Evaluation of coal char gasification kinetics and pore development in high pressure steam and carbon dioxide

LC Mgano

Orcid.org/0000-0002-6104-749X

Dissertation accepted in fulfilment of the requirements for the degree Master of Engineering in Chemical Engineering at the North-West University

Supervisor:	Prof HWJP Neomagus
Co-Supervisor:	Prof JR Bunt
Co-Supervisor:	Prof RC Everson

Graduation:	October 2020
Student Number:	23037326

DECLARATION

I, Lebohang Clement Mgano, hereby declare that the dissertation entitled: ***"Evaluation of coal char gasification kinetics and pore development in high pressure steam and carbon dioxide."***, submitted in the fulfilment of the requirements for the degree of Master's in Chemical Engineering, is my own work except where acknowledged in the text, it has been language edited as required and has not been submitted to any other tertiary institution in whole or in part.

I understand that the copies handed in for examination are the property of the North-West University.

Signed at Potchefstroom on the *11th* day of *August 2020*

LC Mgano (Student)

23037326

University number

CONFERENCE PROCEEDINGS

The conference proceedings which include the conference presentations from the investigations conducted in this study are as follows:

- Gouws, S.M., **Mgano, L.C.**, Neomagus, H.W.J.P. **(Presenter)**, Bunt J.R., Everson R.C. and Roberts, D.G. (2018). The effect of carbon dioxide partial pressure on the gasification rate and pore development of Highveld coal chars at elevated pressures. Results presented at the 9th International Freiberg Conference on IGCC and XtL technologies, 3-8 June 2018, Berlin, Germany. **(Oral presentation)**

- **Mgano, L.C. (Presenter)**, Neomagus, H.W.J.P., Bunt J.R., and Everson R.C. (2018). Evaluation of coal char gasification kinetics and pore development in high pressure steam and carbon dioxide. Presented at the Fossil Fuel Foundation (FFF) Conference on Clean Coal Technologies for Southern Africa: Can coal clean up its act?, 20-21 November 2018, Johannesburg, South Africa. **(Oral presentation)**

- **Mgano, L.C.,** Neomagus, H.W.J.P. **(Presenter)**, Bunt J.R., and Everson R.C. (2019). Evaluation of coal char gasification kinetics and pore development in high pressure steam and carbon dioxide. Presented at International Conference on Coal Science and Technology (ICCS&T), 24-28 November 2019, Krakow, Poland. **(Oral presentation)**

ACKNOWLEDGEMENTS

The author wishes to acknowledge and thank the following persons/institute with sincere gratitude for their contribution in the accomplishment of this dissertation:

- My supervisors, Professor Hein Neomagus, John Bunt and Raymond Everson for their wisdom and guidance throughout the conducted work and much more.
- Mr Ted Paarlberg for his technical assistance and guidance towards the commissioning of the experimental rig.
- The workshop personnel for their help and useful insights throughout this investigation.
- The financial personnel for their assistance and effortless follow-ups on administration throughout the study.
- Dr Gregory Okolo for his insightful knowledge on pore development and the operation of the surface analysis equipment.
- Mr Andrei Koekemoer for his insightful knowledge in the conducted investigations and mentorship.
- My dearest Mother for her support and colleagues.
- Sasol team for the financial support towards the project.
- The financial assistance of the National Research Foundation (NRF) towards this research is hereby acknowledged (Coal Research Chair Grant No. 86880).

The work presented in this paper is based on the research support by the South African Research Chairs Initiative of the Department of Science and Technology and National Research Foundation of South Africa (Coal Research Chair Grant No. 86880). Any opinion, finding, conclusion or recommendation expressed in this material is that of the author(s) and the NRF does not accept liability in this regard.

ABSTRACT

Coal is utilised in the coal-to-liquid (CTL) process on a large scale in South Africa and significantly contributes to the country's energy demand. In this conversion process, the primary step is the high pressure gasification of coal, and only limited studies have related to high pressure gasification kinetics with CO_2, and specifically steam for South African coals. In this study, inertinite-rich coal from the Highveld coalfield was used to evaluate the coal char gasification kinetics and the associated surface area development at high steam and CO_2 partial pressures up to 20 and 30 bar, respectively. A coal char sample of -150+75 µm was prepared through mechanical size reduction of lump coal and charred at 950 °C in a N_2 atmosphere. The coal char gasification experiments were subsequently conducted at isothermal conditions at a temperature of 780 °C for CO_2 and 740 °C for steam in the chemical-controlled regime. The reaction rate was determined by the analysis of the carbon-based products, and the micropore surface area of the raw and reacted chars (conversion of ~10, 20, and 30%) was analysed by CO_2 adsorption with use of the Dubinin-Astakhov (D-A) method.

From the reaction rate and the subsequent micropore surface area data, the intrinsic rate ($g/m^2.s$) was determined for the quantification of the kinetic parameters described by the Langmuir-Hinshelwood (LH) rate type model. The Random-Pore Model (RPM) was used to model the development of micropore surface area with the extent of carbon conversion. From the obtained results, it was found that the specific reaction rate and micropore surface area were significantly affected by the extent of carbon conversion and more pronounced for steam. With an increase in reactant partial pressure, the intrinsic reaction rate increased with a reaction order of 0.57 (±0.09) and 0.32 (±0.05) for steam and CO_2 respectively at a reactant partial pressure of up to 10 and 20 bar, decreasing to a value of close to zero with a further increase. The LH type model was suitable for describing the effect of partial pressure on the reaction rate. The development of micropore surface area was found to be not affected by the reactant partial pressure for steam gasification in contrast to CO_2 gasification.

A mixed model (combination of LH type model and RPM) was used to model the specific rate and it was found that the model can fairly predict the reaction rate and a directly fitted RPM rate type was suitable to describe better the specific rate. The intrinsic reaction rate was found to be only a function of partial pressure for steam gasification, which was described well by a single LH type model with the intrinsic $[Ct]k_1$ and k_1/k_3 values of $7.4x10^{-9}$ ($g/m^2.s.bar$) and 0.13 (1/bar), respectively over the studied conversion range. For CO_2 gasification, intrinsic $[Ct]k_1$ and k_1/k_3 values were found to be in the range of $4.6\text{-}5.7x10^{-9}$ ($g/m^2.s.bar$) and 0.11-0.12 (1/bar), respectively.

Keywords: High pressure steam and CO_2 gasification kinetics, intrinsic reaction rates, pore development, Highveld coal char

TABLE OF CONTENTS

CHAPTER 3: COAL AND CHAT CHARACTERISATION

CHAPTER 4: EXPERIMENTAL METHODS: GASIFICATION

LIST OF TABLES

LIST OF FIGURES

NOMENCLATURE

List of symbols

Symbol	Description	Units
$C(CO)$	carbon-CO surface complex	$-$
$C(O)$	carbon-oxygen surface complex	$-$
$C(H)$	carbon-hydrogen surface complex	$-$
C_f	free carbon sites	$1/g$
$C_{s,g}$	reactant gas concentration	$vol\%$
$[C_t]$	total number of sites	$1/g$
$[C_t]k_i$	LH rate type parameter	$1/bar.s$
c	intrinsic $[C_t]k_i$ term	$g/m^2.s.bar$
E_a	apparent activation energy	kJ/mol
E	activation energy	kJ/mol
k_0	pre-exponential factor	$g.bar^n/g/s$
k_i	rate constant	$1/s$
K_i'	lumped constant of k_i	$1/s$
k_p	RPM rate constant	$1/s$
k_s	specific rate constant	$1/s$
L_o	pore length per unit volume	m/m^3
m	reaction order	$-$
$m_{c,o}$	initial mass of carbon	g
$m_{c,t}$	instantaneous mass of carbon	g
$m_{char,0}$	initial mass of coal char	g
m_t	instantaneous mass of coal char	g
MW_c	molecular weight of carbon	g/mol
n	apparent reaction order	$-$
n_i	moles of species i	mol

Symbol	Description	Units
$\dot{n}_T$	total molar flow rate	mol/s
p_i	reactant partial pressure	bar
p_j	partial pressure of species j	bar
P_{STP}	standard pressure	bar
R	universal gas constant	$J/mol.K$
r_s	specific reaction rate	$g/g/s$
$r_{s,0}$	initial specific rate	$g/g/s$
r_i''	intrinsic reaction rate	$g/m^2/s$
S	Surface area	m^2/g
S_0	initial surface area	m^2/g
S_m	micropore surface area	m^2/g_c
$S_{m,0}$	initial micropore surface area	m^2/g_c
S_v	surface area	m^2/m^3
$S_{v,0}$	initial surface area	m^2/m^3
T	temperature	$K\ or\ °C$
T_a	actual/observed temperature	$K\ or\ °C$
T_{STP}	standard temperature	K
t	time	$s\ or\ min$
$\dot{V}_a$	actual/observed flow rate	L/min
$\dot{V}_{STP}$	flow rate at standard conditions	NL/min
X	char or carbon conversion	$-$
X_C	carbon conversion	$-$
x_i	mass fraction of species i	$-$
y_i	mole fraction of species i	$-$
	Greek symbols	
θ	site occupancy	$-$
ψ	structural parameter	$-$
ε_0	initial porosity	$-$

List of abbreviations

adb – Air-dried basis

BET – Brunauer-Emmet-Teller

BJH – Barrett-Joyner-Halenda

CI – Confidence interval

CTL – Coal-to-Liquid

D-A – Dubinin-Astakhov

D-R – Dubinin-Raduschkevich

daf – Dry-ash free basis

db – Dry basis

EPC – Electronic pressure controller

HK – Horvath-Kawazoe

HPFBR – High pressure fixed-bed reactor

ISO – International standards organisation

LH – Langmuir-Hinshelwood

MFC – Mass flow controller

MFM – Mass flow meter

mmfb – Mineral matter-free basis

MW – Molecular weight

PL – Power law

PSD – Particle size distribution

RPM – Random-Pore Model

SANS – South African National Standard

SAXS – Small-angle X-ray scattering

SCM – Shrinking core model

STP – Standard pressure and temperature

TGA – Thermo-gravimetric analyser

TPD – Temperature-programmed desorption

VM – Volumetric model

XRF – X-ray fluorescence

“Hard work does not necessarily guarantee success, but no success is possible without hard work.”

-Dr T.P. Chia-

Chapter 1

(GENERAL INTRODUCTION)

CHAPTER 1

(GENERAL INTRODUCTION)

1.1 Background and motivation

1.1.1 Importance of coal in energy sector

The demand for energy increases worldwide (IEO, 2016) and to secure sufficient supply, various energy sources have been explored and used in different parts of the world depending on availability and economic feasibility. The most commonly used primary energy sources are natural gas, crude oil, nuclear, renewables, and coal (Lee *et al.*, 2014b; Oakey, 2015; Speight, 2012; WEC, 2019). In both the past and recent years, coal has been contributing widely to electricity generation, accounting for almost 40% of the world's demand (Speight, 2012; WEC, 2019). In countries such as Poland, South Africa, China, and Australia where there are large coal deposits, the use of coal for electricity generation is even more predominant (Speight, 2012; WEC, 2019). Due to coal abundance in South Africa, coal is also used in several other applications for the production of chemicals, synthetic fuels and steel (DOE, 2017).

Almost 23% of the countries coal is used in Coal-to-Liquid (CTL) technology for the production of liquid fuels and various chemicals such as alcohols, acids and solvents (DOE, 2017; van Dyk *et al.*, 2006; WEC, 2019). The liquid fuels produced from coal contribute more than 40% of the countries demand (van Dyk *et al.*, 2006). Considering that South Africa has insignificant oil reserves (WEC, 2019), the use of coal through CTL technology remains imperative.

1.1.2 Coal-to-Liquid technology

CTL technology has been the backbone of South Africa's petrochemical industry for converting coal into a wide range of liquid hydrocarbons through indirect coal liquefaction (van Dyk *et al.*, 2006). In this process, coal gasification is the initial and most crucial step of the technology where the coal is fed into a gasifier together with steam and oxygen at relatively high pressures to primarily produce synthesis gas (Gräbner, 2014; Lee *et al.*, 2014b; Oakey, 2015). This gas mixture consists mainly of CO and H_2, which is further processed through several technologies to produce liquid fuels and chemicals (Bell *et al.*, 2010; Lee *et al.*, 2014b).

During coal gasification, coal is subjected to sequential processes, namely drying, devolatilisation, coal gasification and combustion (Gräbner, 2014). Amongst these processes, the gasification of

coal char from the devolatilisation stage with the co-fed steam has a large impact on the degree of coal conversion and the gasification unit size (Gräbner, 2014; Lee *et al.*, 2014b; Oakey, 2015). This impact is the resultant of the slow heterogeneous chemical reactions that occur during char gasification, making coal char gasification the slowest step that essentially controls the overall gasification process (Bell *et al.*, 2010; Gräbner, 2014; Park & Ahn, 2007). In this regard, the coal char gasification step has attracted many studies to provide essential information regarding the thermodynamics and kinetics of various reactions associated with coal char gasification.

1.1.3 Coal char gasification kinetics

The understanding of the char gasification kinetics together with the thermodynamic behaviour is of importance to improve gasification processes. The gasifier performance-related aspects have been described through mathematical models taking into account, reaction conditions and the nature of the coal (Lee *et al.*, 2014b; Tremel & Spliethoff, 2013). Modelling requires the knowledge of kinetics and the extent of conversions to predict the behaviour of coal char during gasification (Govind & Shah, 1984; Molina & Mondragon, 1998). Coal char gasification kinetics obtained at a laboratory scale provides the intrinsic kinetic data which forms an essential part of reactor modelling attempts. Several studies have been conducted to determine the kinetics using CO_2, steam, or a mixture of the two in the absence or presence of inhibition products (Gouws *et al.*, 2018; Jayaraman & Gokalp, 2015; Kajitani *et al.*, 2013; Roberts & Harris, 2000; Roberts & Harris, 2012; Tremel & Spliethoff, 2013).

As new technological developments and concepts in coal gasification technology are arising, specifically with regards to a smaller carbon footprint, the continuous study of coal char gasification kinetics remains vitally important. Commercial gasifiers are typically operated at high pressures (Gräbner, 2014; van Dyk *et al.*, 2006), however, the intrinsic kinetic data have been widely obtained at low pressures and mostly using CO_2 as the gasifying agent. Furthermore, coal char gasification kinetics obtained at high partial pressures of steam is limited, particularly for South African coals making a study in this field relevant.

1.2 Problem statement

Coal char gasification studies have been mostly performed at low pressures and generated essential fundamental knowledge in the field. Most of these studies have been done using CO_2, steam and a mixture of the two to quantify the gasification reactions and kinetic parameters for different types of coals ranging from lignite to anthracite. (Everson *et al.*, 2006; Jayaraman *et al.*, 2015; Kwon *et al.*, 1988; Roberts & Harris, 2000; Roberts & Harris, 2007; Zhang *et al.*, 2006; Zhang *et al.*, 2017). Coal char gasification kinetics depends on a variety of variables of which

reactant concentration or partial pressure is of significant importance (Irfan *et al.*, 2011; Li *et al.*, 2018; Park & Ahn, 2007). Since data at high pressures, specifically for South African coal chars are scarce, measurement of char gasification kinetics at high reactant pressures needs to be addressed.

Currently, there is a lack of high reactant pressure studies describing char gasification kinetics in CO_2 and steam atmospheres. CO_2 gasification studies at high pressures for Australian coal chars have shown that the reactant pressure has a strong influence on the gasification kinetics up to a certain extent, specifically in the absence of mass transfer limitations (Roberts & Harris, 2000; Roberts & Harris, 2006). As for South African coals, the measurements of the gasification kinetics have mainly been obtained at low pressures (Coetzee *et al.*, 2015; Du toit, 2013; Everson *et al.*, 2006; Veca & Adrover, 2014). In recent CO_2 gasification studies, coal char gasification kinetics have been obtained at total pressures up to 30 bar and reactant pressures up to 9 bar (Gouws *et al.*, 2018). The data obtained in that study contributed to the knowledge of CO_2 gasification kinetics, however, measurements of steam-char gasification kinetics at high pressures are limited. This study will focus on measuring the char gasification kinetics at conditions similar to industrial operation pressures in the atmosphere of steam and CO_2 which include the evaluation of pore development in relation to the pressure as the gasification proceeds.

1.3 Research aim and objectives

The aim of this investigation is to evaluate and compare the reaction kinetics of steam and CO_2 gasification for the selected Highveld coal at elevated reagent partial pressures. To achieve this aim, the objectives of this investigation are to:

- Characterise the parent coal and subsequent char by means of conventional characterisation such as the chemical, petrographic, mineralogical, and surface area analysis.

- Determine the influence of steam and CO_2 partial pressures on the intrinsic reaction rate obtained under chemical-controlled and isothermal conditions.

- Evaluate the char surface area development by means of determining the effects on the char micropore surface area of the partially converted chars related to the reagent pressures.

- Model the char intrinsic rate and pore development by making use of well-established models.

1.4 Scope of investigation

The scope of the investigation is to conduct char gasification experiments at controlled laboratory conditions using a high pressure fixed-bed reactor (HPFBR) which allows determination of char reactivity from the analysis of the main carbon-containing gasification products (CO and CO_2). To address the research objectives, the scope is narrowed down to three sections which focus mainly on (1) char-CO_2 reactivity, (2) char-steam reactivity, and (3) char surface area analysis of the unreacted and partially reacted chars.

- **Coal char gasification experiments**

The coal char gasification experiments will be conducted at isothermal conditions and partial pressures of up to 20 and 30 bar of steam and CO_2, respectively. To perform the steam gasification experiments, a slight modification on the HPFBR rig will be done to incorporate the feed and removal of the water and steam. The experiments will be carried out in the chemical-controlled regime and regime identification will be verified beforehand. In this case, the experiments will be conducted at different steam and CO_2 partial pressures to measure the reactivity at carbon conversions of 10, 20 and 30%. The reactivity data will then be used to determine a suitable kinetic model and the associated constants.

- **Char surface area analysis**

The char surface area analysis will be conducted on the unreacted and partially reacted chars at different reactant (for both steam and CO_2) partial pressures quenched at the carbon conversions of 10, 20 and 30%. The analysis will be based on determining the micropore surface area by making use of CO_2 adsorption at 0 °C.

- **Modelling**

The intrinsic reaction rate ($g/m^2/s$) determined from the specific reaction rate and pore development data will be modelled using the kinetic models. The associated intrinsic kinetic parameters together with the description of pore development from the Random-Pore Model (RPM) will be used to provide a model that describes the specific reaction rate.

- **Limitations and shortcomings**

— In this study, the experiments will be performed at a single temperature since the related Arrhenius plots and the resultant activation energies of the particular South African coal have been well-established and concurs with previous studies (Du toit, 2013; Everson *et al.*, 2006; Gouws *et al.*, 2018; Henning, 2016).

— One Highveld coal which has similar characteristics as typical coal for the CTL technology in South Africa (van Dyk *et al.*, 2006) is used.

— The investigations undertaken in this study do not cover the inhibitions of CO or/and H_2, char gasification of demineralised coal char, and the evaluation of the catalytic effect of the mineral matter.

— The pore development during gasification will be evaluated on the micropore size range where chemical reactions mainly occur and also dominating the pore surface area by almost 98% (Coetzee *et al.*, 2015).

Chapter 2

(LITERATURE REVIEW)

CHAPTER 2

(LITERATURE REVIEW)

2.1 Introduction

On a commercial scale, coal gasification is carried out in a gasifier where coal char is converted through heterogeneous chemical reactions to produce synthesis gas. These reactions are influenced by several parameters which include primarily reactant pressure, coal char type, and temperature. The fundamental knowledge of the coal char and its kinetic behaviour can be used to describe the overall gasification process.

This chapter includes a literature review and is divided into subsections addressing the relevant fundamentals of the study. Section **2.2** discusses an overview of coal gasification and the associated heterogeneous chemical reactions. This section also addresses the mechanisms of char gasification reactions in the atmosphere of CO_2 and steam together with a review of the three-temperature zones (regimes). In Section **2.3** the variables affecting the char reactivity, especially with regards to the changes in reactant partial pressure and temperature are discussed. The discussion on the associated development of pores and surface area during coal char conversion is provided in Section **2.4**. Section **2.5** provides the modelling of char reactivity using well-known models and also their applicability and limitations. Section **2.6** provides a summary of the chapter.

2.2 Coal char gasification

2.2.1 Overview of coal gasification

Coal gasification is a process wherein coal is converted to synthesis gas (a mixture of CO and H_2) through a series of chemical reactions. Steam and O_2 (or air) are fed into the gasifier operating at relatively high pressures (20-100 bar) and temperatures greater than 700 °C whereby they interact with coal, resulting in the formation of gaseous products (Bell *et al.*, 2010; Gräbner, 2014; van Dyk *et al.*, 2006). In a typical gasifier, the first step that coal undergoes is drying followed by pyrolysis where volatiles are removed and resulting in a formation of coal char. Thereafter, coal char is mainly converted to CO and H_2 in the gasification stage through heterogeneous chemical reactions (Aydar *et al.*, 2014; Figueiredo & Moulijn, 2012; Gräbner, 2014; Harvey & Ruch, 1984; Lee *et al.*, 2014b). The last stage involves the combustion of the resultant carbonaceous material from the gasification stage which also provides heat for the endothermic gasification reactions (Bell *et al.*, 2010; Collot, 2006; Dupont *et al.*, 2016; Gräbner, 2014; La Villetta *et al.*, 2017).

Amongst these processes, the gasification of the coal char material is the slowest step that ends up controlling the overall gasification process (Roberts & Harris, 2006; Tremel *et al.*, 2012). Table 2-1 summarises the major reactions taking place in the gasification process which also include gas-phase reactions (Bell *et al.*, 2010; Bunt, 2006; McKendry, 2002; Rezaiyan & Cheremisinoff, 2005).

Table 2-1: Summary of char gasification and gas reactions

Reaction	Reaction process	ΔH^0_{rxn} (kJ/mol)	Equation no.
$C+CO_2 \rightarrow 2CO$	Gasification with carbon dioxide	172.7	(R2.1)
$C + H_2O \rightarrow CO+H_2$	Gasification with steam	131.5	(R2.2)
$C+2H_2 \rightarrow CH_4$	Gasification with hydrogen	-74.9	(R2.3)
$CO+H_2O \rightarrow CO_2 + H_2$	Water-gas shift	-41.2	(R2.4)
$CO+3H_2 \rightarrow CH_4+H_2O$	Methanation	-206.2	(R2.5)

Coal char gasification involves heterogeneous primary reactions taking place between the carbon within the char material and the gasifying agent (steam and CO_2). These reactions are ascribed to a series of reaction mechanisms which then result in the formation of CO and H_2. As shown in Table 2-1, the formation of CO (R2.1 and R2.2) is influenced by the secondary water-shift reaction (R2.4), which results in the formation of CO_2. On the other hand, the formation of methane (CH_4) can also occur and is strongly depended on the H_2 partial pressure (Blackwood & McGrory, 1958; Hüttinger & Merdes, 1992). The char-steam and char-CO_2 reactions have been extensively studied due to their significant influence on the gasification rate since they are primary reactions and much slower than the gas-phase reactions (Gräbner, 2014; Kabe *et al.*, 2004; Smoot & Smith, 1985). The kinetics of these reactions are influenced by the material and heat transfer phenomena which are described based on reaction regimes (Smoot & Smith, 1985; Walker Jr *et al.*, 1959).

2.2.2 Coal char reaction regimes

The regime in which the coal char gasification reactions occur influences the char reactivity and kinetics. It has been proposed that heterogeneous gas-solid reactions can occur in three-temperature zones (regimes) which are described from the relation of the reaction rate and the particle temperature (Walker Jr *et al.*, 1959). Figure 2-1 illustrates the rate-controlling regimes for coal char gasification (Smoot & Smith, 1985).

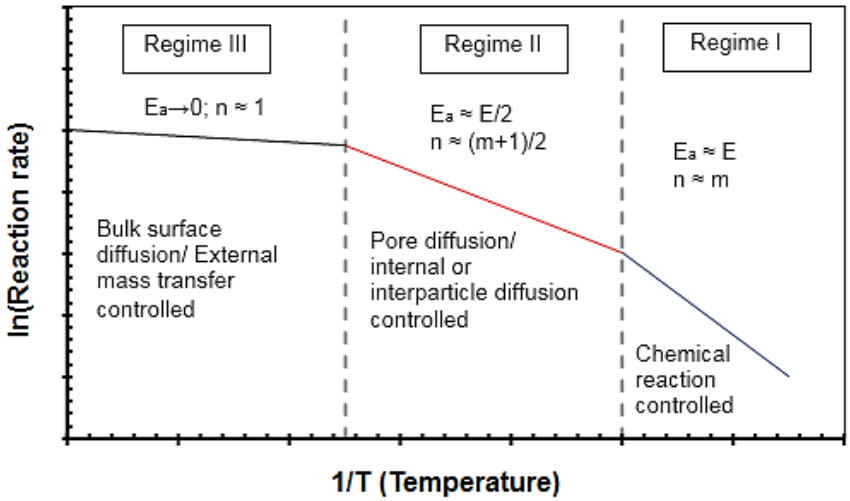

Figure 2-1: Influence of temperature on rate-limiting regimes/zones [***adapted from*** (Gräbner, 2014; Kabe *et al.*, 2004; Kim *et al.*, 2014; Smith *et al.*, 2013; Tanner & Bhattacharya, 2016; Tremel *et al.*, 2012)]

In order to determine intrinsic char reaction rates and kinetic parameters suitable for the development of gasification models, mass transfer limitations have to be decoupled from the surface or chemical reactions that mostly occur at the internal surface area of the particle (Roberts & Harris, 2000; Tanner & Bhattacharya, 2016).

- **Regime I: Reaction controlled**

In the chemical-controlled regime, the heterogeneous char-gas reactions occur at low temperatures in the absence of diffusional limitations. The reaction between carbon within the char and the reagent gas (H_2O, CO_2) uniformly occurs at the inner surface area of the char at a slow rate and these chemical reactions are the rate-limiting step (Irfan *et al.*, 2011; Lee *et al.*, 2014a; Smoot & Smith, 1985; Tanner & Bhattacharya, 2016; Tremel & Spliethoff, 2013). Because of the relative fast external and internal mass transfer, the reagent gas concentration at the bulk film and the surface of the coal char particle are the same (Fogler, 2013; Sahini & Sahimi, 2003; Szekely, 2012). Therefore, change in total pressure at a constant reagent partial pressure and flow rate will not have an effect on the reaction rate (Fogler, 2013; Harris & Smith, 1991; Roberts *et al.*, 2010; Tremel & Spliethoff, 2013). It has also been found that a change in char particle size does not show an effect on the reaction rate (Fogler, 2013; Roberts & Harris, 2000; Tremel *et al.*, 2012). To measure the intrinsic reaction rates of char-steam and char-CO_2 reactions, these conditions have to be precisely chosen and evaluated (Smoot & Smith, 1985).

- **Regime II&III: Pore and bulk diffusion-controlled**

The effects of external and internal mass transfer limitations on reaction rate have been reported to occur at high temperatures of around 1000 °C where chemical reactions are predominantly

faster (Adschiri *et al.*, 1986; Fogler, 2013; Gräbner, 2014; Smith *et al.*, 2013; Tanner & Bhattacharya, 2016; Tremel *et al.*, 2012). The apparent activation energy of the char gasification in the atmosphere of steam and CO_2 has been reported almost one-half of the "true" value and in the order of about or less than 190 kJ/mol (Gräbner, 2014; Smith *et al.*, 2013; Smoot & Smith, 1985; Tanner & Bhattacharya, 2016). In these regimes, the reaction rate is limited by pore diffusion of reagent gases into the char pore structure and external mass transfer through the boundary layer surrounding the char particle (Fogler, 2013; Smith *et al.*, 2013; Tanner & Bhattacharya, 2016; Tremel & Spliethoff, 2013). Due to a difference in reagent gas concentration and surface of char particle, a change in total pressure and flow rate have a significant influence on the reaction rate (Figueiredo & Moulijn, 2012; Fogler, 2013; Tremel & Spliethoff, 2013). These observations are more profound during coal char gasification of larger particle size (Figueiredo & Moulijn, 2012; Fogler, 2013; Irfan *et al.*, 2011). Therefore, the measurement of char gasification rates at low temperatures, the use of high flow rates and small particle sizes are essential in order to eliminate mass transfer limitations (Fogler, 2013; Irfan *et al.*, 2011; Kabe *et al.*, 2004; Molina & Mondragon, 1998).

2.2.3 Char-CO_2 and char-steam reactions

CO_2 and steam gasification reactions occur through a series of steps based on the fundamental heterogeneous gas-solid reactions which involve (1) diffusion of gaseous reactants and products from the bulk-gas phase to the internal surface of the reacting solid particle, (2) diffusion of gaseous reactant or product through the pores of a partially reacted solid, (3) adsorption and desorption of gaseous reactant or/and reaction products from the solid surfaces, and (4) chemical reactions between the adsorbed gas and the solid material (Smith *et al.*, 2013; Szekely, 2012). Amongst these steps, the chemical reaction step takes place at a slow rate (rate-limiting step) and therefore, limiting the gasification rate (Roberts & Harris, 2006; Tremel & Spliethoff, 2013).

2.2.3.1 CO_2-char reaction mechanism

Several char-CO_2 reaction mechanisms have been proposed which involve the intermediate elemental steps associated with the chemical reactions and the commonly used mechanism is the two-step reaction scheme (Blackwood & Ingeme, 1960; Gadsby *et al.*, 1948; Strange & Walker Jr, 1976; Walker Jr *et al.*, 1959). The two-step mechanism for C-CO_2 gasification reaction was initially proposed by Gadsby *et al.* (1948) and further confirmed by Walker Jr *et al.* (1959) as presented in Equation R2.6 and R2.7.

$$C_f + CO_2 \rightleftharpoons C(O) + CO \qquad (k_1, k_2) \qquad \text{(R2.6)}$$

$$C(O) \longrightarrow CO \qquad (k_3) \qquad \text{(R2.7)}$$

where C_f is a free active site on the char surface, $C(O)$ is the adsorbed surface complex, and k_i is a rate constant. These reaction steps indicate that during the char-CO_2 reaction, CO_2 attaches onto the free active sites and dissociate into an adsorbed-oxygen surface complex and CO in the gas phase (Equation R2.6). This reaction step is influenced by the quantity of free active sites available on the char surface. The last step (Equation R2.7) illustrates the desorption of the adsorbed surface complexes into the CO molecule in the gas phase. The desorption of the surface complexes is regarded as the rate-limiting step observed at low and high CO_2 partial pressures (Roberts & Harris, 2006). The reaction rate derived from this reaction mechanism is expressed in Equation 2.1 based on the Langmuir-Hinshelwood (LH) rate type (Gadsby *et al.*, 1948; Hüttinger & Merdes, 1992).

$$r_{CO_2} = \frac{[C_t]k_1 p_{CO_2}}{1 + {k_1}/{k_3}\, p_{CO_2} + {k_2}/{k_3}\, p_{CO}} \qquad (2.1)$$

where $[C_t]$ is the concentration of the active sites related to the sum of the free and occupied sites (Ergun, 1956; Lee *et al.*, 2014b; Roberts & Harris, 2006; Wang & Bell, 2017), p_{CO_2} is the CO_2 partial pressure, p_{CO} is the partial pressure of CO, and k_i is the reaction constant that can be described by the Arrhenius equation. As illustrated in Reaction R2.6, the CO formed can inhibit the reaction rate through the oxygen-exchange mechanism of the reverse reaction which result to CO_2 formation (Ergun, 1956; Meijer *et al.*, 1994; Molina & Mondragon, 1998; Smith *et al.*, 2013). Blackwood and Ingeme (1960) proposed a more detailed reaction mechanism describing the inhibition effects of CO by adding two additional steps which describe the formation of CO_2 and sites occupancy.

$$CO_2 + C(CO) \longrightarrow 2CO + C(O) \qquad (k_4) \qquad \text{(R2.8)}$$

$$CO + C(CO) \rightleftharpoons CO_2 + 2C_f \qquad (k_5, k_6) \qquad \text{(R2.9)}$$

where $C(CO)$ is the chemisorbed molecule in which CO is adsorbed onto the active site on the char surface. The reaction rate incorporating these two steps is then expressed as follows:

$$r_{CO_2} = \frac{K_1' p_{CO_2} + K_5' p_{CO_2}^2}{1 + K_2' p_{CO_2} + K_3' p_{CO}} \qquad (2.2)$$

where K_i' is a lumped (product) constant of individual reaction rate constant (k_i). The inhibition effects by chemisorbed CO surface complexes on the reaction rate are believed to occur at high CO concentrations due to (1) the accumulation of chemisorbed species which reduces the amount of active sites available on the char surface (Ergun, 1956; Lee *et al.*, 2014b; Meijer *et al.*, 1994) and (2) stronger inhibitions due to high CO concentrations favouring reaction R2.9 (Huang *et al.*, 2010). The proposed reaction scheme was found to be able to describe the reaction rate of C-CO_2 at high pressures (Blackwood & Ingeme, 1960; Kajitani *et al.*, 2006; Mühlen *et al.*, 1985), however, Nozaki *et al.* (1992) found the reaction rate associated with additional steps not applicable to describe the C-CO_2 reactions at high pressures.

2.2.3.2 Steam-char reaction mechanism

Similar to the char-CO_2 reaction mechanism, different char-steam reaction mechanisms have been proposed and a two-stage mechanism proposed by Gadsby *et al.* (1946) has been commonly used (Nozaki *et al.*, 1991; Walker Jr *et al.*, 1959).

$$C_f + H_2O \rightleftharpoons C(O) + H_2 \qquad (k_7, k_8) \qquad \text{(R2.10)}$$

$$C(O) \longrightarrow CO \qquad (k_9) \qquad \text{(R2.11)}$$

This reaction mechanism shows that steam (H_2O) is chemisorbed onto a free active site where it then dissociates into a surface complex $C(O)$ and H_2 in the gas phase. The adsorbed surface complex also desorb from the active site into CO in the gas phase (Equation R2.11). The reverse reaction in Equation R2.10 enables the reduction of $C(O)$ surface complexes through the reaction between the chemisorbed $C(O)$ and the H_2 which ends up retarding the reaction rate. At high H_2 concentrations, the inhibition of H_2 can follow a different path other than the one described from Equation 2.10 reverse reaction (Hüttinger & Merdes, 1992). Two ways in which H_2 inhibition occur have been reported and found to be associated with sites occupancy (Hüttinger & Merdes, 1992; Molina & Mondragon, 1998; Moulijn & Kapteijn, 1995).

$$C_f + H_2 \rightleftharpoons C(H)_2 \qquad (k_{10}, k_{11}) \qquad \text{(R2.12)}$$

$$C_f + {}^1/_2 H_2 \rightleftharpoons C(H) \qquad (k_{12}, k_{13}) \qquad \text{(R2.13)}$$

Equation R2.12 and R2.13 indicate H_2 inhibition occurring through associative and dissociative adsorption occupying free active sites. A general reaction rate based on the LH rate type for this reaction mechanism is provided in Equation 2.3.

$$r_{H_2O} = \frac{[C_t]k_7 p_{H_2O}}{1 + {k_7}/{k_9}\, p_{H_2O} + f(p_{H_2})} \tag{2.3}$$

where $f(p_{H_2})$ is the inhibition term and can be expressed based on the nature of inhibition as follows:

$$f(p_{H_2}) = {k_8}/{k_9}\, p_{H_2} \quad \textit{: Oxygen-exchange mechanism} \tag{2.3a}$$

$$f(p_{H_2}) = {k_{10}}/{k_{11}}\, p_{H_2} \quad \textit{: Associative } H_2 \textit{ adsorption} \tag{2.3b}$$

$$f(p_{H_2}) = {k_{12}}/{k_{13}}\, p_{H_2}^{0.5} \quad \textit{: Dissociative } H_2 \textit{ adsorption} \tag{2.3c}$$

At low pressures, dissociative adsorption has been observed to be more dominant (Fushimi *et al.*, 2011; Huttinger, 1989; Kajitani *et al.*, 2013; Lussier *et al.*, 1998). H_2 inhibition through associative H_2 adsorption and oxygen-exchange reaction between H_2 and $C(O)$ has been found to be more applicable at high pressures (Lussier *et al.*, 1998; Zhang *et al.*, 2000). However, some authors have found these effects dominating at low pressures (Azimi *et al.*, 2012; Kajita *et al.*, 2009). Several studies have found the reaction rate expressed in Equation 2.3, with the incorporation of Equation 2.3a, to be applicable at low and high pressures due to insignificant methane formation (Chen *et al.*, 2013; Everson *et al.*, 2006; Roberts & Harris, 2006; Zhang *et al.*, 2017). At high steam and H_2 partial pressures, methane formation is significant and therefore, incorporation of its formation is necessary (Blackwood & McGrory, 1958; Hüttinger & Merdes, 1992; Mühlen *et al.*, 1985; Zhang *et al.*, 2000). To describe the possible formation of methane, Blackwood and McGrory (1958) proposed a reaction scheme through the modification of the two-stage reaction scheme and incorporating an additional intermediate step as follows:

$$C_f + H_2O \rightarrow C(O) + C(H_2) \qquad (k_1) \tag{R2.14}$$

$$C(H_2) \rightleftharpoons H_2 \qquad (k_{14}, k_{15}) \tag{R2.15}$$

$$C(O) \rightarrow CO \qquad (k_9) \tag{R2.16}$$

$$C(H)_2 + C_f + H_2O \longrightarrow CH_4 + C(O) \qquad (k_{16}) \tag{R2.17}$$

From this reaction scheme, steam is firstly chemisorbed onto the free active sites and forms $C(H_2)$ and $C(O)$ surface complexes through dissociation. Some of the adsorbed-hydrogen complexes transform into H_2 in a gas phase and untransformed surface complex can further react

with steam to form methane. The reaction rate for this reaction mechanism is shown in Equation 2.4.

$$r_{H_2O} = \frac{K_1' p_{H_2O} + K_4' p_{H_2O} p_{H_2} + K_5' p_{H_2O}^2}{1 + K_3' p_{H_2O} + K_2' p_{H_2}} \quad (2.4)$$

where K'_i is a lumped (product) constant of individual reaction rate constant (k_i). The applicability of the reaction rate expressed in Equation 2.4 is observed in cases where methane formation is significant (Blackwood & McGrory, 1958; Mühlen *et al.*, 1985; Schmal *et al.*, 1983).

2.3 Factors affecting char reactivity

The char gasification reactivity and kinetics have been established to be affected by a wide range of process parameters which include: coal rank, the chemical structure of coal/char, char preparation conditions, mineral matter contents and dispersion, porosity and surface area of coal char, inhibition of product gases, pressure and gasification temperature (Coetzee *et al.*, 2015; Everson *et al.*, 2006; Irfan *et al.*, 2011; Molina & Mondragon, 1998; Ng *et al.*, 1988; Porada *et al.*, 2017).

2.3.1 Coal char properties

Coal properties such as rank have a significant influence on the char gasification kinetics and reactivity since different coals exhibit different thermal behaviour and extent of coal conversion during gasification. The char reactivity is largely dependent on the type and maturity of the parent coal, whereby reactivity decreases with an increase in coal rank (Di Blasi, 2009; Porada *et al.*, 2017; Ye *et al.*, 1998). The porosity and pore volume of the derived chars also decreases with an increase in rank (Ng *et al.*, 1988), resulting in a decrease in gasification reactivity. This analogy is attributed to the high concentration of active sites within the coal matrix of the low-rank coals as compared to high-rank coals (Zhang *et al.*, 2006). Low-rank coals are associated with a high volatile matter content which plays a major role in increasing the pore structure when released, resulting in an increased gasification reactivity (Shadle *et al.*, 2002). Coal mineral matter such as the content of alkali and alkaline earth elements have a catalytic influence on the coal char reactivity (Kabe *et al.*, 2004; Ng *et al.*, 1988; Smith *et al.*, 2013). At lower temperatures, the mineral matter constituents catalyse the gasification reactions, which then result in a greater coal char reactivity (Ma *et al.*, 2013). At higher temperatures, the mineral matter can also reduce the coal char reactivity due to a result of a decrease in the micropore surface area (pore blockage) at which gasification reactions occur (Ma *et al.*, 2013).

2.3.2 Reactant partial pressure

The effect of reactant partial pressure on char reactivity has been evaluated by the variations in the total pressure at a fixed reactant concentration or variations in reactant concentration at a fixed total pressure. Several investigations have been conducted to evaluate the effect of reactant partial pressure on the char-steam and char-CO_2 reactivity at low and high pressures (Ahn *et al.*, 2001; Blackwood & Ingeme, 1960; Blackwood & McGrory, 1958; Everson *et al.*, 2008; Gonzalez *et al.*, 2018; Gouws, 2017; Harris & Smith, 1991; Megaritis *et al.*, 1998; Mühlen *et al.*, 1985; Porada *et al.*, 2017; Roberts & Harris, 2006; Sha *et al.*, 1990; Tremel & Spliethoff, 2013). From these studies, it has been observed that an increase in reactant partial pressure increases reaction rate while the reaction rate is not significantly influenced anymore at high reactant partial pressures.

2.3.2.1 Low pressure studies

At low pressures, the reaction rate is significantly influenced by the changes in reactant partial pressure whereby an increase in reaction rate is observed. As the reactant partial pressure is increased, the amount of reactant gas molecules adsorbing onto the active sites on the char surface are also increased, resulting in an increase in the concentration of surface complexes (C(O)), and hence the reaction rate (Mühlen *et al.*, 1985; Roberts & Harris, 2000; Roberts & Harris, 2006; Wall *et al.*, 2002). The apparent reaction order with respect to the effect of CO_2 partial pressure has been widely reported in the range of 0.4-0.6 (Du toit, 2013; Everson *et al.*, 2008; Harris & Smith, 1991; Kajitani *et al.*, 2006) and 0.4-0.7 for steam gasification (Du toit, 2013; Harris & Smith, 1991). The reaction order has been observed to vary with pressure and approaches an order of zero at high pressures (Blackwood & Ingeme, 1960; Wall *et al.*, 2002).

2.3.2.2 High pressure studies

An increase in reaction rate with reactant partial pressure has been found to occur at reactant partial pressure of up to 15-20 bar (Gonzalez *et al.*, 2018; Gouws *et al.*, 2018; Mühlen *et al.*, 1985; Roberts & Harris, 2000; Sha *et al.*, 1990). This effect is attributed to an increase in the concentration of surface complexes with the observed reaction order of about 0.4-0.5 and 0.4-0.7 for steam and CO_2 gasification, respectively (Roberts & Harris, 2006). A further increase in reactant partial pressure pertains to saturation of active sites and an unaffected reaction rate (Mühlen *et al.*, 1985). Several studies have been conducted to evaluate the effect of reactant partial pressure on gasification rate at reactant partial pressures of up to 60 bar and the remarks are summarised in Table 2-2.

Table 2-2: Remarks on the effect of reactant pressure on reactivity and saturation at high pressures

Author(s)	Operating conditions	Gasified material	Particle size	Rank/type	Reagent gas	Partial pressures	Level off range	Reaction order (n)
Blackwood and Ingeme (1960)	1.2-40 bar at 790-870 °C	Purified carbon	-7+14 B.S.	Coconut shells	CO_2	1.2-40 bar	Not observed	Approaches zero
Mühlen *et al.* (1985)	1-70 bar at 800- 1000 °C	Coal char	NR[a]	2 Sub-bituminous	CO_2 & H_2O	1-60 bar	Above 20 bar	NR
Sha *et al.* (1990)	1.2-31 bar at 850 and 900 °C	Coal char	-800+420 µm	4 Lignites, 2 Bituminous, 1 Sub-bituminous	CO_2 & H_2O	1.2-31 bar	Above 15 bar	Approaches zero
Megaritis *et al.* (1998)	1-30 bar at 1000 °C	Coal	-150+106 µm	NR[a]	CO_2	2-30 bar	Not observed	NR
Roberts and Harris (2006)	1-30 bar at 850 and 900 °C	Coal char	-1+0.6 mm	3 Bituminous	CO_2 & H_2O	1-30 bar	20-30 bar	0.5-0.7 CO_2, 0.4-0.5 H_2O
Tremel and Spliethoff (2013)	25 bar at 750 °C	Coal char	-160+80 µm	1 Lignite and 1 Bituminous	CO_2	5-25 bar	Not observed	0.41
Liu *et al.* (2015)	1-20 bar at 950 and 1050 °C	Coal char	~ 200 µm	1 Bituminous	CO_2	1-20 bar	Not observed	NR

NR - Not reported

Although the effect of reactant partial pressure above 15 bar has shown an unaffected reaction rate, some authors have observed an increase in reaction rate with reactant partial pressure up to 40 bar (Blackwood & Ingeme, 1960; Megaritis *et al.*, 1998; Tremel & Spliethoff, 2013). These results indicate that some effects of coal rank might have an effect (Liu *et al.*, 2000b; Molina & Mondragon, 1998; Park & Ahn, 2007; Wall *et al.*, 2002). When comparing the char reactivity of steam and CO_2, it has been found that the char-steam reaction rates were higher in the order of 3-6 showing that steam is more reactive (Mühlen *et al.*, 1985; Roberts & Harris, 2000; Sha *et al.*, 1990; Tremel & Spliethoff, 2013; Zhang *et al.*, 2006).

To understand or evaluate the observed saturation effect at high pressures, the quantification of the adsorption-desorption reaction rates is vital (Mühlen *et al.*, 1985). The degree of saturation also referred to as the occupancy or surface coverage can be used to explain the saturation effect on reaction rate because it describes the desorption of the intermediate surface complexes which has been also found to control the apparent reaction rate (Roberts & Harris, 2006; Wang & Bell, 2017). The degree of saturation can be quantified using an empirical method which is based on the char-gas reaction mechanism that is described by the LH expressions and temperature-programmed desorption (TPD) (Roberts & Harris, 2006). Based on the LH rate expression for the char-gas mechanism described in the Section 2.2.3 the degree of surface coverage which is the ratio of adsorbed surface complexes to the total concentration of active sites is given by Equation 2.5 for CO_2 and steam adsorption (Roberts & Harris, 2006):

$$\theta_{CO_2} = \frac{{k_1}/{k_3}\, p_{CO_2}}{1 + {k_1}/{k_3}\, p_{CO_2}} \; ; \theta_{H_2O} = \frac{{k_7}/{k_9}\, p_{H_2O}}{1 + {k_7}/{k_9}\, p_{H_2O}} \qquad (2.5)$$

Based on the observations by Roberts and Harris (2006) on Australian coal chars, the degree of saturation increased with the reactant pressure from 1-30 bar using both the TPD and LH expression method (Equation 2.5 and 2.6). These results correspond with the observed unaffected reaction rate at the CO_2 partial pressure range of 20-30 bar. This implies that at elevated reactant partial pressures, the reactive surface becomes more saturated with the surface complexes in such a way that a further increase in the reactant pressure will not significantly influence the reaction rate (Mühlen *et al.*, 1985; Roberts & Harris, 2006).

2.3.3 Reaction temperature

It has been reported that the reaction temperature has a large influence on char reactivity, whereby an increased reaction rate with temperature has been observed (Bai *et al.*, 2017; Everson *et al.*, 2006; Gomez & Mahinpey, 2015; Jayaraman *et al.*, 2015; Jayaraman *et al.*, 2017;

Porada *et al.*, 2017; Wang *et al.*, 2016). As the temperature is increased, the chemical reactions become faster resulting in an increased reaction rate (Smoot & Smith, 1985; Tanner & Bhattacharya, 2016). When the chemical reaction rate is controlling the overall gasification rate, the apparent activation energy of 200-292 kJ/mol at low and high pressures is observed (Everson *et al.*, 2006; Harris & Smith, 1991; Krishnamoorthy *et al.*, 2019; Roberts *et al.*, 2010). As the temperature increases, the apparent activation energy reduces to lower values in the order of less than 190 kJ/mol (Ahn *et al.*, 2001; Kim *et al.*, 2014). These results indicate that the overall gasification rate is influenced by mass transfer limitations (Roberts *et al.*, 2010).

2.4 Char structural development

A coal char particle is understood to consist of different sizes of pores of which the micropores (pore width < 2 nm) serve as the gas-solid reaction platform, while the mesopores (2 nm < pore width < 50 nm) and macropores (pore width > 50 nm) mainly serve as channels for transport of gaseous reactant also referred to as feeder pores (Fatehi & Bai, 2017; Kajitani *et al.*, 2002; Komarova *et al.*, 2015; Wang & Bhatia, 2001). The micropore or internal surface area of the coal char has been measured using different methods such as the adsorption-desorption, SEM (Scanning electron microscopy) and SAXS (Small-angle X-ray scattering) (Coetzee *et al.*, 2015; Jin *et al.*, 2018b; Pan *et al.*, 2016). However, it is challenging to quantify the specific surface area through the SEM technique due to its limitation to smaller pore size distributions (Wang *et al.*, 2015). The adsorption isotherms obtained at certain relative pressure range are interpreted through theoretical equations which include Langmuir, BET, D-A (Dubinin-Asthakov), D-R (Dubinin-Radushkevich), t-plot, and DFT (Density-functional theory) (Chang *et al.*, 2017; Jin *et al.*, 2018a; Kajitani *et al.*, 2002; Komarova *et al.*, 2015; Lowell *et al.*, 2012; Marsh, 1987). Amongst these interpretation methods, the D-R and D-A methods are normally used to describe the micropore surface area measured from CO_2 adsorption isotherms as compared to other methods (Burevski, 1982; Komarova *et al.*, 2015; Marsh, 1987).

2.4.1 Degree of conversion

During coal char gasification, the micropore surface area generally increases, and these developments on the physical coal char structure influence the char reactivity (Komarova *et al.*, 2015). The physical structural development during gasification involves the concept of the opening of closed pores, formation of micropores, development of micropores to mesopores and also coalescing or overlapping of micropores as the carbon is continuously consumed during the reaction (Bai *et al.*, 2018; Chang *et al.*, 2017; Fatehi & Bai, 2017; Liu *et al.*, 2015). The micropore surface area measured from CO_2 adsorption has been found to increase with an increase in conversion up to 40% because of the development of smaller pores into larger pores (Hurt *et al.*,

1991; Jin *et al.*, 2018a; Kajitani *et al.*, 2002; Krishnamoorthy *et al.*, 2019). This development of pores has also been observed at an early stage of conversion and more profound for steam gasification (Coetzee *et al.*, 2015; Huan *et al.*, 2019). Gouws *et al.* (2018) investigated the pore development of the coal chars gasified to conversions of 10 and 20% at constant pressures of up to 30 bar. It was found that the development of pores is also affected by the CO_2 partial pressure indicating a significant effect on micropore surface area and the discussion is provided in Section 2.4.2.

The changes in the char surface area with the degree of conversion is generally quantified by the Random-Pore Model (RPM) with the knowledge of the initial surface characteristics as described by Bhatia and Perlmutter (1980).

$$S = S_0\sqrt{1 - \psi ln(1 - X)} \tag{2.6}$$

Volume basis;

$$S_v = S_{v,0}(1 - X)\sqrt{1 - \psi ln(1 - X)} \tag{2.7}$$

where $S_{v,0}$ is the initial surface area per volume, S_0 is the initial surface area per mass and ψ is a structural parameter given by Equation 2.8.

$$\psi = \frac{4\pi L_0(1 - \varepsilon_0)}{S_0^2} \tag{2.8}$$

L_0 is the total length per unit volume, ϵ_0 is the initial porosity, and S_0 is the initial surface area. Although the structural parameter is theoretically related to the initial structural properties, it is often indirectly obtained by fitting the surface area development or reactivity data (Section 2.5.2) (Feng & Bhatia, 2003; Kajitani *et al.*, 2006). Kajitani *et al.* (2006) investigated the development of surface area measured from CO_2 adsorption analysis of two coal chars (PSD of about 40 µm) reacted to conversions of up to 85% and found a fitted ψ value of about 1 and 10 to well describe the measured surface areas. Feng and Bhatia (2003) evaluated the development of the surface area (obtained from CO_2 adsorption analysis) with a carbon conversion of 0-75% for the coal chars (PSD of < 200 µm) gasified in a CO_2 atmosphere and a ψ value of about 3. However, it was observed that the measured structural parameter from the initial pore properties is not in agreement with the fitted ψ value and this might be due to unaccounted pore development in the early stage, or inaccessibility of certain pores to the physical adsorption (Chi & Perlmutter, 1989; Feng & Bhatia, 2003; Ochoa *et al.*, 2001).

2.4.2 Reagent partial pressure

Despite the well-understood effect of degree of conversion on char surface development and char reactivity during gasification, the reactant partial pressure also plays a major role in the development of coal char structural properties. Few studies have been done on the evaluation of pore development with CO_2 partial pressure and to a less extent for steam gasification. Roberts and Harris (2007) gasified three coal chars to a conversion of 10% at 850 °C in the atmosphere of steam and CO_2. From the variation of steam and CO_2 partial pressure from 5-10 bar, it was observed that the micropore surface area measured using the CO_2 adsorption and D-R method slightly increase with CO_2 partial pressure and decreases with steam partial pressure. Similar observations were found by Gouws *et al.* (2018) from the evaluation of the effect of CO_2 partial pressure over a range of 0.1-9 bar on the gasified coal chars to a conversion of 10 and 20%. The observed development of micropore surface area with CO_2 partial pressure is associated with pore development (Gouws *et al.*, 2018). The pore volume in the micropore range increases with an increase in CO_2 partial pressure resulting in an increased micropore surface area (Gouws *et al.*, 2018; Howaniec, 2019). However, in this case, it was observed that the mesopore surface area was lower than the micropore surface area indicating the domination of micropores on the coal char surface.

2.5 Modelling char reactivity

Several models have been proposed to describe the coal char gasification behaviour and most commonly used models are structural and kinetic models. Structural models provide the predictions of changes in the coal char structure during gasification. The kinetic models such as the n^{th}-order (Power law) and LH type model are the most used models describing the intrinsic reaction rate of char-gas reactions at low and high pressures. These models are widely used to describe the influence of reagent partial pressure on the char reaction rate since they incorporate the partial pressure term in the rate expression (Tremel & Spliethoff, 2013).

2.5.1 Kinetic models

2.5.1.1 Power law (n^{th}-order) model

The n^{th}-order or power-law model has been utilised to represent the reaction rate in relation to the partial pressure and also to determine the kinetic parameters of char gasification at various temperatures and pressures with the incorporation of Arrhenius law. This model is described in Equation (2.9) and it is generally correlated to the specific reaction rate.

$$r_s = k_0 \exp\left(\frac{-E_a}{RT}\right) {p_i}^n \quad (2.9)$$

where p_i is the reagent partial pressure which can be steam or CO_2, n is the reaction order attributed to the effect of reagent partial pressure, k_0 is the pre-exponential factor, E_a is the apparent activation energy, T is the reaction temperature and R is the universal gas constant. At low pressures, it has been reported that the power-law rate equation can well describe the measured coal char reactivity (Everson *et al.*, 2008; Harris & Smith, 1991). Harris and Smith (1991) evaluated the intrinsic reactivity of brown coal chars in the atmosphere of steam and CO_2. The apparent reaction order was found to be about 0.6 for a steam partial pressure range of 0.1-0.3 atm and CO_2 partial pressure of 0.1-1.0 atm. These results are in agreement with the reported results by Everson *et al.* (2008) for a Highveld coal char gasified in the atmosphere of CO_2 at partial pressures of 0.6-2.875 bar. Similar apparent reaction orders of about 0.40-0.6 were found in high pressure studies (Ahn *et al.*, 2001; Gouws, 2017; Kajitani *et al.*, 2006; Roberts & Harris, 2006; Tremel & Spliethoff, 2013), however, the applicability of the power-law model to describe experimental data at high pressures has also been reported to be unsuitable (Blackwood & Ingeme, 1960; Kajitani *et al.*, 2006; Molina & Mondragon, 1998; Roberts & Harris, 2000; Roberts & Harris, 2006). This is due to the associated changes of reaction order at high pressures and also that the saturation effect is not encountered in the power law model (Kajitani *et al.*, 2006; Roberts & Harris, 2006). At high pressures, the apparent reaction order tends to approach zero due to the saturation of active sites which can be better explained and quantified using LH type models (Blackwood & Ingeme, 1960; Molina & Mondragon, 1998; Roberts & Harris, 2000).

2.5.1.2 LH reaction models

The Langmuir-Hinshelwood (LH) model has been developed from mechanistic principles in coal gasification (Botero *et al.*, 2013; Irfan *et al.*, 2011; Keller *et al.*, 2018; Wall *et al.*, 2002) as described in Section 2.2.3 and more applicable at high pressures (Gouws *et al.*, 2018; Kajitani *et al.*, 2013; Lee *et al.*, 2014b; Roberts & Harris, 2006; Tomaszewicz *et al.*, 2017). At controlled laboratory conditions, several authors have observed low concentrations of CO and H_2 formed during high pressure steam and CO_2 gasification of which had no significant effect on reaction rate (Gouws *et al.*, 2018; Keller *et al.*, 2018; Krishnamoorthy *et al.*, 2019; Liu *et al.*, 2017; Roberts & Harris, 2006; Saito *et al.*, 2017; Tomaszewicz *et al.*, 2017; Tremel & Spliethoff, 2013; Wang & Bell, 2017). Under these conditions, the LH rate expression given in Equation 2.1 and 2.3 is simplified to the LH model shown in Equation 2.10.

$$r_{CO_2} = \frac{[C_t]k_1 p_{CO_2}}{1 + {}^{k_1}/_{k_3}\, p_{CO_2}} \;;\; r_{H_2O} = \frac{[C_t]k_7 p_{H_2O}}{1 + {}^{k_7}/_{k_9}\, p_{H_2O}} \qquad (2.10)$$

Gouws (2017) investigated the effect of CO_2 partial pressure over a range of 0.1-9 bar on specific reaction rate for three coal chars at different temperatures. From the measured coal char reactivity, the LH kinetic parameters were obtained and the $[C_t]k_1$ term was found to be in the range of 0.29-3.30 (1/bar.s x 10^5) and k_1/k_3 of 0.24-0.70 (1/bar). Similar results have been reported by Roberts and Harris (2006) over a CO_2 partial pressure range of 1-30 bar for three gasified coal chars. From the investigations of the effect of steam partial pressure over a range of 1-30 bar and the use of the LH model, Roberts and Harris (2006) found the $[C_t]k_1$ term to vary from 0.87-9.20 (1/bar.s x 10^5) with k_1/k_3 value of 0.24-0.70 (1/bar). These results are in agreement to the results obtained by Saito *et al.* (2017) who evaluated the effect of steam partial pressure on coal char reactivity at a total pressure of 30 bar. The LH kinetic parameters associated with the $[C_t]k_1$ and k_1/k_3 terms are determined from the measured specific reaction rate at carbon conversions of about 10% or lower of which is inferred to as the initial char reactivity (Gouws *et al.*, 2018; Liu *et al.*, 2017; Roberts & Harris, 2006; Saito *et al.*, 2017). These kinetic parameters are influenced by the reaction temperature, changes in char surface structure and pressure (Ergun, 1956; Gouws, 2017; Roberts & Harris, 2006; Wang & Bell, 2017).

The LH rate expressions are more applicable in describing the dependency of char reactivity on reagent partial pressure as compared to the n^{th}-order rate model, particularly at elevated pressures (Botero *et al.*, 2013; Irfan *et al.*, 2011; Keller *et al.*, 2018; Roberts & Harris, 2006). This is because the LH reaction rates can describe the reaction rates with regards to the surface saturation by surface complexes and the inhibition effects thereof (Botero *et al.*, 2013; Irfan *et al.*, 2011; Tomaszewicz *et al.*, 2017; Tremel & Spliethoff, 2013).

2.5.2 Structural models

Several structural models such as the Volumetric model (VM), Grain model (GM) or Shrinking-core model (SCM), and Random-Pore Model (RPM) have been widely used to model the char reactivity data. The VM and SCM are more preferred for describing the relations of char conversion and time (Chen *et al.*, 2013; Molina & Mondragon, 1998). However, it has been observed that the RPM is the most practical model in describing the char reactivity due to incorporation of the changes in char surface area that are associated with pore development and coalescence during char conversion (Bhatia & Perlmutter, 1980; Duman *et al.*, 2014; Kabir *et al.*, 2016; Kajitani *et al.*, 2002; Keller *et al.*, 2018; Liu *et al.*, 2017; Morin *et al.*, 2017; Porada *et al.*, 2017; Wang *et al.*, 2015). The most commonly used expression of the RPM was derived by Bhatia

and Perlmutter (1980) and has been found to describe the experimental data obtained in the chemical-controlled regime and isothermal conditions accurately (Jayaraman & Gokalp, 2015; Kabir *et al.*, 2016; Kajitani *et al.*, 2002; Keller *et al.*, 2018; Molina & Mondragon, 1998; Porada *et al.*, 2017; Tomaszewicz *et al.*, 2017; Wang & Bell, 2017).

$$\frac{dX}{dt} = k_p(1-X)\sqrt{1-\psi ln(1-X)} \tag{2.11}$$

This equation can also be expressed in terms of specific reaction rate as shown in Equation 2.12.

$$r_s = \frac{dX}{dt}\Big/_{(1-X)} = r_{s,0}\sqrt{1-\psi ln(1-X)} \tag{2.12}$$

where $r_{s,0}$ is the initial specific reaction rate ascribed to the initial char structural properties as shown in Equation 2.13.

$$r_{s,0} = \frac{k_s S_0}{(1-\varepsilon_0)} \tag{2.13}$$

The structural parameter can be obtained by means of measuring the pore structural properties, however, it has been widely used as a fitting parameter (Fatehi & Bai, 2017; Kabir *et al.*, 2016; Kajitani *et al.*, 2002; Liu *et al.*, 2017; Wang & Bell, 2017). From the measured conversion-time profiles, a structural parameter ranging from 0.7-6.3 has been observed by several authors (Everson *et al.*, 2008; Kabir *et al.*, 2016; Tomaszewicz *et al.*, 2017) and found to be dependent on reagent gas (Kajitani *et al.*, 2002) and less on temperature (Everson *et al.*, 2008; Tomaszewicz *et al.*, 2017). Kajitani *et al.* (2002) found ψ values ranging from 3-130 from the fitting of the reaction rate data. The larger ψ value indicates that the development of pores during coal char gasification is more significant (Kajitani *et al.*, 2002; Wang & Bell, 2017). Although the RPM model has been found to model the char reactivity well, it has been reported by Kajitani *et al.* (2002) that the structural parameter obtained from the initial pore properties (Equation 2.8) and surface area (expressed in Equation 2.6) cannot describe the reaction rate well. That is, the ψ value determined from the fitting of surface area and reaction rate is not the same due to onset pore development that is not incorporated when ψ is assumed to remain constant during coal char conversion, and therefore the improvement of the Random-Pore Model has to be considered (Bhatia & Vartak, 1996; Kajitani *et al.*, 2002).

2.6 Summary

Coal gasification is a vital process for the conversion of coal to liquid fuels which is undertaken in a typical gasifier operating at high temperatures and pressures using steam and oxygen as gasifying reagents. Amongst the processes occurring during coal gasification, the heterogeneous gas-solid reactions (char-steam and char-CO_2 reactions) in the gasification stage takes place at a slower rate and hence, controls the overall gasification rate. Several studies have been conducted to understand the reaction kinetics of these reactions and the effects thereof at different reaction regimes. However, only limited studies have been done at high pressures and little of them relates the development of reactant partial pressure to the development of coal char surface area and intrinsic reaction rate ($g/m^2/s$). Incorporation of the pore development to the apparent reaction rate measured under chemical-controlled regime has not been evaluated extensively and this provides reaction rate that is less dependent on the development of the surface area and mass transfer limitations suitable for the development of gasification models.

The influence of temperature and its kinetic parameters for coal char gasification have been widely reported. The surface area of the coal chars reacted in the atmosphere of steam and CO_2 indicated some pore development as the reactions proceed to conversions of 40-50%, however, the results have been widely reported at low pressures. From the obtained results, it has been observed that the reactant partial pressure has a significant effect on the gasification rate and also on the surface area development. The reaction rate was observed to increase significantly with an increase in reactant partial pressure up to 20 bar with reaction orders of about 0.4-0.6. At high pressures above 20 bar, the effects of reactant partial pressure were found to be less significant on the gasification rate due to the saturation of the active sites available for reaction. The development of pore structure has been well described by the existing models such as the Random-Pore Model (RPM) which is associated with the changes in the char structural characteristics with the degree of conversion and the effects of reactant partial pressure have not yet been incorporated. Other models such as the Power law) model and Langmuir-Hinshelwood (LH) rate type model have been commonly used to describe the effects of the reactant partial pressure on gasification rate but some limitations in terms of applicability have been observed. The LH model has been found to model the experimental data at high pressures well while the n^{th}-order model was more suitable at low pressures.

Chapter 3

(COAL AND CHAR CHARACTERISATION)

CHAPTER 3

(COAL AND CHAR CHARACTERISATION)

3.1 Introduction

Coal properties and coal char generation have a large influence on coal char gasification kinetics. The assessment of these properties such as mineralogical, chemical, and physical properties is essential and provides insight into the thermal and reactivity behaviour of particular coal.

This chapter is divided into sections that address the origin and characteristics of the coal and coal char together with the preparation techniques. Section **3.2** provides the background on the origin and type of coal. Section **3.3** discusses the preparation techniques and conditions that were used to generate the coal char sample. Section **3.4** describes the analyses methods used to characterise relevant properties of the coal and char samples. Section **3.5** and **3.6** provide the results and discussions including a summary of the characterised coal and char properties.

3.2 Coal sample and origin

A South African coal from the Highveld coalfield is used. The coal has no swelling and caking propensity and is rich in inertinite. This coal has similar characteristics as typical coal used in a commercial gasifier (van Dyk *et al.*, 2006), hence suitable for CTL technology. For confidentiality reasons, the coal colliery is not disclosed.

3.3 Coal and char preparation

3.3.1 Coal preparation

A 10 kg coal sample was obtained in lump size (-60+5 mm) and subjected to mechanical size reduction methods to obtain the desired particle size distribution (PSD). Figure 3-1 illustrates the subsequent steps that were followed in the preparation process.

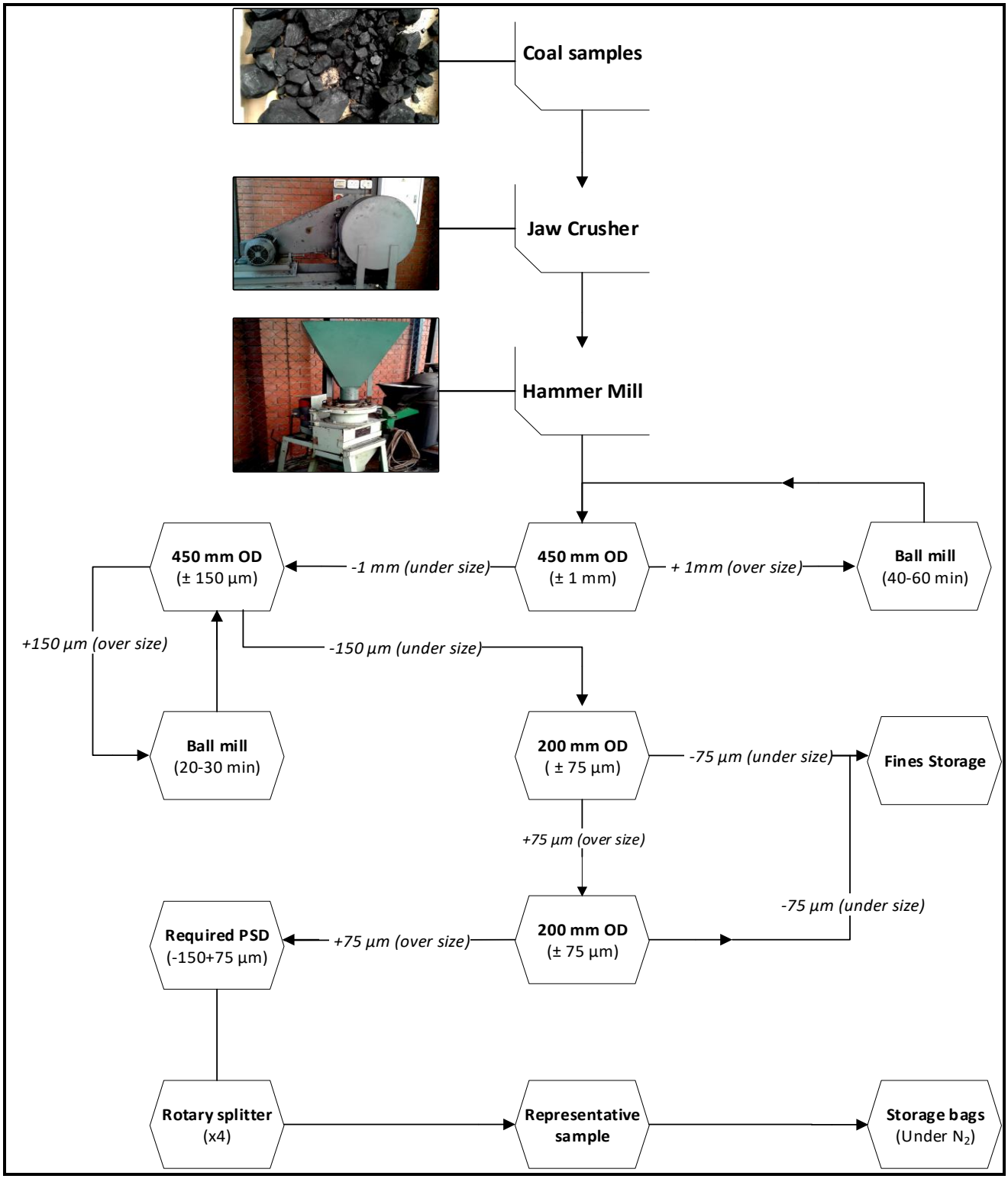

Figure 3-1: Coal sample preparation

The bulk sample of the coal was air-dried for 48 hours and subjected to particle size reduction. The air-dried sample was crushed in batches by making use of an in-house jaw crusher followed by a hammer mill to reduce the lump coal to a particle size range less than 2 mm. Coal fractions above 1 mm aperture size were further ground using a lab-scale ball mill containing ceramic balls.

The liberated coal was sieved using a series of laboratory sieves to obtain a bulk coal sample with a particle size range of -150+75 µm.

A representative sample of the bulk was obtained from the liberated coal using sample division methods as prescribed by Wills and Finch (2015). In this case, a rotary sample splitter was used because of its efficiency to split and handle granular or powdered material (Wills & Finch, 2015). Batches of coal (about 3.5 kg) were fed into the rotary splitter and continually divided into 6 sub-samples at a constant controlled feed rate (~50 g/min). The sub-samples were intermixed and the sample splitting was repeated to obtain 12 representative samples of about 150 g. These samples were packed in sealable bags and flushed with nitrogen gas and stored in a refrigerator.

3.3.2 Char preparation/generation

The prepared coal samples were used to produce batches of char samples for the gasification experiments. The char preparation was conducted with an in-house atmospheric pyrolysis rig.

3.3.2.1 Charring setup and description

Figure 3-2 illustrates the pyrolysis setup consisting of a horizontal tube furnace and a gas inlet stream. The horizontal tube furnace (Lenton®, TMH16/75/610) comprises of a 130 cm tube with an inside diameter (I/D) of 100 mm. A ceramic sample-boat with a length of 270 mm and a width of 35 mm was used as a sample holder with a capacity of 200 g of pulverised coal.

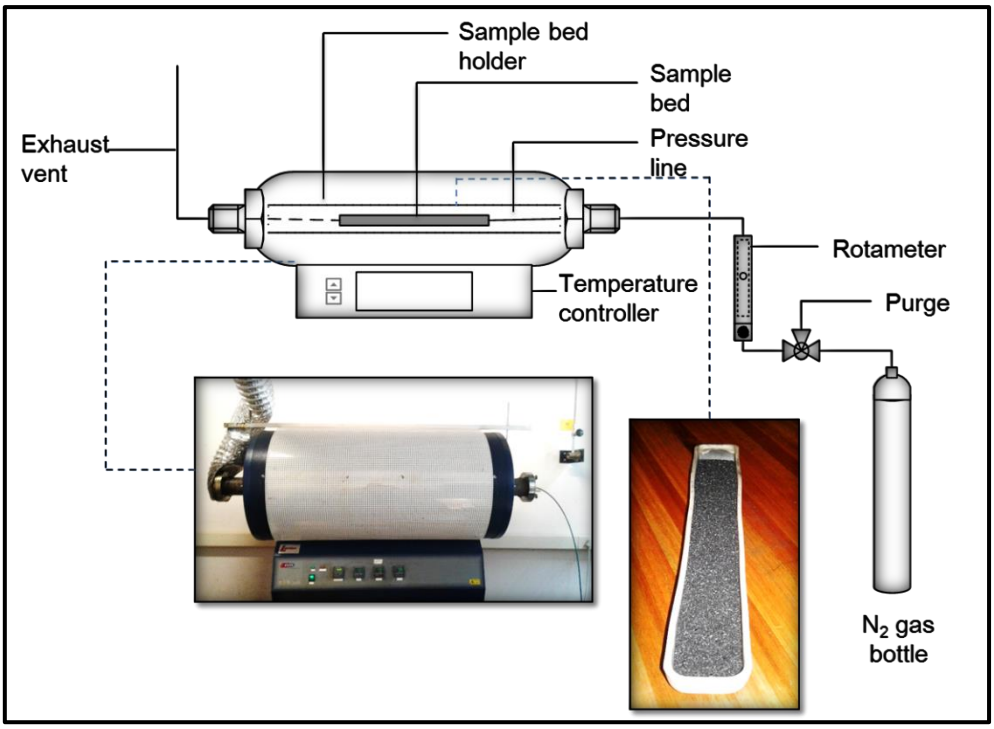

Figure 3-2: Coal pyrolysis setup

The furnace comprises of three-heating zones which are controlled through set-point retransmission. It provides operating temperatures up to 1600 °C and heating rates up to 15 °C/min.

3.3.2.2 Procedure and operation

Batches of coal were pre-dried at a temperature of 80 °C for 4 hours. Pyrolysis experiments were carried out at non-isothermal conditions to a temperature of 950 °C in an N_2 atmosphere (purity > 99.999%). A sample holder containing 150 g (±4 g) was placed within the determined isothermal heating zone (see Appendix A.2.1) and heated at a rate of 10 °C/min to the pyrolysis temperature and held for 30 minutes similar to the pyrolysis conditions in a typical gasifier (Bunt, 2006). The furnace was allowed to cool down to room temperature at a natural cooling rate, and the produced char samples were retrieved and stored in zip-lock bags for further experimental work and characterisation.

The pyrolysis conditions that were used to generate the coal chars are summarised in Table 3-1. These conditions were selected to significantly devolatilise similar coal resulting in the formation of porous coal char (Everson *et al.*, 2008) and the temperature used is similar to the reaction zone in a typical gasification process (Gräbner, 2014; van Dyk *et al.*, 2006).

Table 3-1: Charring operational conditions

Variable/Property	Conditions
Mass per batch	±150 g
Temperature	950 °C
Pressure	~87.5 kPa
Heating rate	10 °C/min
Hold time	30 min
N_2 flow rate	1.2 NL/min

3.4 Characterisation analyses

Chemical, mineralogical and petrographic properties were carried out at external laboratories (Bureaus Veritas) for the prepared coal and generated char samples. Analysis of the structural properties was conducted in-house on the reacted and unreacted coal chars. Table 3-2 summarises the characterisation analyses that were conducted including the standards that were applied.

Table 3-2: Summary of characterisation analyses and standards

Parameter/property	Standard Method	Laboratory
	Proximate analysis	**(Bureaus Veritas)**
Inherent moisture (wt%)	ISO 11722: 2013 (SANS 11722, 2017)	
Ash yield (wt%)	ISO 1171: 2010 (SANS 131, 2011)	
Volatile matter (wt%)	ISO 562: 2010 (SANS 50, 2011)	
Fixed carbon (wt%)	By difference	
	Ultimate analysis	**(Bureaus Veritas)**
Carbon (wt%)	ISO 29541: 2010 (SANS 29541, 2014)	
Nitrogen (wt%)	ISO 29541: 2010 (SANS 29541, 2014)	
Hydrogen (wt%)	ISO 29541: 2010 (SANS 29541, 2014)	
Oxygen (wt%)	By difference	
Total sulphur (IR Spectroscopy (%))	ISO 19579: 2007 (SANS 19579, 2007)	
	Gross calorific value	**(Bureaus Veritas)**
CV (MJ/kg)	ISO 1928: 2009 (SANS 1928, 2009)	
	Mineralogical analysis	**(Bureaus Veritas)**
Ash composition (XRF)	ASTM D4326	
	Petrographic analysis	**(Bureaus Veritas)**
Maceral composition (Vol,%)	ISO 7404-3: 2009 (SANS, 2016)	
Rank	ISO 11760: 2005 (SANS 11760, 2007)	
	Surface area analysis	**(NWU)**
Micropore surface area (m^2/g)	Dubinin-Astakhov (D-A) method	

- **Chemical and mineralogical properties**

The chemical properties and ash composition were analysed using proximate, ultimate and XRF analysis methods.

- **Petrographic properties**

The petrographic analysis was only done on the parent coal to provide the maceral composition and the classification of coal in terms of rank.

- **Structural properties: surface area analysis**

The surface area measurements were conducted using a Micrometrics surface and porosity analyser (ASAP 2020). In this study, the focus was on the micropore surface area and this was analysed using CO_2 adsorption isotherms and the Dubinin-Astakhov (D-A) method (Burevski, 1982; Kajitani *et al.*, 2002; Komarova *et al.*, 2015; Marsh, 1987; Tomaszewicz *et al.*, 2017). The CO_2 adsorption isotherms were measured at a temperature of 273 K and relative pressure (P/P_0) range between 0 and 0.035. The char samples (~200 mg) were initially dried at a temperature of 105 °C for 4 hours. Furthermore, the chars were degassed in a vacuum (10 µmHg) at a temperature of 380 °C for 24 hours.

3.5 Results and discussion

3.5.1 Chemical properties

The proximate, ultimate analysis and gross calorific value (CV) results of the parent coal and the produced char sample are presented in Table 3-3.

Table 3-3: Summary of the chemical properties and energy content results of the parent coal and char

Parameter	Parent coal			Coal char		
	adb	*db*	*daf*	*adb*	*db*	*daf*
Proximate analysis						
Inherent moisture (wt%)	2.5	-	-	0.7	-	-
Ash yield (wt%)	29.8	30.6	-	38.0	38.3	-
Volatile matter (wt%)	21.3	21.8	14.4	1.1	1.1	0.7
Fixed carbon (wt%)	46.4	47.6	85.6	60.2	60.6	99.3
Ultimate analysis						
Carbon (wt%)	53.1	54.5	78.4	58.7	59.1	95.8
Hydrogen (wt%)	3.0	3.1	4.5	0.4	0.4	0.7
Nitrogen (wt%)	1.4	1.4	2.0	1.1	1.1	1.8
Oxygen (wt%)	9.1	9.3	13.4	-	-	-
Total Sulphur (wt%)	1.2	1.2	1.7	1.0	1.0	1.7
Gross calorific value						
CV (MJ/kg)	20.7			17.6		

adb – air-dry basis, *db* – dry basis, *daf* – dry-ash free basis

As shown in Table 3-3, the inherent moisture and volatile matter results of the coal char sample are significantly less as compared to the parent coal. The char sample consists of traces of volatile matter with little inherent moisture; these results correspond to the volatiles that were driven off during coal pyrolysis (see Appendix D.1). After coal pyrolysis, it was also found that the carbon content increased from the preparation of coal to coal char. Similar observations have generally been observed in literature and the results are in agreement with other reported results of Highveld coal derived chars (Everson *et al.*, 2008; Gouws *et al.*, 2018; Hattingh *et al.*, 2011). The parent coal properties based on the ash yield (> 19 wt%, *adb*) and volatile matter (14-22 wt%, *adb*) indicate that the coal sample is a high-ash and low-volatile coal (ISO 1171, 2010; ISO 11760, 2005).

3.5.2 Ash composition (XRF)

Table 3-4 shows a summary of the XRF results (on wt%) reported on loss of ignition (LOI) free basis.

Table 3-4: Ash composition results of the coal sample

Elemental component	**wt%**
Al_2O_3	28.1
CaO	7.5
Fe_2O_3	4.6
K_2O	0.6
MgO	1.7
Na_2O	0.1
P_2O_5	0.6
SiO_2	50.3
TiO_2	1.5
ZrO_2	0.1
BaO	0.2
SrO	0.2
SO_3	4.3
Other	0.2
Total (wt%)	**100**
Alkali Index (-)	**5.5**

The ash composition was found to be rich in Si and Al containing elements and these results are in accordance with results reported by several authors for bituminous high-ash coals (Gräbner,

2014; Hattingh *et al.*, 2011; Kajitani *et al.*, 2006; Porada *et al.*, 2017; Zou *et al.*, 2018). A high content of Si and Al containing elements indicate that the ash of the parent coal constitutes a high amount of mineral grains of quartz and kaolinite (Porada *et al.*, 2017; Zhang *et al.*, 2015), which has been observed for similar coals (Hattingh *et al.*, 2011).

3.5.3 Petrographic properties

3.5.3.1 Vitrinite reflectance

The mean maximum (RoV max) and random vitrinite (RoV random) reflectance were determined with the standard deviation of 0.10%. The results obtained, which illustrate the vitrinite reflectance V-class distribution, are summarised in Table 3-5.

Table 3-5: Vitrinite reflectance distribution

Vitrinite reflectance distribution	Random vitrinite reflectance (Rr) distribution (%)
V4 (0.40 – 0.49)	0
V5 (0.50 – 0.59)	15
V6 (0.60 – 0.69)	34
V7 (0.70 – 0.79)	30
V8 (0.80 – 0.89)	14
V9 (0.90 – 0.99)	7
V10 (1.00 – 1.09)	0
RoV max	**0.71**
RoV random	**0.66**

As shown in Table 3-5, the vitrinite reflectance distribution measurements which account for about one-third fell into the V-class 6. The mean random vitrinite reflectance in this V-class range was found to be 0.66%; these results show that the sample is a bituminous – medium rank C coal (ISO 11760, 2005), which is very typical for Highveld coals (Everson *et al.*, 2008; Gouws *et al.*, 2018; Hattingh *et al.*, 2011).

3.5.3.2 Maceral composition

The maceral composition results of the coal are presented in Table 3-6. The parent coal was found to be rich in inertinite and consists of traces of liptinite. Within the inertinite macerals, reactive and inert semifusinite account for 90% of the total inertinite macerals with inert

semifusinite dominating. The dominance of inert semifusinite as compared to the reactive semifusinite was also found in the characterisation of similar coals (Hattingh *et al.*, 2013; Okolo *et al.*, 2015b; Roberts *et al.*, 2015).

Table 3-6: Coal Maceral composition results

Maceral/parameter	Coal sample	
	(*mmb*)	(*mmfb*)
Vitrinite (vol.%)	14.2	17.1
Liptinite (vol.%)	1.3	1.6
Inertinite (vol.%)	67.7	81.4
Reactive semifusinite	22.4	26.9
Inert semifusinite	38.6	46.4
Fusinite + secretinite	6.7	8.1
Total reactives (vol.%)	37.9	45.6
Mineral matter (vol.%)	16.8	-

3.5.4 Surface area analysis

Table 3-7 summaries the results of the coal char surface area analyses.

Table 3-7: Summary of char structural properties

Parameter	Method/technique	Char sample	
		(*db*)	(*daf*)
Micropore SA (m^2/g)	D-A method	154	249
Monolayer capacity (cm^3/g)	D-R method	34	54
Average micropore diameter (Å)	H-K method	3.7	-

SA – surface area; *db* – dry basis; *daf* – dry ash-free basis

The average micropore diameter of the char sample was found to be less than 20 nm and therefore, the char surface area is dominated by the micropores ((Sing, 1985; Speight, 2012)). The characteristics of these pores can be related to the internal surface area which serves as the reaction platform for gasification reactions. The micropore surface area determined from the D-A method is in the range of the unreacted coal chars investigated by several authors on Highveld coal chars (Coetzee *et al.*, 2015; Gouws *et al.*, 2018; Okolo *et al.*, 2015a).

3.6 Summary

Characterisation analyses were conducted on the parent coal and the prepared char sample following ISO/ASTM standards. Table 3-8 shows a summary of the coal and char characterisation results.

Table 3-8: Summary of the conventional coal and char characterisation results

Parameter/property	Parent coal	Coal char
	Proximate analysis (wt%-db)	
Ash yield	30.6	38.3
Volatile matter	21.8	1.1
Fixed carbon	47.6	60.6
	Ultimate analysis (wt%-daf)	
Carbon	78.4	95.8
Nitrogen	4.5	0.7
Hydrogen	2.0	1.8
Oxygen	13.4	0.0
Total sulphur	1.2	1.7
	Gross calorific value (MJ/kg-adb)	
CV	20.7	17.6
	Maceral composition (vol.%-mmfb)	
Total Vitrinite	17.1	ND
Total Liptinite	1.6	ND
Total Inertinite	81.4	ND
Total Reactives	45.6	ND
	Vitrinite reflectance	
Reflectance (%)	0.66	ND
Rank (Bituminous)	Medium C	ND
	Micropore surface area (m^2/g-daf)	
D-A method	ND	257

ND – not determined; *db* – dry basis; *daf* – dry ash-free basis; *mmfb* – mineral matter-free basis

The parent coal was found to be a medium rank C bituminous coal and classified as a high-ash and low-volatile coal, rich in mineral grains of quartz. From the maceral composition, it was found that the parent coal is rich in inertinite in which inert semifusinite dominants. The volatile and moisture contents after pyrolysis were found to be consistent with the volatiles driven off during the coal char preparations.

Chapter 4

(EXPERIMENTAL METHODS)

CHAPTER 4

(EXPERIMENTAL METHODS: GASIFICATION EXPERIMENTS)

4.1 Introduction

A Highveld coal char sample (-150+75 µm), which was prepared with the methods discussed in Section 3.3, was used for steam and CO_2 gasification experiments. This chapter discusses the high-pressure fixed bed reactor (HPFBR) used for determining char gasification rates with steam and CO_2 from the carbon-based product gas analysis. The experimental rig was previously used by Gouws *et al.* (2018) to conduct CO_2 gasification experiments at pressures of up to 30 bar. To perform steam gasification experiments, the rig was modified to feed a high pressure steam and water removal downstream the reactor. Section **4.2** describes the materials used for conducting the experiments and Section **4.3** provides detail on the experimental rig. Section **4.4** discusses the experimental procedure followed to obtain the experimental data. Section **4.5** describes the mathematical expressions to determine char reactivity and kinetic parameters. Section **4.6** discusses the manner at which the experimental data is processed and the evaluation of carbon balance. Section **4.7** provides the results and discussions on the identification of the chemical-controlled regime. The experimental uncertainties with regards to the measurements of char reactivity and micropore surface area are quantified and discussed in Section **4.8**. In Section **4.9**, a summary of the chapter is provided including the experimental plan and conditions.

4.2 Materials used

Table 4-1 shows a summary of the materials used which include coal char, the reactants, gases, and the moisture adsorbent.

Table 4-1: Summary of the materials used

Substance	Specification/purity	Supplier
Coal char	Table 3-8	-
CO_2	> 99.9%	Afrox®
N_2	> 99.999%	Afrox®
CO calibration gas	2800 and 1450 ppm	Afrox®
CO_2 calibration gas	1900 and 1050 ppm	Afrox®
De-ionized water	Ultra-high purity	Immuno-Vet Services®
3Å molecular sieves	-	Sigma-Aldrich®

4.2.1 Gases

Instrument grade N_2 and CO_2 were used to perform CO_2 gasification experiments. N_2 was used as a balanced reagent gas for both steam and CO_2 experiments and also used as an inert atmosphere during the heating of the coal char sample to the desired reaction temperature. Prior to the gasification experiments, mixtures of CO and CO_2 balanced with N_2 were used to calibrate the gas analysers (see Appendix B.5).

4.2.2 Moisture trap

A moisture trap (desiccant) was built in-house and a UOP type 3Å molecular sieve (3.2 mm pellets) was used as a moisture adsorbent to ensure the removal of moisture downstream the water condenser. The application of this material was chosen based on its capability to adsorb moisture without removal of product gases such as CO_2, CH_4, H_2, CO, and other hydrocarbons (Farag *et al.*, 2011).

4.3 Experimental setup and description

A High Pressure Fixed Bed Reactor (HPFBR) rig was commissioned in-house for conducting low and high pressure steam/CO_2 gasification experiments of fine coal char particles (-1000+75 µm). Figure 4-1 illustrates a schematic presentation of the experimental setup and a detail description is presented in Appendix A.1.

The experimental rig is equipped with several facilities and consists of a vertical split furnace (temperatures up to 1200 °C) that provide the required heat for the endothermic gasification reactions. This furnace is used to heat a C267 alloy pipe, which consists of a porous quartz frit (nominal pore size of -40+15 µm) mounted to a flange at the centre of the pipe. The heated length of the pipe is about 40 cm at the centre with an isothermal zone of 5 cm (Gouws, 2017). The reaction temperature inside the pipe is monitored by a K-type thermocouple located 5 mm above the sample bed. The feed to the pipe consists of N_2, CO_2 and steam (from the steam generation unit) lines which are introduced at the top. The N_2 and CO_2 gas were stored in the standard gas cylinders and the inlet conditions were controlled by two-staged regulators (gauge pressure of 0-52 bar) and mass flow controllers (MFC) (calibration provided in Appendix B.1.1 and B.1.2). The steam is generated by pumping de-ionised water from the water reservoir through stainless steel coils, which are heated to a temperature of 360 °C (±12 °C).

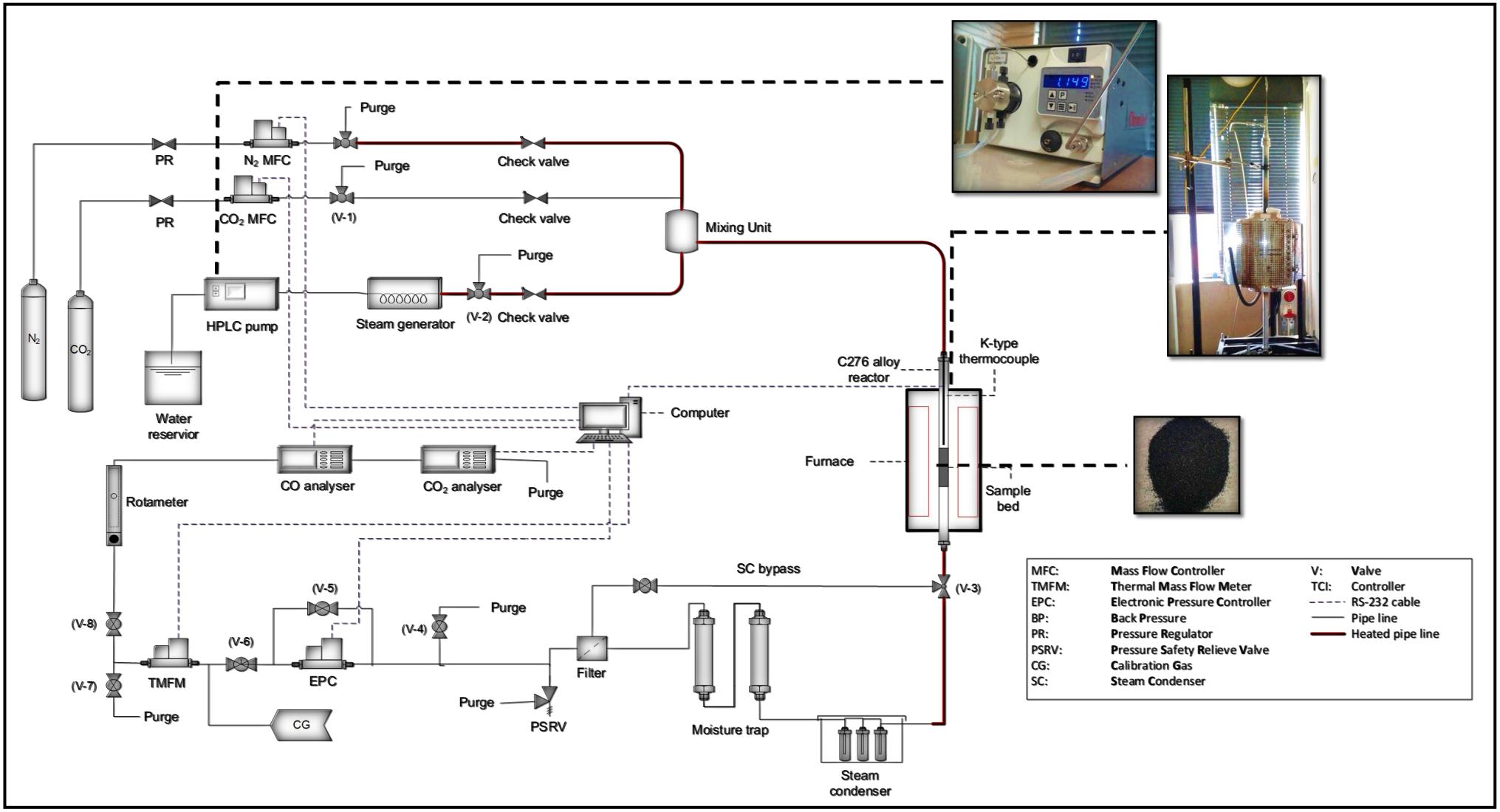

Figure 4-1: Schematic of the experimental setup

The steam generation unit comprises of a water pre-heater, de-ionised water reservoir (5 L storage capacity) and HPLC pump (flow calibration provided in Appendix B.3). The steam pre-heater is equipped with cartridge heaters mounted through an aluminium round bar and stainless steel coils (1/8” pipe) connected to the pump.

The gas feed line to the reactor (upstream) is pre-heated at a maintained temperature of 320 °C using heating tapes. The temperature is monitored using a K-type thermocouple. At the outlet of the reactor, the product gas line comprises of a water removal unit (water condenser and trap), electronic pressure controller (EPC) and gas analysers. The water removal unit consists of moisture traps and an ice-water bath system constructed in-house, which is capable of condensing about 2 L of water. Before the water removal unit, the product gas line is pre-heated at a maintained temperature of 250 °C and monitored using a K-type thermocouple. The pre-heated upstream and downstream of the reactor are insulated.

After the water removal unit downstream the reactor, an EPC is installed to maintain constant total system pressure. The EPC is capable of regulating and maintaining pressures up to 80 bar, which is measured at the upstream using a pressure transmitter. A thermal mass flow meter (TMFM) is used to measure the total gas flow rate going through the EPC to the gas analysers. The gas analysers consist of non-dispersive infra-red (NDIR) sensors, which operate at a maximum flow rate of 1 NL/min. The total flow rate going to the analysers can be adjusted through the downstream purge that is equipped with a rotameter (calibration profile provided in Appendix B.2) and purge valve (V-7 in Figure 4-1). The experimental rig can be operated at total pressure and flow rate up to 50 bar and 5 NL/min, respectively.

The operational conditions which include the total pressure (see Appendix A.2.3), the temperature in the reaction zone and steam generation unit (see Appendix A.2.2) are monitored and logged into a computer using RS232 communication. Similarly, the concentrations of CO and CO_2 are also continuously logged into the computer at intervals of 2 s. Table 4-2 shows a specification summary of the major equipment used.

Table 4-2: Summary of the equipment used

Equipment	Description/model	Range/ precision
Furnace	Carbolite® VST 12/100/200	Ambient to 1200 °C
Reactor pipe	Multi-alloys® C276 alloy	Ambient up to 120 bar and 1000 °C
Cartridge heaters	Thermon SA® cartridge elements	Ambient to 450 °C
Heating tapes	Hi-tech elements®	Ambient to 300 and 400 °C
HPLC pump	Chrome-tech® LS-Class pump	Flow rate of 0.000-4.999 ml/min. Pressure of ambient to 49 MPa
CO analyser	ADC® MGA3000 analyser	NDIR: 50-5000 ppm
CO_2 analyser	ADC® MGA3000 analyser	NDIR: 200-40000 ppm
EPC	Bronkhorst® type El-Press	Ambient to 80 bar
Pressure transmitter	Wika® Unitrans	Ambient up to 120 bar
N_2 MFC	Bronkhorst® type El-Flow	0.000-5.000 NL/min
CO_2 MFC	Bronkhorst® type El-Flow	0.000-0.750 NL/min
TMFM	Bronkhorst® type El-Flow	0-2.0 NL/min

4.4 Experimental procedures

4.4.1 Char-CO_2 gasification

To conduct CO_2 gasification experiments, the CO analyser was only used and the steam condensation system was by-passed (Valve V-3). A char sample of approximately 0.50 g was weighed using a Mettler Toledo laboratory scale (Microsep®, MS-TS analytical balance) and inserted onto the quartz frit placed in the reactor. The furnace was pre-heated to the desired reaction temperature and enclosed around a reactor. The reaction temperature was monitored using a thermocouple placed inside the reactor. Meanwhile, N_2 was allowed to flow through the experimental rig during the pre-heating of the sample at the desired flow rate and also for 60 minutes after the reaction temperature had stabilised.

After reaching isothermal conditions and constant flow, the rig was pressurised to the desired system (total) pressure with N_2 controlled by the EPC. The N_2 pressure was regulated using a two-stage regulator and set to a pressure that is 4 bar above the desired total pressure. When this pressure was reached, the CO_2 flow rate and pressure were set and CO_2 was introduced into the reactor. The data logging of reaction temperature, total pressure and CO concentration were then started. The char gasification runs were conducted at various times, depending on the acquired char conversion. After completion, the data-logging and CO_2 flow rate were stopped and

N_2 was left running while dislocating the furnace and depressurising the rig. This allowed the converted chars to be flushed with N_2 while the reactor was cooled to ambient conditions. When the reactor reached ambient pressure and temperature, the N_2 flow was stopped and the reacted char was collected.

4.4.2 Char-Steam gasification

The steam gasification experiments were performed in a similar manner as the CO_2 gasification experiments but in this case, CO_2 measurements and water removal were incorporated. A char sample of about 0.5 g was prepared and placed into the reactor. The N_2 flow rate and pressure were set accordingly and introduced into the reactor. The upstream and downstream lines the reactor were pre-heated at the maintained temperature. Thereafter, the sample was preheated to the reaction temperature in the N_2 atmosphere until the isothermal conditions were reached and the rig was pressurised. During the sample pre-heating and rig pressurisation, the steam generation and water removal unit (steam condenser) were prepared. The steam generation unit was pre-heated to a temperature of 360 °C (±12 °C) and water was fed at the desired flow rate (obtained from Appendix B.3 and B.4) and purged. The steam was purged until the reaction conditions were met and this allowed a time for the steam flow rate and temperature to stabilise.

As the acquired total pressure and temperature stabilises, the data logging was started, and then steam was directed into the reactor (V-2). The steam discharge pressure and flow rate are set on the HPLC pump. After completion of an experiment, the steam flow rate and data logging were stopped while the N_2 remained flowing. The condensers were firstly depressurised through the drain system in order to collect condensed water. Thereafter, the experimental rig was fully depressurised and the furnace was dislocated from the reactor. When the reactor reached ambient temperature and pressure, the N_2 flow was stopped and the reacted chars were collected and stored accordingly.

4.5 Determination of char reactivity and modelling

In order to evaluate the char reactivity and kinetics, the reaction rate of char gasification in the atmosphere of steam and CO_2 was determined. This was done by determining the carbon conversion from the carbon-based product gas analysis.

4.5.1 Carbon conversion measurements

The measurements of the carbon conversion for the char gasification experiments were based on the reaction stoichiometry of carbon-containing product gas(es) and the use of ideal gas law due to concentration profiles measured at ambient conditions. Because of the insignificant

formation of methane (evaluated through carbon mass balance), the carbon was determined from the CO and CO_2 concentrations only. Equation 4.1 (char-CO_2) and 4.2 (char-steam) show the mathematical expressions used for determining the carbon conversion and detailed procedures are discussed in Appendix C.1.

Char-CO_2 gasification:

$$X_{C,CO_2} = \frac{\Delta n_{CO} \cdot MW_C}{2m_{C,0}} \tag{4.1}$$

Char-steam gasification:

$$X_{C,steam} = \frac{\left(\Delta n_{CO} + \Delta n_{CO_2}\right) MW_C}{m_{C,0}} \tag{4.2}$$

where MW_c is the molecular weight of carbon, and Δn_i is the change in product gas concentration of species i (CO or CO_2) from initial time to a specific time and calculated using Equation 4.3.

$$\Delta n_i = \int_0^t y_i . \dot{n}_T dt \tag{4.3}$$

where $\dot{n}_T$ is the total molar flow rate determined from the total flow rate of the reagent gas for CO_2 gasification and nitrogen flow rate for steam gasification (steam removal), t is the instantaneous time at which the product gas concentrations was measured, and y_i is the fraction of the species i in the product gas. Equation (4.1) and (4.2) can be further expanded by Equation 4.4.

$$X_C = \frac{m_{C,0} - m_{C,t}}{m_{C,0}} = \frac{\Delta m_{C,t}}{m_{Char,0}\left(1 - x_{ash,db}\right) x_{C,daf}} \tag{4.4}$$

where $m_{C,0}$ is the initial mass of carbon, $m_{C,t}$ is the instantaneous mass of carbon, $x_{ash,db}$ is the weight fraction of the ash yield on a dry (moisture-free) basis and $x_{C,daf}$ is the weight fraction of the initial carbon content present within the coal char on a dry-ash free basis.

4.5.2 Specific reaction rate

After determining the carbon conversion, the specific reaction rate for both steam and CO_2 experiments was determined using Equation (4.5).

$$r_s\ (g/g_c/s)\ = \frac{1}{1-X}\frac{dX}{dt} = \frac{1}{m_{C,t}}\frac{dm_{C,t}}{dt} \tag{4.5}$$

The specific reaction rate described by Equation (4.5) quantifies the rate of reacted carbon relative to the unconverted carbon mass at a specific time. From the literature, this expression has been used for describing the char reactivity (Krishnamoorthy *et al.*, 2019; Liu *et al.*, 2015; Roberts & Harris, 2007; Steibel *et al.*, 2017).

4.5.3 Intrinsic reaction rate

The intrinsic reaction rate was determined by normalising the specific reaction rate to the subsequent measured internal surface area of the coal chars reacted to a specific carbon conversion (10, 20 and 30%). This form (Equation 4.6) provides a reaction rate that is not dependent much on the changes in internal surface area, from which the "true" kinetic data such as the reaction order and the activation energy can be obtained (Roberts & Harris, 2006).

$$r_i^{"}(g/m^2/s) = r_s/S_{m,daf} \tag{4.6}$$

where $S_{d.a.f}$ is the micropore surface area on a dry-ash free basis described by;

$$S_{m,daf} = \frac{S_{m,db}}{1-x_{ash,d.b}} \tag{4.7}$$

where $S_{m,db}$ is the micropore surface area on a dry basis and $x_{ash,d.b}$ is the ash yield corrected to a specific carbon conversion. The micropore surface area of the reacted coal chars was determined using the CO_2 adsorption and D-A method as described in Section 3.4.

4.5.4 Determination of the model and kinetic parameters

Amongst the well-established coal char kinetic models, the Langmuir-Hinshelwood (LH) model was used from which kinetic parameters were obtained (see Appendix C.2.2). The Random-Pore Model (RPM) was used to evaluate the char reactivity and surface area development with the extent of carbon conversion (see Appendix C.2.3). In this study, the activation energy of the heterogeneous reactions was not evaluated due to the well-established data at both low and high pressure studies conducted for the Highveld coals (Du toit, 2013; Everson *et al.*, 2006; Gouws *et al.*, 2018).

The modelling and determination of kinetic parameters was done on the intrinsic reaction rate measured at conversions of 10, 20 and 30% using Equation 4.8

$$r_i^{"} = \frac{c\, p_i}{1 + {k_1}/{k_3}\, p_i + {k_2}/{k_3}\, p_j} \tag{4.8}$$

where p_i is the partial pressure of steam or CO_2, p_j is the partial pressure of CO or H_2 and c is the intrinsic $[C_t]k_1$ term. For comparison with literature, the specific reaction rate data at carbon conversion of 4% has also been used to determine the kinetic parameters as shown in Equation (4.8) and (4.9).

$$r_{s,4\%} = \frac{[C_t]k_1 p_i}{1 + {k_1}/{k_3}\, p_i + {k_2}/{k_3}\, p_j} \tag{4.9}$$

Due to the low observed concentrations, the inhibition effects of CO and H_2 were negligible and the p_j term in Equation 4.8 and 4.9 is then approximately zero, and the effect of product inhibition was not taken into account.

4.6 Carbon balance and data processing

4.6.1 Carbon conversion and balance

In order to demonstrate data processing and a carbon mass balance, the steam and CO_2 gasification experiments were performed at a temperature of 875 °C and a pressure of 30 bar and 20 bar with 66.7% steam and 30% CO_2, respectively. These conditions were chosen such that an almost complete conversion was achieved and also to evaluate the accuracy of the system based on the measurements of CO only (CO_2 gasification) and CO+CO_2 (steam gasification). After obtaining the CO and CO_2 concentrations (see Appendix D.2.1) the carbon conversion was determined using the methods described in Section 4.5.1 and the results are shown in Figure 4-2.

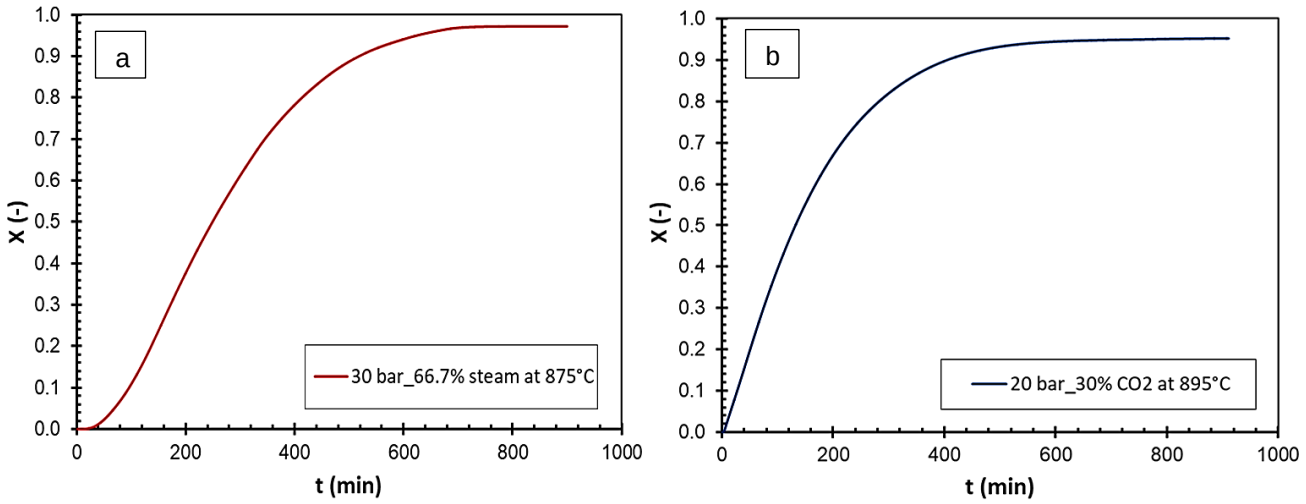

Figure 4-2: Carbon conversion profile of (a) 20 bar steam at 875 °C and (b) 6 bar CO_2 at 895 °C

The carbon conversion was found to reach a plateau with gasification time at a conversion of 97.2 and 95.2% for 20 bar steam and 6 bar CO_2 run, respectively. The remaining residue after the experimental runs was found to be significantly rich in ash as illustrated in Figure 4-3.

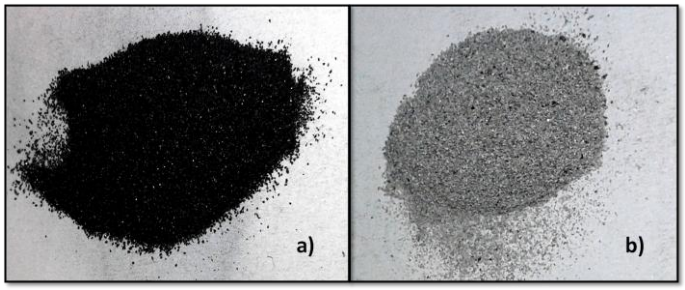

Figure 4-3: A 0.5 g char sample (a) before gasification and (b) after gasification

From the performance of proximate analysis in accordance to the ISO standards (ISO 1171:2011, ISO 562:2011, ISO 11722:1999) on the remaining residue, an ash yield of 98.5 and 98.9 wt% was found for steam and CO_2, respectively as expected for a converted coal char. A comparison of the calculated and experimental conversion was done (see Appendix D.2.2) from which it was found the carbon mass balance closure was larger than 95%. These results demonstrated that the proposed rig and procedures are sound, and results also demonstrate that the measurement of $CO+CO_2$ alone for steam gasification is sufficient in describing the carbon conversion.

4.6.2 Specific reaction rates

From the measurements of carbon conversion (Section 4.6.1), the specific reaction was determined using the procedures discussed in Section 4.5.2 and the results are shown in Figure 4-4.

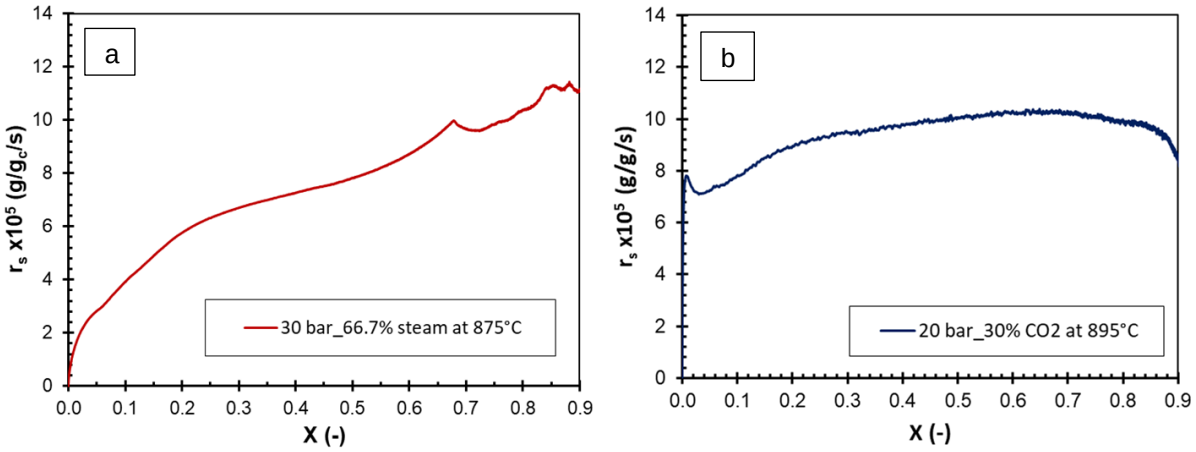

Figure 4-4: Specific reaction rate against conversion of (a) 20 bar steam at 875 °C and (b) 6 bar CO_2 at 895 °C

The specific reaction rate was found to have an increasing trend with carbon conversion up to 80%. At the early stage of conversion, especially for CO_2 gasification, it was observed that the

specific reaction rate increases and reaches a maximum and thereafter decreases. This effect might be attributed to flow dynamics and change in atmosphere at the start of the experiment. Similar observations have been reported in the literature and the specific reaction rate data lower than 5% will therefore not be reported in this study (Gomez *et al.*, 2014; Gouws, 2017).

The measured specific reaction rates for both steam and CO_2 gasification described in this section are not entirely free from the effects of mass transfer limitations. Therefore, the operating conditions where the effects of mass transfer limitations are negligible will be evaluated.

4.7 Evaluation of operating regime

As noted in the literature, the char gasification rate is dependent on the operating regime controlling the overall gasification rate. To evaluate the intrinsic chemical reaction kinetics, the dependence of the reaction rate on several parameters were conducted to decouple the chemical reaction limitations from diffusional limitations. The test experimental runs were performed at different to total pressure, flow rate and particle size to evaluate the effects thereof.

4.7.1 Influence of total pressure

The influence of total pressure on the specific reaction rate at a certain temperature was studied by means of varying the total pressure and reactant concentration while keeping the reactant partial pressure constant. These studies were carried at a total flow rate of 2 NL/min for steam and CO_2, and a summary of selected experimental conditions is given in Table 4-3.

Table 4-3: Operational conditions for evaluating the effect of total pressure

Variable	5 bar CO_2	15 bar CO_2	2.5 bar steam	10 bar steam
Temperature (°C)	780-900	780	740-780	740
Total pressure (bar)	5, 10, 25	15, 25, 30	5, 10	12, 15
Concentration (vol%)	100, 50, 20	100, 60, 50	25, 50	83.3, 66.7

The effect of total pressure on specific rate was studied at a temperature range of 780-900 °C and 740-780 °C for CO_2 and steam, respectively. It was observed that the total pressure does not have a significant influence on the specific reaction rate at a temperature of 780 °C for CO_2 experiments and 740 °C for steam experiments. The results on the effect of total pressure on the reaction rate are shown in Figure 4-5.

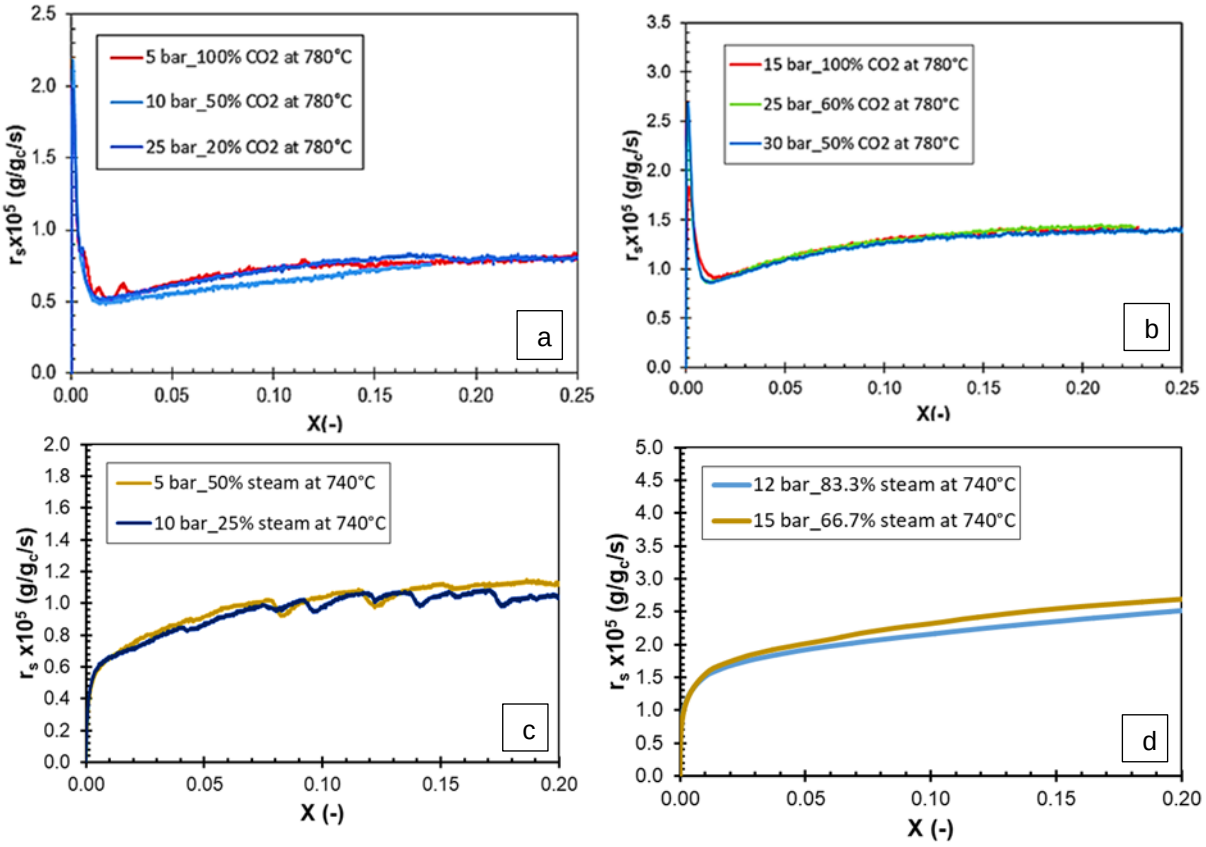

Figure 4-5: Effect of total pressure on specific rate at 780 °C for (a) 5 bar CO_2, (b) 15 bar CO_2 and 740 °C for (c) 2.5 bar steam, (d) 10 bar steam.

Based on the results shown in Figure 4-5, the specific reaction rate was shown not to be dependent on the total pressure at fixed steam and CO_2 partial pressure. For a similar coal char, Gouws (2017) has found that the total pressure had no significant effect on the reaction rate at temperatures similar to the ones observed in this study. These observations are also in agreement with the reported results by other authors (Roberts *et al.*, 2010; Tremel & Spliethoff, 2013). In order to demonstrate the absence of mass transfer limitations at the observed temperatures, the effect of particle size and total flow rate were investigated and only on CO_2 gasification experiments.

4.7.2 Influence of particle size

A coal char with a particle size range of -500+425 µm was selected to evaluate the influence of particle size on the conversion rate. The sample was prepared and charred with the methods described in Section 3.3. The conversion rate determined for both coal char samples (particle size range of -500+425 µm and -150+75 µm) at a temperature of 780 °C was compared and the results are shown in Figure 4-6.

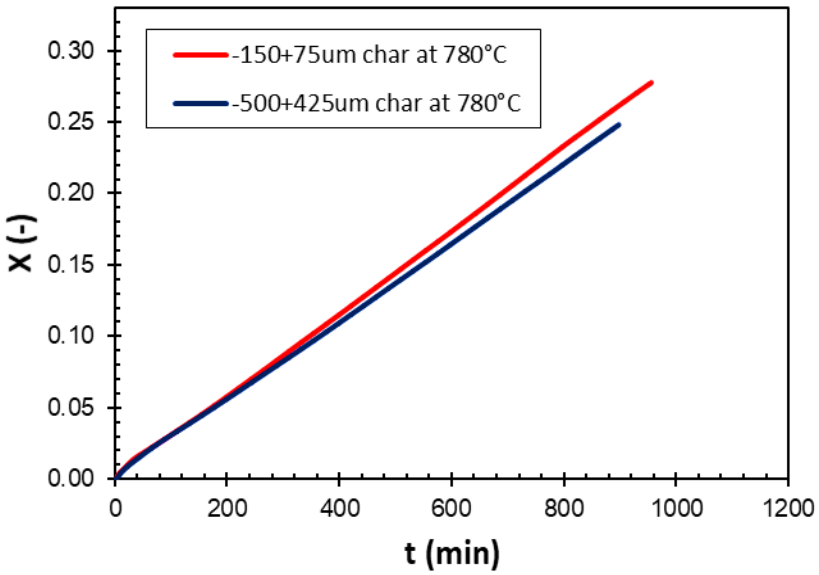

Figure 4-6: Influence of particle size on conversion at 780 °C

From the experimental results, it was observed that the coal char particle size did show a significant effect on the conversion rate at a temperature of 780 °C, which indicates the absence of internal mass transfer limitations. Therefore, at the temperature ranges ≤ 780 °C, the effects of internal mass transfer limitations does not play a vital role on the char-CO_2 gasification rate and therefore on steam gasification rate at 740 °C (Kabe *et al.*, 2004).

4.7.3 Influence of total flow rate

The total pressure and particle size dependency tests showed that the char-CO_2 gasification rates are controlled by the chemical surface reactions only at 780 °C. To ensure that the char-gas reactions are not dependent on the external mass transfer limitations, the influence of the total gas flow rates was studied. Based on the studies conducted by Gouws (2017) it was found that a total gas flow rate of 1 NL/min was adequate for conducting char-CO_2 gasification studies for South African Highveld coals.

The effect of the total gas flow rate on the specific reaction rate was evaluated using a total flow rate of 1 and 2 NL/min. The influence of total flow rate on the specific reaction rate is illustrated in Figure 4-7.

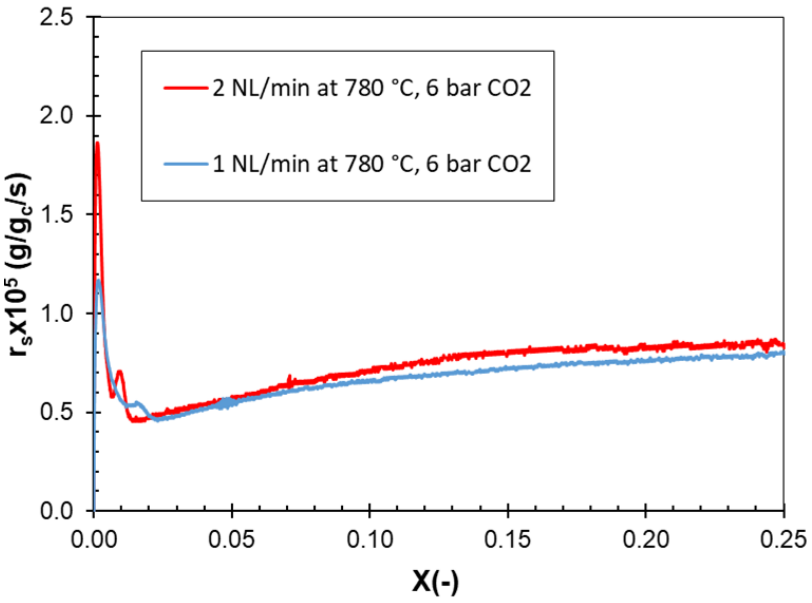

Figure 4-7: Influence of total flow rate on reaction rate at a constant partial pressure

As shown in Figure 4-7, it was observed that total flow rate does not a significant effect on the char-CO_2 reaction rate at 780 °C and therefore similar conclusions can be made for measurements of steam gasification reactions at 740 °C.

4.8 Experimental uncertainties

The experimental uncertainties were evaluated for the measurement of the gasification reaction rate using the experimental rig discussed in Section 4.3 and also on the surface area measurements using the CO_2 adsorption method as discussed in 3.4.

4.8.1 Char reactivity uncertainties

The char reactivity uncertainties associated with several variables such as the measurements of the product gases, the precision of equipment and calibration were quantified on the specific reaction rate data. To determine the experimental uncertainties, three repeated experimental runs at a steam and CO_2 partial pressure of 15 bar and the results are shown in Figure 4-8.

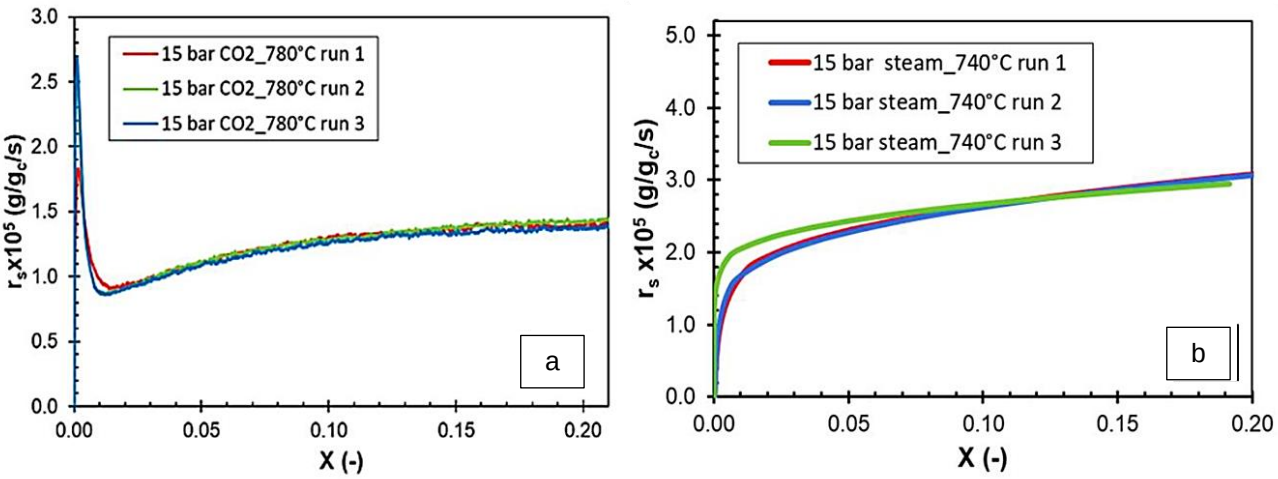

Figure 4-8: Experimental repeatability results for (a) 15 bar CO_2 and (b) 15 bar steam

A t-distribution test with a 95% confidence interval was used to quantify the experimental uncertainties as described in Appendix C.3.1. Based on the results obtained, it was found that the average uncertainties were 4% and 8% for the 15 and 30 bar CO_2 pressure, respectively and 6% for steam. These results indicate good repeatability of the experimental runs, also demonstrates that the experimental method used to measure the char reactivity is reliable.

4.8.2 Surface area uncertainties

The micropore surface area for the unconverted and the partially converted chars was measured by making use of the Micrometrics surface and porosity analyser as described in Section 3.4. The analysis equipment is fully automated, and three runs were selected for the determination of uncertainties of which were quantified based on the t-distribution test with a 95% confidence interval. After doing three measurements on the three unreacted coal chars from the same batch, an uncertainty of less than 4% was found, which is in agreement with the observed results on similar analysis methods (Gouws, 2017). The micropore surface area of the converted coal chars to a certain conversion at the selected conditions are summarised in Table 4-4.

Table 4-4: The micropore surface area uncertainties results for the converted chars

Sample	Carbon conversion	Run 1	Run 2 (m^2/g_c,*daf*)	Run 3	Uncertainties
7.5 bar steam	~30%	937.3	919.2	923.4	2.1%
30 bar CO_2	~10%	239.9	247.2	246.1	4.0%
	~30%	314.0	315.8	317.5	1.4%

The maximum uncertainties for the analysis of the micropore surface area for the repeated runs were found to be < 5% indicating good reliability and accuracy.

4.9 Summary and experimental program

The char gasification tests with regards to finding the operating conditions at which the reaction rate is only controlled by chemical surface reactions and evaluation of the carbon balance at relatively high temperatures were conducted. Based on the observed results, it was concluded that the use of only CO for CO_2, and $CO+CO_2$ for steam was sufficient to describe the carbon conversion during the steam and CO_2 gasification. A constant total flow rate of 2 NL/min was used for conducting the gasification experiments.

A coal char sample with a particle size range of -150+75 µm was used for both steam and CO_2 gasification with a fixed sample amount of about 0.5 g. From the evaluation of the effect of total pressure, particle size and flow rate on reaction rate, it was found that a temperature range less than 780 °C (for CO_2 experiments) and 740 °C (for steam experiments) will provide the kinetic data that is not influenced by the effects of mass transfer limitations.

The coal chars will be reacted to relative low carbon conversions of 10, 20 and 30% (at fixed reactant partial pressures) to minimise the effect of the mineral matter since the parent coal shows high ash yields. To obtain the specific partial pressure (1-30 bar CO_2 and 2.5-20 bar steam), the total pressure and reactant concentrations will be varied accordingly. To determine the micropore surface area of the reacted coal chars, the extent of carbon conversion was used to correct for the actual mineral matter content, according to Equation 4.7.

Table 4-5 summarises the experimental conditions and variables used for conducting the char-steam and char-CO_2 gasification experiments.

Table 4-5: Operating conditions for the gasification experiments

Parameters	**Char-CO_2 gasification**	**Char-steam gasification**
Particle size (PSD)	-150+75 µm	-150+75 µm
Reaction temperature	780 °C	740 °C
Sample mass	~0.50 g	~0.50 g
Total flow rate (STP)	2 NL/min	2 NL/min
Reactant partial pressure	1-30 bar	2.5-20 bar
Reactant concentrations	5-100%	50-83.3%
System total pressure	1-30 bar	5-30
Conversion (X)	10, 20 and 30%	10, 20 and 30%

Chapter 5

(RESULTS AND DISCUSSION)

CHAPTER 5

(RESULTS AND DISCUSSION)

5.1 Introduction

The steam and CO_2 gasification experiments were done at an isothermal temperature of 740 °C and 780 °C respectively by making use of the modified HPFBR, from which the char reactivity and kinetics were obtained. The experiments were carried out at different reactant pressures and carbon conversions of up to 30% and the subsequent specific surface area of reacted chars were determined. Section **5.2** discusses the effects of conversion and reactant partial pressure on the reaction rate and surface area for CO_2 gasification. For steam gasification experiments, these effects are discussed in Section **5.3**. Section **5.4** provides the modelling results of the reaction rate and surface area including the evaluation of sites occupancy. In Section **5.5**, the comparison of steam and CO_2 results is addressed and a summary of the main findings is given in Section **5.6**.

5.2 CO_2 gasification

5.2.1 Effect of conversion on CO_2 specific rate

Figure 5-1 illustrates the specific rate results determined at a conversion of up to 30% (±2%) for different CO_2 partial pressures (conversion-time profiles are provided in Appendix D.2.3).

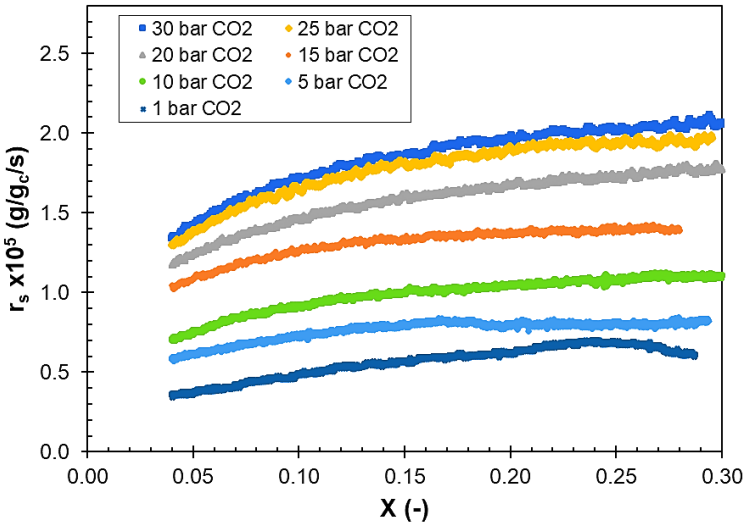

Figure 5-1: Effect of conversion on CO_2 specific rate

The specific rate was found to increase with an increase in carbon conversion for the complete CO_2 partial pressure range. Similar results have been reported by several authors and this

increase has been found to be associated with pore development during conversion (Gouws, 2017; Krishnamoorthy *et al.*, 2019; Liu *et al.*, 2015; Tremel & Spliethoff, 2013). Krishnamoorthy *et al.* (2019) evaluated the effect of the extent of conversion on specific reaction rate at CO_2 partial pressures of 3.4-21.7 bar over the conversion range of 0-40% (±10%). It was found that the specific reaction rate increased with an increase in conversion and more profound at high pressures. As the carbon conversion increases, the micropore surface area increases even at low conversions due to development of pores (Coetzee *et al.*, 2015; Feng & Bhatia, 2003; Gouws, 2017) and causing an increased specific reaction rate (Bai *et al.*, 2018; Feng & Bhatia, 2003; Kabe *et al.*, 2004; Smith *et al.*, 2013; Wang & Bhatia, 2001). At higher CO_2 partial pressures, the increase in specific rate with conversion was found to be more profound indicating some effect of partial pressure similar to the results observed by Krishnamoorthy *et al.* (2019). This effect has been reported to be a result of an increased pore development at high CO_2 partial pressures compared to lower pressures (Gouws *et al.*, 2018; Liu *et al.*, 2015; Tremel & Spliethoff, 2013).

5.2.2 Effect of CO_2 partial pressure on specific rate

The results on the effect of CO_2 partial pressure on specific rate over the range of 1-30 bar are presented in Figure 5-2.

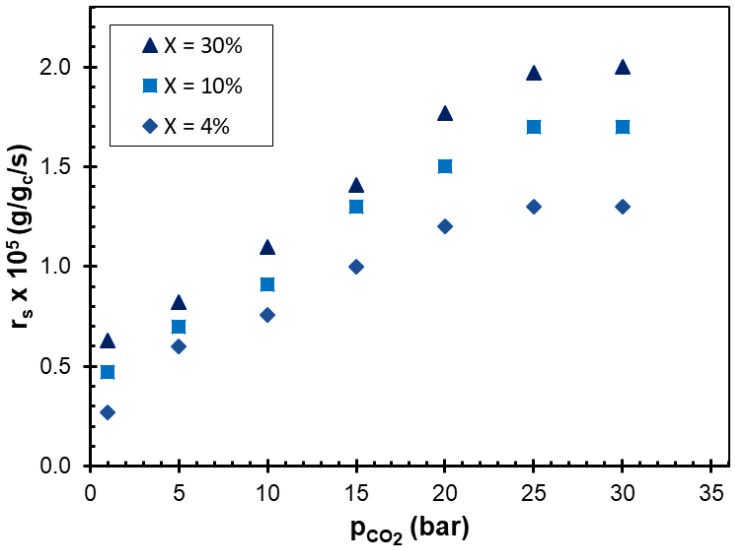

Figure 5-2: Effect of CO_2 partial pressure on specific rate

The specific rate was found to significantly increase with an increase in CO_2 partial pressure from 1-25 bar with an increase of almost five-fold. A further increase in CO_2 partial pressure from 25 to 30 bar did not show a significant. Similar observations have been reported at a CO_2 partial pressure of about 20 bar (see Table 2-2) and this effect was found to be related to the site coverage of adsorbed species (Gouws *et al.*, 2018; Liu *et al.*, 2000b; Roberts & Harris, 2006; Tremel & Spliethoff, 2013; Wall *et al.*, 2002). As the CO_2 partial pressure increases, the

concentration of surface complexes (adsorbed on active sites) increases resulting in an increased specific reaction rate (Gouws *et al.*, 2018; Liu *et al.*, 2000b; Roberts & Harris, 2006; Tremel & Spliethoff, 2013; Wall *et al.*, 2002) and a further increase causes saturation of the active sites pertaining to unaffected specific rate generally observed at high pressures (Mühlen *et al.*, 1985; Roberts & Harris, 2006; Sha *et al.*, 1990). Roberts and Harris (2006) evaluated the effect of CO_2 partial pressure on the reaction rate and it was found that the reaction rate did not change significantly at a CO_2 partial pressure above 20 bar, which is also consistent with the previously reported results by Mühlen *et al.* (1985).

The observed reaction order attributed to the effect of CO_2 partial pressure from 1-25 bar was found to be in the range of 0.46-0.50 (see Appendix D.3.1) of which is similar to the order measured at atmospheric pressures (Everson *et al.*, 2008; Harris & Smith, 1991). Several authors have reported similar results on high pressure studies with a reaction order varying from 0.5-0.7 (Gouws *et al.*, 2018; Kajitani *et al.*, 2002; Liu *et al.*, 2017; Malekshahian & Hill, 2011; Roberts & Harris, 2006) and approaching zero at high CO_2 partial pressures (Ahn *et al.*, 2001; Blackwood & Ingeme, 1960; Roberts & Harris, 2000; Sha *et al.*, 1990).

5.2.3 Effect of conversion on surface area

Figure 5-3 shows the results on the effect of conversion on micropore surface area on the chars reacted to conversions of 10% (±2%), 20% (±3%) and 30% (±2%) for the selected CO_2 partial pressures.

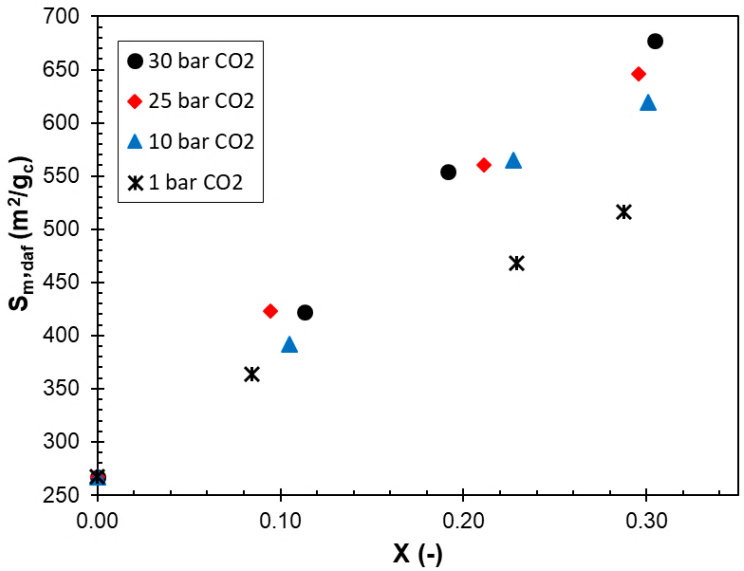

Figure 5-3: Effect of conversion on micropore surface during CO_2 gasification

It is clearly observed that an increase in conversion results in a significant increase in micropore surface area over the conversion range of 0-30% irrespective of the CO_2 partial pressure. The

micropore surface area was found to increase by almost 50% for the chars reacted to 10% indicating a significant pore development from the onset of the gasification reactions. These observations are in accordance with the reported results and were found to be due to pore development occurring with the extent of conversion (Coetzee *et al.*, 2015; Feng & Bhatia, 2003; Gonzalez *et al.*, 2018; Gouws *et al.*, 2018; Jin *et al.*, 2018a; Kajitani *et al.*, 2002; Liu *et al.*, 2000a; Tilghman & Mitchell, 2015; Wang & Bhatia, 2001). Since the reaction takes place in the micropores (Bhatia & Perlmutter, 1980; Wang & Bhatia, 2001), generally, an increase in carbon conversion result in pore growth in the micropore size range causing an increased micropore surface area (Coetzee *et al.*, 2017; Coetzee *et al.*, 2015; Gouws *et al.*, 2018; Huan *et al.*, 2019). A more pronounced increase in micropore surface area is observed at high CO_2 partial pressures, which indicates some effect of CO_2 partial pressure on pore development.

5.2.4 Effect of CO_2 partial pressure on surface area

Figure 5-4 shows the results of the micropore surface area of the reacted chars to conversions of about 10, 20 and 30% as a function of CO_2 partial pressure.

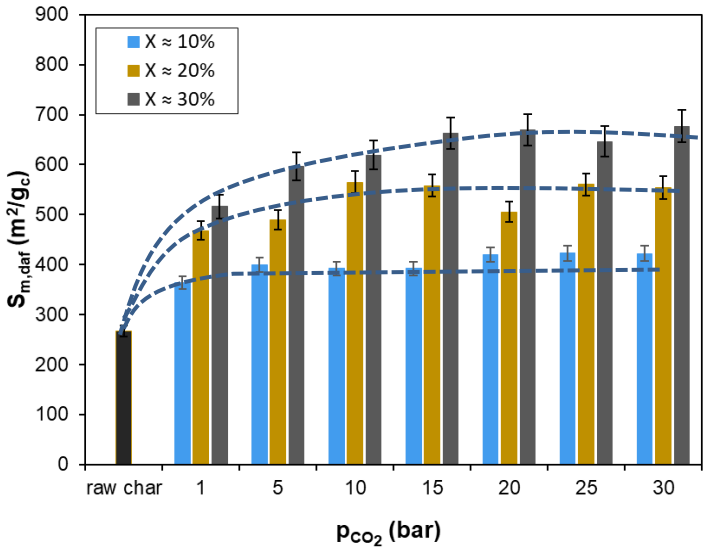

Figure 5-4: Effect of CO_2 partial pressure on the development of micropore surface area at a constant conversion

An increase in the micropore surface area was observed for the reacted chars at any CO_2 partial pressure despite the extent of carbon conversion. These results show the development of the micropore surface area of the unreacted chars with CO_2 partial pressure which is attributed to pore development (Gouws *et al.*, 2018). Similar to the discussions provided in Section 5.2.3, the development of micropore surface area with CO_2 partial pressure is also dependent on the extent of carbon conversion whereby the effect of CO_2 partial pressure is more profound at a fixed conversion of about 30%.

At a fixed conversion of 10%, an increase in CO_2 partial pressure from 1-30 bar did not show a significant effect on the micropore surface area. Similar observations were reported by Roberts and Harris (2007) from the evaluation of micropore surface area development at an early stage over the CO_2 partial pressure of 5 to 10 bar. At a fixed conversion of 20 and 30%, it was observed that the micropore surface area increases with an increase in CO_2 partial pressure from 1-10 bar and 1-15 bar, respectively. A further increase in CO_2 partial pressure up to 30 bar did not significantly show further development of micropore surface area. These results indicate increased pore growth with an increase in CO_2 partial pressure which depends on the extent of gasification. Similar results on the development of micropore surface area with CO_2 partial pressure have been reported by a few authors and this was found to mainly be associated with the pore growth in the micropore size range (Gouws *et al.*, 2018; Howaniec, 2019; Krishnamoorthy *et al.*, 2019). Howaniec (2019) evaluated the development of micropore surface area with CO_2 partial pressure over a range of 1-30 bar and the level-off of micropore surface area at high partial pressures was not observed which might be a result of surface area analysis method (N_2 adsorption analysis) and the gasified material (lignite char). The observed unaffected micropore surface area with an increase in CO_2 partial pressure in this study is in accordance with the observed effect of CO_2 partial pressure on specific rate (discussed in Section 5.2.2) and similarly, the effect might be attributed to surface saturation at high CO_2 partial pressures.

5.2.5 Effect of conversion and CO_2 pressure on intrinsic reaction rate

The results on the effect of conversion and CO_2 partial pressure on the intrinsic reaction rate ($g/m^2.s$) are presented in Figure 5-5.

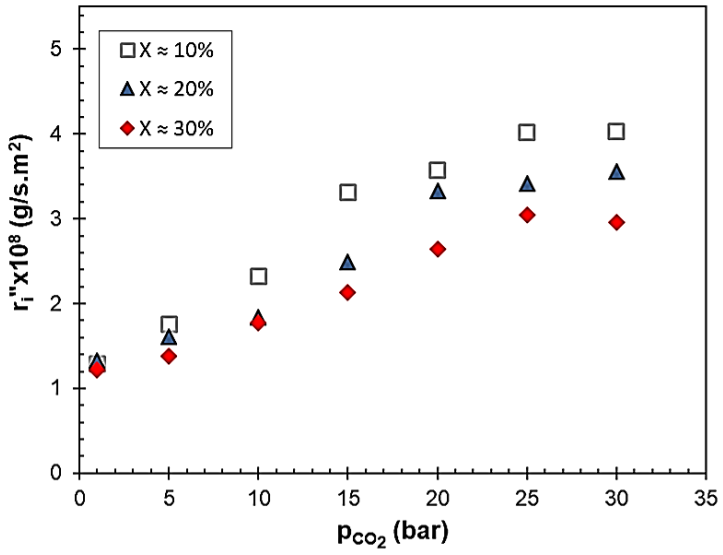

Figure 5-5: Effect of conversion and CO_2 partial pressure on the intrinsic rate

The effect of conversion on the intrinsic rate was evaluated over a conversion range of 10-30% at a fixed CO_2 partial pressure of 1-30 bar. An increase in conversion was found to have no significant effect on the intrinsic rate at a CO_2 partial pressure range of 1-5 bar. At a fixed CO_2 partial pressure of 10-30 bar, the intrinsic rate was found to exhibit a decreasing trend with an increase in conversion. The observed decrease of intrinsic rate with conversion has been reported by several authors for chars reacted to carbon conversions of up to 50% (Adschiri & Furusawa, 1986; Feng & Bhatia, 2003; Huan *et al.*, 2019). Feng and Bhatia (2003) evaluated the intrinsic rates at different carbon conversions from early stage to conversions greater than 50% at ambient pressure. It was observed that the intrinsic rate decrease significantly with conversion up to 20% and tends to decrease slowly at greater conversions up to 75%. These effects were found to be caused by the initial rapid conversion of carbon in the pore structure resulting to pore growth and less reactive crystalline matter (Feng & Bhatia, 2003; Huan *et al.*, 2019). As a result, the intrinsic rate at low conversions tends to be greater (Feng & Bhatia, 2003). These results are in agreement with the observed increase in micropore surface area with conversion (see Figure 5-3).

At a fixed conversion, the intrinsic rate was found to be dependent on the CO_2 partial pressure whereby it was observed to increase with an increase in CO_2 partial pressure from 1-20 bar. A further increase from 20 to 30 bar resulted in an insignificant effect on the intrinsic rate. These results are in accordance with reported results (Krishnamoorthy *et al.*, 2019; Liu *et al.*, 2000b; Roberts & Harris, 2000) and the effect was found to be associated with an increase in the concentration of surface complexes and the subsequent result of the saturation effect (Krishnamoorthy *et al.*, 2019; Roberts & Harris, 2000).

The observed intrinsic reaction order of the CO_2 partial pressure effect from 1-20 bar was found to be in the range of 0.27-0.37 (see Appendix D.3.1) which is lower than the observed reaction order measured from the specific rate data (reported in Section 5.2.2). This implies that the intrinsic rate provides the gasification rate in which the effects of CO_2 partial pressure are less pronounced as compared to specific rates, which again is related the surface area development during conversion (Liu *et al.*, 2000b; Roberts & Harris, 2000). Therefore, the normalisation of the intrinsic rate to the amount of surface complexes can provide with a gasification rate that is not dependent on changes in micropore surface area (observed at lower CO_2 partial pressures) and CO_2 partial pressure (Krishnamoorthy *et al.*, 2019; Roberts & Harris, 2006).

5.3 Steam gasification

5.3.1 Effect of conversion on steam specific rate

The effect of conversion on specific reaction (conversion-time profiles are provided in Appendix D.2.3) was evaluated at a steam partial pressure of 2.5-20 bar and a conversion of 4-30% (±2%). Figure 5-6 shows the specific reaction rate against conversion results for the evaluated steam partial pressure range.

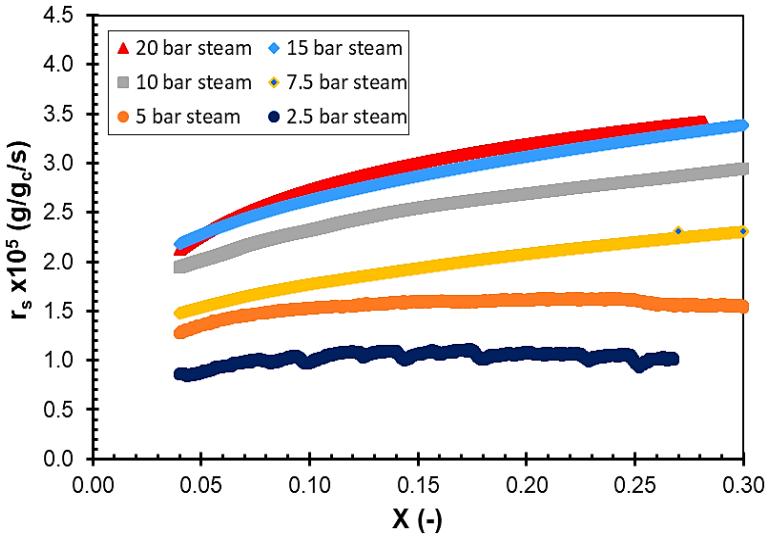

Figure 5-6: Effect of conversion on the steam specific rate

It can be seen that the specific rate increase with an increase in conversion up to 30% regardless of the steam partial pressures, and similar to the observations on CO_2 gasification. These results are in agreement with the generally reported results in the literature and it is due to the development of pores with conversion, which result to an increased specific rate (Aranda *et al.*, 2016; Huan *et al.*, 2019; Molina & Mondragon, 1998; Roberts & Harris, 2000; Wang *et al.*, 2013).

At high steam partial pressures, the increase in specific rate was found to be almost 4 times greater as observed at 2.5 bar of which is also more pronounced as compared to CO_2 gasification. The increase in specific rate with the conversion for different steam pressures demonstrated some dependency of specific rate on steam partial pressure.

5.3.2 Effect of steam partial pressure on specific rate

The results on the effect of steam partial pressure from 2.5 up to 20 bar on specific rate are shown in Figure 5-7.

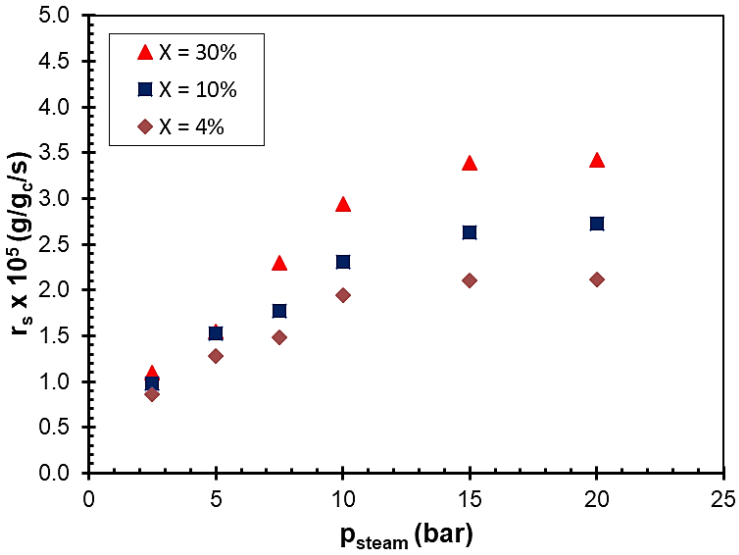

Figure 5-7: Effect of steam partial pressure on specific rate

The specific rate was found to increase with an increase in steam partial pressure almost three-fold from 2.5 to 15 bar. An increase in steam partial pressure from 15 to 20 bar showed no significant increase in the specific rate. Similar observations have been found by several authors, especially at a steam partial pressure above 15 bar (see Table 2-2) and these effects were also found to be a result of an increase in the quantity of surface complexes (concentration of C(O)) and site coverage of adsorbed specifies (Aranda *et al.*, 2016; Huan *et al.*, 2019; Mühlen *et al.*, 1985; Roberts & Harris, 2000; Sha *et al.*, 1990). When the steam partial pressure increases, the quantity of surface complexes also increases which result in an increased specific rate (Roberts & Harris, 2006). At high steam partial pressures, the increase in the quantity of surface complexes causes saturation of active sites and that results in an unaffected specific rate with a further increase in steam partial pressure (Mühlen *et al.*, 1985; Roberts & Harris, 2000; Roberts & Harris, 2006) in agreement to the observed results around 15 bar.

The observed reaction order with regards to steam partial pressure effect from 1-15 bar was found to be in the range of 0.46-0.60 (see Appendix D.3.1) which is in accordance with the observed reaction order for CO_2 gasification. Similar reaction order results with respect to the effect of steam partial pressure on the reaction rate at low and high pressures have been found (Everson *et al.*, 2006; Harris & Smith, 1991; Mühlen *et al.*, 1985; Roberts & Harris, 2006; Sha *et al.*, 1990). At low pressures, the effect of steam partial pressure on the reaction rate has been widely reported with the observed reaction orders of about 0.55 (±0.15) (Du toit, 2013; Harris & Smith, 1991). At high pressures, Roberts and Harris (2006) found the reaction order of 0.45 (±0.05) with regards to the effect of steam partial pressure on the reaction rate at steam partial pressures of up to 20 bar. At higher steam partial pressures, the observed reaction order has been found to approach an order of zero (Blackwood & McGrory, 1958; Mühlen *et al.*, 1985).

5.3.3 Effect of conversion on surface area

The results on the effect of conversion on the development of micropore surface area measured at conversions of 10%, 20% and 30% (±2%) are presented in Figure 5-8 for the selected steam partial pressures.

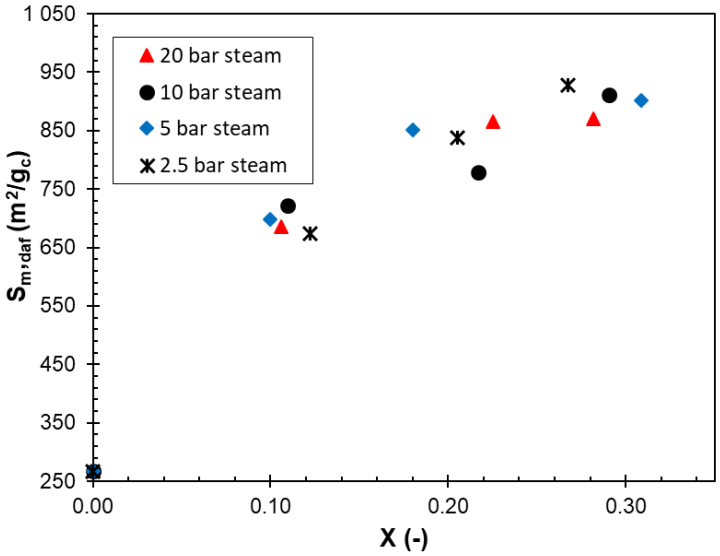

Figure 5-8: Effect of conversion on micropore surface area during steam gasification

At a fixed steam partial pressure, a general increase in micropore surface area with an increase in carbon conversion up to 30% was found. These results are in agreement with the reported results in the literature and the effect is associated with pore development that occurs as the conversion proceeds (Bai *et al.*, 2018; Coetzee *et al.*, 2015; Huan *et al.*, 2019; Jin *et al.*, 2018a; Kajitani *et al.*, 2002; Molina & Mondragon, 1998; Tilghman & Mitchell, 2015; Wang *et al.*, 2013), which is again similar to the observed pore development during CO_2 gasification. However, the magnitude of the development is larger for steam gasification, which might be attributed to the steam reacting even in much smaller pores due to its smaller kinetic diameter, causing a more pronounced micropore surface area. Therefore, these results demonstrate some dependency of reactant medium on the development of micropore surface area during conversion. Similar observations have been found by Coetzee *et al.* (2015) who evaluated and compared the pore development over a conversion range of 0-50%.

When comparing the micropore surface area development with conversion (10-30%) over the whole steam partial pressure range, it was observed that a change in steam partial pressure does not show greater effects with an average difference of less than 5%. These results indicate that the variation in steam partial pressure from 2.5-20 bar might have an insignificant influence on the micropore surface area development at the evaluated conditions.

5.3.4 Effect of steam partial pressure on surface area

The results on the effect of steam partial pressure on the development of micropore surface area for the coal chars reacted at a fixed carbon conversion of 10-30% are shown in Figure 5-9.

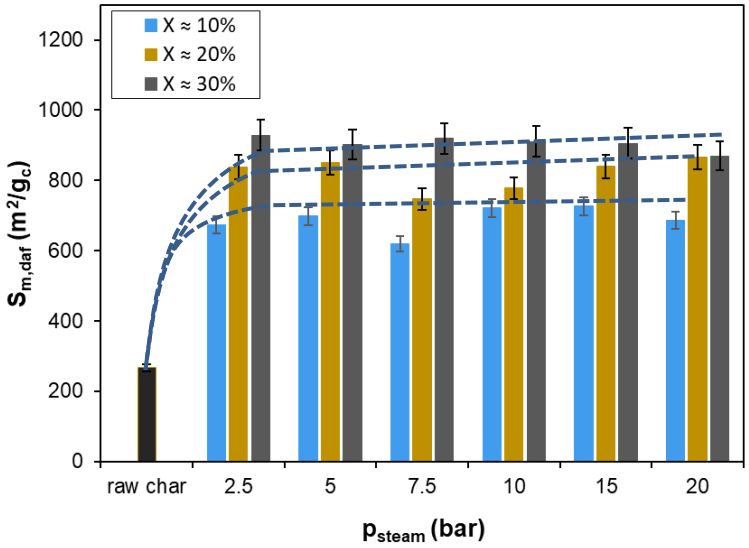

Figure 5-9: Effect of steam partial pressure on the micropore surface area at a constant conversion

The development of micropore surface area is observed from the onset of the gasification reactions regardless of the extent of conversion and steam partial pressure. This might be due to a greater pore growth occurring during conversion that might be related to the steam reacting in the smallest pores, which then results in a fast increase in surface area (Coetzee *et al.*, 2015; Wang *et al.*, 2013). However, at a fixed conversion, an increase in steam partial pressure from 2.5-20 bar result to an insignificantly increase by less than 8% in the early stage of conversion and less than 4% at the later stage. These results show that an increase in steam partial pressure results in a small micropore surface area development that seems to be fairly the same. In this case, the pore development during steam gasification seems to be more affected by the extent of carbon conversion as compared to the steam partial pressure.

In contrast to the observed micropore surface area development for the CO_2 gasification, the micropore surface area seems to be fairly independent of steam partial pressure over the whole conversion range and this behaviour is not well-reported in the literature. This might be associated with the better accessibility of smaller pores with steam as compared to CO_2, especially in the probed pore size range.

5.3.5 Effect of conversion and steam pressure on intrinsic rate

Figure 5-10 shows the results of the intrinsic rate as a function of conversion and steam partial pressure obtained at constant partial pressure and conversion.

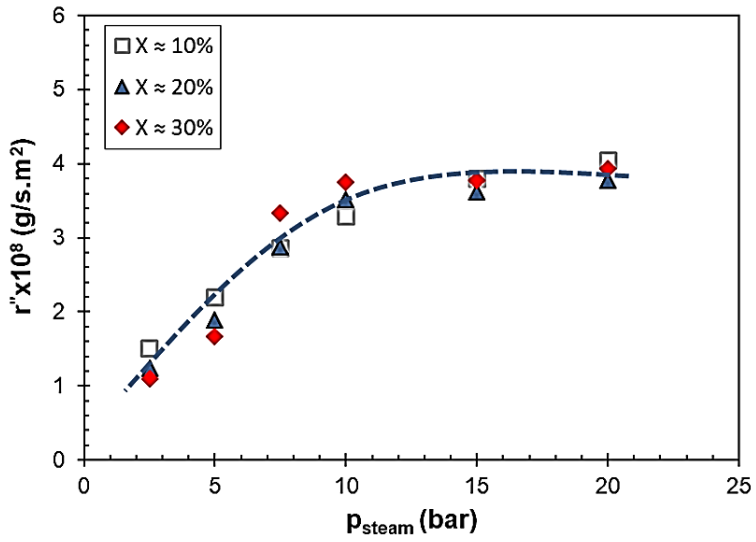

Figure 5-10: Effect of conversion and steam partial pressure on the intrinsic rate

As illustrated in Figure 5-10, the variation in conversion at a fixed steam partial did show a significant effect on the intrinsic reaction rate and similar observations have been reported in the literature (Huan *et al.*, 2019; Wang *et al.*, 2013). In contrast to the CO_2 gasification, the intrinsic rate is independent of conversion and the effect of conversion on the intrinsic rate over the conversion range of 10-30% can be fairly described by a single reaction rate. Huan *et al.* (2019) evaluated the effect of carbon conversion on intrinsic reaction rate over a conversion range of 10-50% at a constant steam partial pressure. It was found that the intrinsic reaction rate was independent of conversion at the evaluated conditions. These results indicate that the reaction rate normalised to the changes in surface area is solely dependent on the steam partial pressure as shown in Figure 5-10.

At a fixed conversion, a pronounced increase in intrinsic rate with an increase in steam partial from 2.5 up to 10 bar was observed with a reaction order of 0.57 (±0.09). A further increase from 10-20 bar had an insignificant increase in the intrinsic rate. Roberts and Harris (2000) reported similar observations and this effect of steam partial pressure is mainly associated with the quantity of surface complexes. Similar to CO_2, an increase in steam partial pressure causes an increase in surface complexes concentration which to an increased intrinsic rate and saturation effect of the active sites (Roberts & Harris, 2000; Roberts & Harris, 2006).

5.4 Modelling and sites occupancy

Modelling of the intrinsic reaction rate was evaluated using an LH type rate model and the results are discussed in Section 5.4.1, which was further used to evaluate the sites occupancy (Section 5.4.4). The RPM was also used to evaluate the relation of specific reaction rate (discussed in Appendix D.4.1) and surface area development with conversion (Section 5.4.2). From the

modelling of the intrinsic rate, surface area, and reactant partial pressure, a mixed model was developed to predict the specific reaction rate in relation to the conversion and compare with the experimental data.

5.4.1 Intrinsic reaction rate

The LH model was used to describe the intrinsic reaction rate for CO_2 and steam measured at carbon conversions of about 10, 20 and 30%. The detailed method is presented in Appendix C.2.2 which include the determination of the intrinsic $[C_t]k_1$ (denoted by c) and the k_1/k_3 term. A comparison of the intrinsic rate determined from the experimental data and LH rate equation with regards to the measured parameters is illustrated in Figure 5-11.

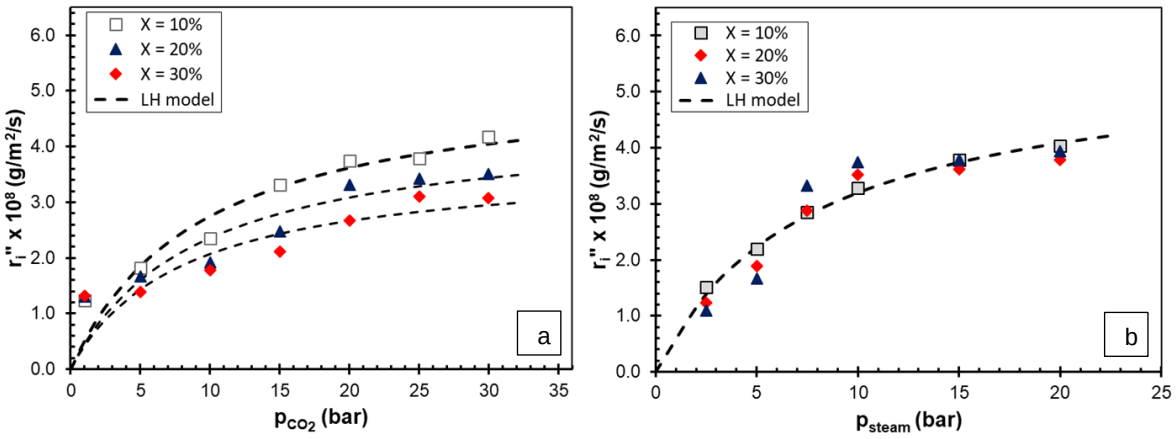

Figure 5-11: Comparison of experimental data and LH model results for (a) CO_2 and (b) steam

As shown in Figure 5-11(a) and (b) the LH model seems to fairly describe well the intrinsic rate data for steam and CO_2 with a relative error (see Appendix C.3.2) of less than 11% and 13%, respectively over the evaluated conversion range. The deviations between the LH model and the intrinsic rate data measured from the CO_2 gasification are due to the underprediction at lower CO_2 partial pressure of 1 bar and maybe of the probed surface area which is more representative for steam than CO_2. The observed results on the prediction of the reaction rate at a CO_2 partial pressure of 1 bar are in accordance with the generally reported applicability of the LH model at low pressures (Liu *et al.*, 2000b; Mühlen *et al.*, 1985; Roberts & Harris, 2006; Tremel & Spliethoff, 2013) and the reasons thereof are not clearly provided.

As for steam gasification (Figure 5-11(b)), it can be seen that a single reaction rate based on the LH type rate can fairly describe well the intrinsic rate data for the whole conversion range unlike that of CO_2 gasification. This effect is a result of the observed strong dependency of intrinsic rate on conversion as discussed in Section 5.3.5, which might be associated with the probed size

range that is more representative for steam than CO_2 due to small kinetic diameter. The determined kinetic parameter results are summarised in Table 5-1.

Table 5-1: Summary of the LH intrinsic kinetic parameters results for CO_2

X	CO_2 results		Steam results	
	c $(g/m^2.s.bar)$	k_1/k_3 $(1/bar)$	c $(g/m^2.s.bar)$	k_1/k_3 $(1/bar)$
10%	$5.7x10^{-9}$	0.11	$7.4x10^{-9}$	0.13
20%	$5.0x10^{-9}$	0.11	$7.4x10^{-9}$	0.13
30%	$4.6x10^{-9}$	0.12	$7.4x10^{-9}$	0.13

To compare the determined LH parameters with the values reported in the literature under regime I, the specific rate data obtained at 4% was used (refer to Appendix D.3.2) due to a lack of intrinsic data. The specific $[Ct]k_1$ and k_1/k_3 terms were found to correspond well with the reported results by Gouws *et al.* (2018) and Roberts and Harris (2006) who evaluated the steam and CO_2 gasification over a reactant partial pressure of 1-30 bar.

5.4.2 RPM: pore development

The RPM was used as a fitting tool to describe the relation of specific reaction rate with conversion and also pore development based on the knowledge of micropore surface area. The RPM results that describe the changes of specific reaction rate with conversion are discussed in detail in Appendix D.4.1. The development of micropore surface area with conversion is described by Equation 5.2 which is based on surface area per mass basis, where $S_{m,0}$ is the initial surface area and ψ is the structural parameter (Bhatia & Perlmutter, 1980; Feng & Bhatia, 2003).

$$S_m = S_{m,0}\sqrt{1 - \psi ln(1 - X)} \tag{5.1}$$

The results of the modelled surface area against conversion at some selected steam and CO_2 partial pressures are shown in Figure 5-12.

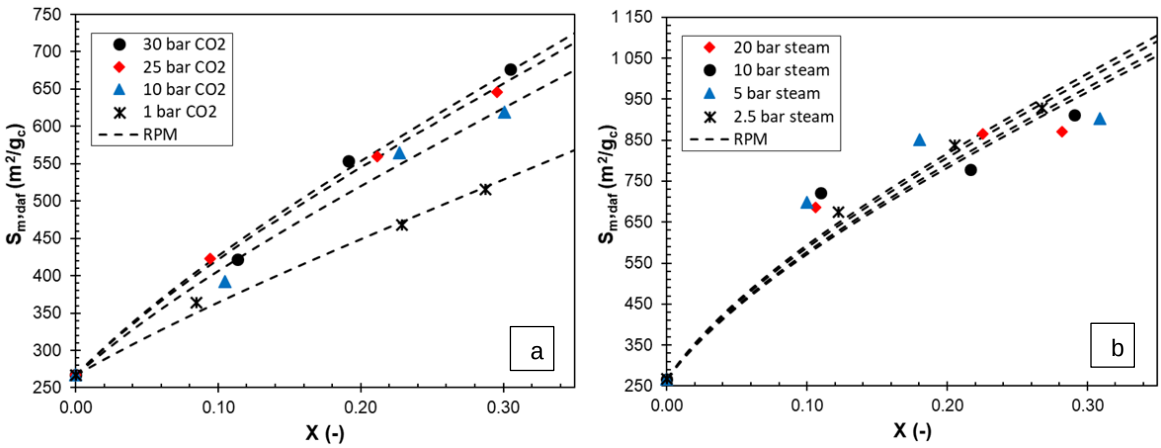

Figure 5-12: Surface area modelling using RPM for chars reacted with (a) CO_2 and (b) steam

As shown in Figure 5-12(a) the RPM can predict the development of the surface area with conversion at any CO_2 partial pressure reasonably. The deviations between the measured surface areas and predicted values were found to be less than 5% for the evaluated CO_2 partial pressure range. Similar observations have been reported from either using the surface area related to the square meter per unit mass or square meter per unit cubic meter (Adschiri *et al.*, 1986; Feng & Bhatia, 2003; Gonzalez *et al.*, 2018; Kajitani *et al.*, 2006; Ochoa *et al.*, 2001). However, the structural parameter (ψ) values are not the same for all the CO_2 partial pressures, which indicates some dependency on the CO_2 partial pressure (presented in Figure 5-13) and this is aligned with the reactivity results.

As shown in Figure 5-12(b) the RPM can fairly predict the micropore surface area for steam gasification during conversion with the deviations of less than 10%. The model was found to underpredict the development of micropore surface area at an early stage of conversion unlike that of CO_2 gasification. These results indicate that the drastic development of micropore surface area during conversion, which results in greater surface areas as compared to CO_2 gasification, cannot be well predicted by the model (Tremel *et al.*, 2012). The prediction of the surface area development for steam gasification seems to be different from that of CO_2 gasification. For steam gasification, the model does not show a pronounced effect of steam partial pressure and therefore indicating less dependence of the structural parameter (ψ).

The determined structural parameter (ψ) values are shown in Figure 5-13 as a function of reactant partial pressure.

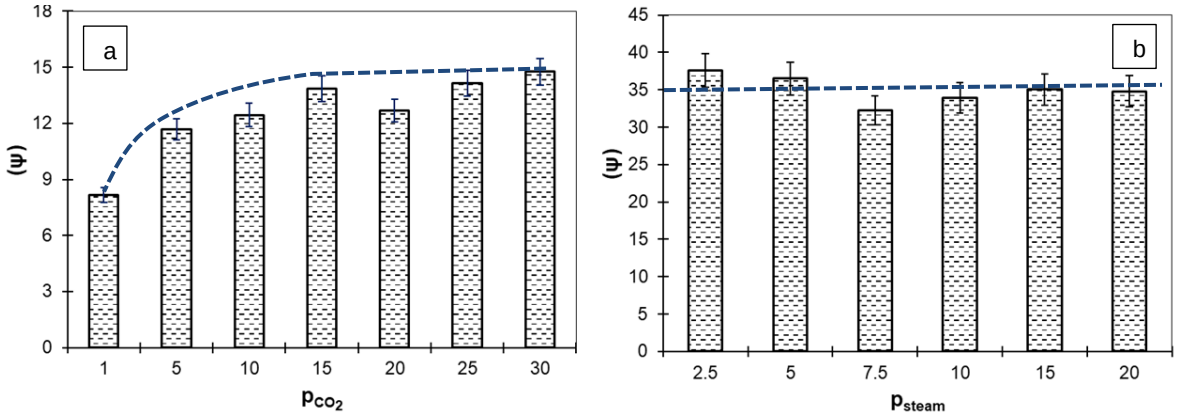

Figure 5-13: Structural parameter as a function of (a) CO_2 and (b) steam partial pressure

The structural parameter as a function of reactant partial pressure shows a similar trend as the previously discussed effect of reactant pressure on the micropore surface area. As shown in Figure 5-13(a) the structural parameter increase with an increase in CO_2 partial pressure up to 15 bar due to the structural changes ascribed to pore development. A further increase in CO_2 partial pressure from 15-30 bar also results in an insignificant influence on the ψ value. As for steam gasification, it can be seen from Figure 5-13(b) that the structural parameter does show an insignificant dependence on the steam partial pressure as compared to the CO_2 gasification. In this case, the ψ value remains unaffected by an increase in steam partial pressure from 2.5 up to 20 bar, which is in agreement with the observed effect on the micropore surface area. Therefore the changes in char physical structure during steam gasification are not dependent on variations in steam partial pressure. The observed structural parameter values correspond with the reported structural parameter results (ψ value of 3-130) determined from the surface area-conversion data for both steam (Kajitani *et al.*, 2002) and CO_2 gasification (Feng & Bhatia, 2003; Kajitani *et al.*, 2006; Ochoa *et al.*, 2001). In contrast to steam gasification results, it was established that the structural parameter is not only a function of conversion as described in the original Random-Pore Model but also a function of CO_2 partial pressure.

When comparing the structural parameter values determined from the surface area results and the reactivity data (see Appendix D.4.1), it was found that ψ values are not the same. Similar observations have been reported in the literature, however, explanations for this phenomenon are not clearly given (Kajitani *et al.*, 2002; Tremel & Spliethoff, 2013).

5.4.3 Mixed model: LH type model and RPM

From the obtained kinetic and structural parameters of the intrinsic reaction rate, the specific reaction rate was determined using Equation 5.2.

$$r_s = r_i^{"} \times S_m = \frac{cp_i}{1 + {k_1}/{k_3}\, p_i} S_{m,0}\sqrt{1 - \psi \ln(1 - X)} \qquad (5.2)$$

This equation relates the specific reaction rate with the effects of partial pressure through LH type intrinsic rate and pore development as described by the RPM, which is more convenient to use for reactor modelling. Based on the findings from the experimental results, the following comments are given:

- The determined ${k_1}/{k_3}$ and c term from the intrinsic rate was found to be independent of conversion for steam gasification with a value of 0.13 (1/bar) and 7.4x10^{-9} (g/m^2.s). For CO_2 gasification, a specific ${k_1}/{k_3}$ and c term value was used due to conversion dependency.

- A constant structural parameter value was used (ψ = 35) for steam gasification since it was found to be not dependent on the changes in steam partial pressure over a range of 2.5-20 bar. As for the CO_2, this parameter was found to dependent on CO_2 partial pressure and well predicted by the nth-order type equation (Equation 5.4) with a correlation coefficient (R^2) of 0.938 (see Appendix D.4.2).

$$\psi = 8.5 \times {p_{CO_2}}^{0.162} \qquad (5.3)$$

Figure 5-14 shows the predicted specific reaction rate results for steam and CO_2 for the evaluated reactant partial pressure and conversion range.

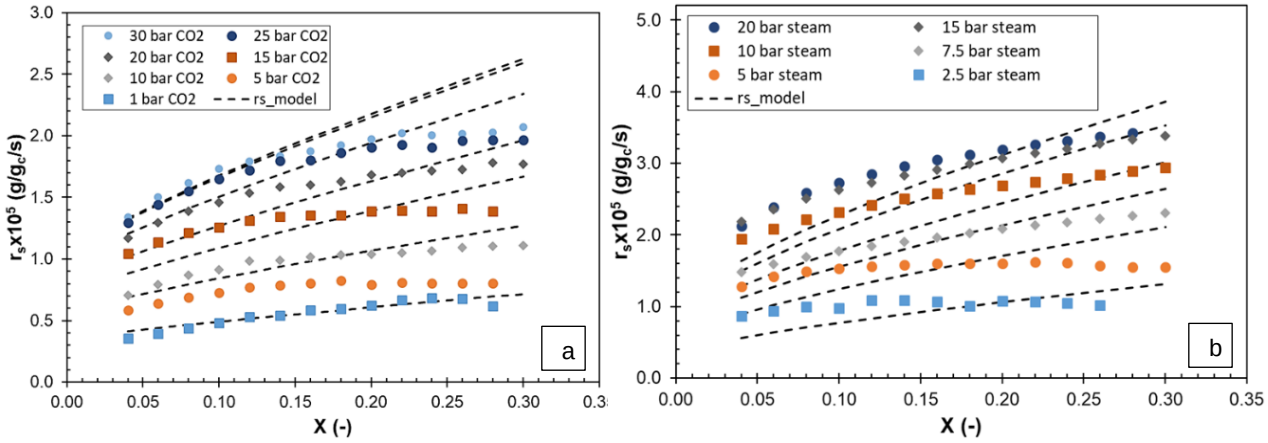

Figure 5-14: Specific reaction rate model (combined models) results against conversion

The quality-of-fit (QOF) (described in Appendix C.3.3) was determined to quantify the accuracy and applicability of the model to predict the experimental and the results are summarised in Appendix D.5 for the evaluated reactant partial pressure range. A QOF value ranging from 82-

90% was found for steam gasification and was slightly greater as compared to CO_2 gasification with a QOF value range of 64-94%, of which indicates that the model can fairly describe the experimental data. For CO_2 gasification, it was found that the model can predict the specific reaction rate at a low partial pressure of 1 bar and also the reaction rate at lower conversions rather well.

Liu *et al.* (2017) evaluated the applicability of a similar model (combined PL and RPM) to predict the reaction rate. From their investigations, it was found that the combined model was not capable of predicting well the reaction rate with the extent of conversion. Conversely, the investigations conducted by Kajitani *et al.* (2006) showed that the kinetic parameters obtained directly from the combined model can predict the reaction rate. This method was based on model fitting and not on the determined kinetic parameters from individual models. In order to improve the accuracy of the proposed combined model, and improvement of the description of pore development through the RPM has to be considered.

The discrepancies between the experimental data and the model might be associated with the non-uniformity of the carbon sites whereby the reactivity does not increase faster as compared to the micropore surface area. During conversion, the micropore surface area increases rapidly resulting in a great availability of the surface area for the reactions to occur, however, the carbon becomes less reactive (Feng & Bhatia, 2003; Huan *et al.*, 2019).

5.4.4 Site coverage/occupancy

The site occupancy or the degree of saturation was estimated from the approximation of the ration of adsorbed surface complexes to the total concentration of active sites as shown in Equation (5.4) (Roberts & Harris, 2006; Wang & Bell, 2017).

$$\theta_i = \frac{\left({}^{k_1}/_{k_3}\right) p_i}{1 + \left({}^{k_1}/_{k_3}\right) p_i} \tag{5.4}$$

where i is the reactant gas (steam or CO_2). Using the determined intrinsic kinetic parameters discussed in Section 5.4.1 and the sites occupancy was estimated and the results are shown in Figure 5-15.

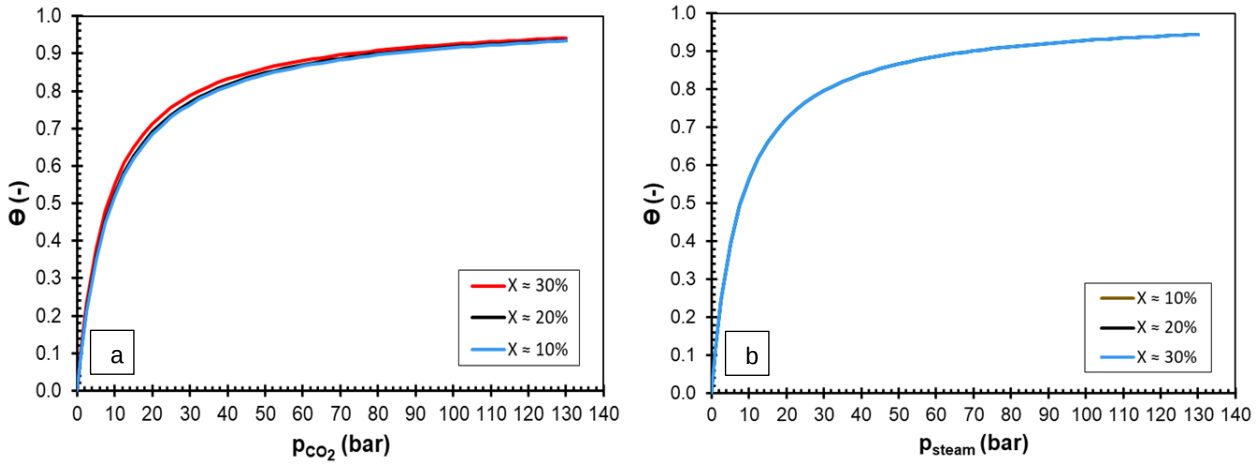

Figure 5-15: Site occupancy as a function of (a) CO_2 partial pressure and (b) steam partial pressure

For both steam and CO_2, the site occupancy was found to increase with an increase in reactant partial pressure. Roberts and Harris (2006) reported similar results using the TPD method and LH kinetic data for both steam and CO_2 over the partial pressure range of 1-30 bar. These results show that the quantity of adsorbed surface species increases rapidly at reactant partial pressures less than 10 bar, which is consistent with the observed increase in reaction rate with reactant partial pressure.

At higher reactant partial pressure, the site occupancy increases slowly indicating saturation of active sites, which results in an unaffected reaction rate with reactant partial as observed from the previous discussions on the reaction rate. Similar observations have been reported (Roberts & Harris, 2006).

5.5 Comparison of steam and CO_2 gasification

Although the steam and CO_2 gasification were performed at different temperatures, a qualitative comparison on the intrinsic reactivity and surface area development was done to illustrate the differences. The intrinsic reactivity measured at a conversion of 30% and the micropore surface area results obtained at similar partial pressures of 5 and 20 bar was used.

The comparison results of the steam and CO_2 char intrinsic reactivity as a function of reactant partial pressure and surface area development for the selected conditions are shown in Figure 5-16.

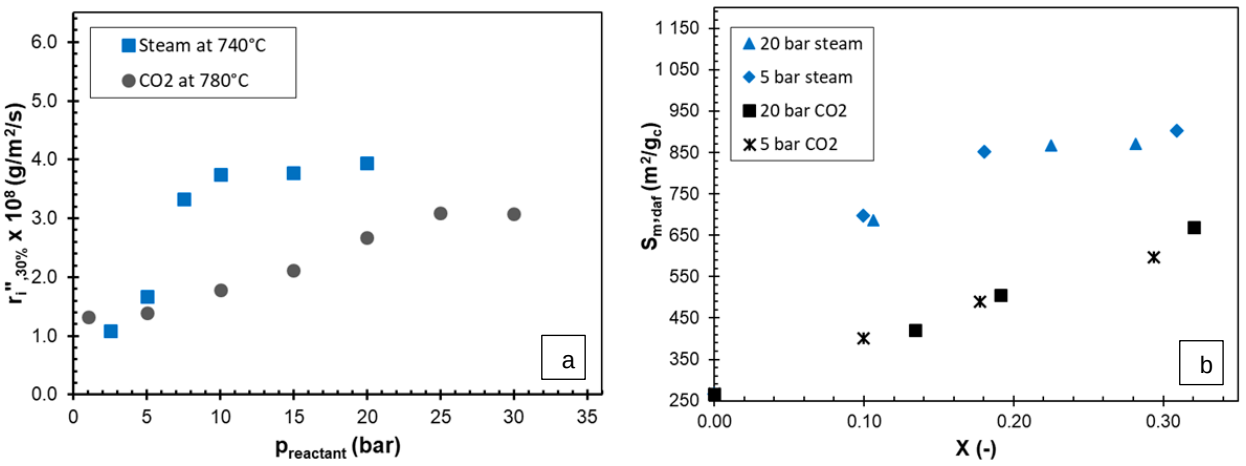

Figure 5-16: Comparison of steam and CO_2 (a) char intrinsic reactivity and (b) surface area development

As shown in Figure 5-16(a) the increase in the intrinsic rate for steam gasification is larger than that of CO_2 gasification indicating that steam is more reactive. When the reaction rate of CO_2 is extrapolated from 780 to 740 °C using the Arrhenius equation and the apparent activation energy reported by Gouws *et al.* (2018) for a similar coal char, a reactivity ratio between steam and CO_2 was found to be 3 based on the intrinsic rate data and 5.5 from the specific rate data. These results agree well with the generally reported ratio of the specific reactivity in the literature with a factor of 3-6 (Huan *et al.*, 2019; Katta & Keairns, 1981; Roberts & Harris, 2006).

From the comparison shown in Figure 5-16(b) on the development of surface area conversion, it was found that steam gasification is not only more reactive than CO_2 gasification but also results in a greater pore development that is almost twice as compared to CO_2. The dominance of steam on pore development as compared to CO_2 has been also reported and these observations were found to be associated with the difference in pore accessibility and kinetic diameter whereby steam can penetrate and develop smaller pores at a greater extent as compared to CO_2 (Coetzee *et al.*, 2017; Coetzee *et al.*, 2015; Huan *et al.*, 2019; Kajitani *et al.*, 2002).

5.6 Summary

The evaluation of coal char intrinsic kinetics and pore development was done at a conversion range of 10-30% in the atmosphere of steam and CO_2 at different partial pressures. It was found that the specific reaction rate and micropore surface area increases with an increase in carbon conversion for both reactants, irrespective of the reactant partial pressure. With the variation in reactant partial pressure, it was observed that the specific reaction increases to a certain extent and reach a plateau with a further increase. It was also found that the development of the surface area is independent of the reactant partial pressure for steam gasification in contrast to the CO_2 gasification, which was observed to be dependent on partial pressure.

The normalisation of the specific rate to the surface area was done to determine the intrinsic rate at different conversions and reactant partial pressure. It was seen that the intrinsic rate for steam gasification was less affected by the changes in carbon conversion but the steam partial pressure to a certain extent, which was found to be similar to the effect on that of specific reaction rate. As for the CO_2 gasification, it was found that the intrinsic rate is dependent on both the CO_2 partial pressure and the extent of carbon conversion. When comparing the char intrinsic reactivity and micropore surface area development of steam and CO_2, it was observed that steam is more reactive and causes greater surface area development as the reactions proceed.

The LH rate type, Random-pore, and the mixed model were used to describe the obtained coal char reactivity and pore development during coal char conversion. It was found that the individual models can predict the experimental data well as compared to the mixed model. From the determined model parameters, it was seen that the structural parameter (ψ) for CO_2 gasification was not only a function of conversion as described in the original RPM but also a function of partial pressure.

Chapter 6

(CONCLUSION AND RECOMMENDATIONS)

CHAPTER 6

(CONCLUSIONS AND RECOMMENDATIONS)

6.1 Introduction

A bituminous (medium rank C) coal sample was obtained in lump size and a representative coal char sample with a particle size range of -150+75 µm was prepared using mechanical size reduction and devolatilisation in a N_2 atmosphere. The coal and char characterisation was carried out, from which it was found that the parent coal was of high ash and rich in inertinite. The prepared coal char sample was subjected to gasification experiments (under regime I) in the atmosphere of steam (2.5-20 bar) and CO_2 (1-30 bar) at conversions of 10, 20, and 30%, and the partially reacted chars were analysed to determine the specific micropore surface area. From both the conversion experiments and the specific surface area development, an intrinsic reaction rate was obtained and further modelled.

This chapter provides the conclusions drawn from the experimental results and discussed in Section **6.2**. Section **6.3** and **6.4** addresses the contributions to science and the recommendations for further studies respectively.

6.2 Conclusions

The coal char reactivity was found to be dependent on reactant partial pressure to a certain extent whereby the reaction rate increased with an increase in reactant partial pressure up to a steam and CO_2 partial pressure of 10 and 20 bar, respectively. In contrast to the intrinsic reaction rate, the specific reaction rate was found to be greatly dependent on the carbon conversion with greater effects during steam gasification. The dependency of the reaction rate on the reactant partial pressure could be described by the Langmuir-Hinshelwood (LH) type model.

The micropore surface area was found to be significantly influenced by the extent of carbon conversion. With the variation in the reactant partial pressure, it was found that the micropore surface area was not dependent on steam partial pressure in contrast to the CO_2 gasification. The observed micropore surface area development was found to be greater in steam gasification as compared to CO_2 gasification.

A mixed model combining the effects of surface area development (RPM) and reactant partial pressure (LH type model) was used to model the specific rate during conversion and compared with the experimental results. It was found that the model can fairly predict the specific rate and

the individual models were applicable to well describe the experimental data. Although the RPM can well predict the experimental data, it was found that the structural parameter (ψ) directly obtained from the surface area development was larger than the one fitted from the rate-conversion results directly. These discrepancies were found to result in an overprediction of the specific rate by the mixed model, specifically at high conversions.

6.3 Contribution to existing knowledge field and science

The following contributions were made to the existing knowledge field and science:

- A systematic determination of coal char reactivity in the chemical-controlled regime at high steam and CO_2 partial pressures for a South African coal char.
- The determination and comparison of the micropore development of coal char as a function of reactant partial pressure at elevated gasification pressures.

6.4 Recommendations

Based on the investigations conducted and conclusions drawn in this study, the following recommendations are made for further studies on the underlying topic:

- The use of different coals from Highveld as well as biomass and comparisons thereof in terms of pore development and reaction kinetics at high pressures of steam and CO_2.
- Evaluate the effects of total pressure on the surface area to decouple this from the effect of reactant.
- Investigate the relation between the pyrolysis pressure and the initial surface area and the subsequent pore development during gasification.
- Detailed surface area characterisation using multiple techniques such as N_2 and CO_2 adsorption and SAXS/SANS to provide further insight into pore development.
- Study the inhibition of product gases (CO and H_2) at high pressures to better understand the char reactivity and applicability of the LH model.
- Evaluation of different coals varying in terms of mineral matter or demineralised coals to understand the impact of mineral matter on pore development and reaction rate.

- Investigation of the RPM to understand the discrepancies on the structural parameter determined from pore development and reaction rate in order to improve the combined kinetic model.

BIBLIOGRAPHY

Adschiri, T. & Furusawa, T. 1986. Relation between CO_2-reactivity of coal char and BET surface area. *Fuel,* 65 (7):927-931.

Adschiri, T., Shiraha, T., Kojima, T. & Furusawa, T. 1986. Prediction of CO_2 gasification rate of char in fluidized bed gasifier. *Fuel,* 65 (12):1688-1693.

Ahn, D., Gibbs, B., Ko, K. & Kim, J. 2001. Gasification kinetics of an Indonesian sub-bituminous coal-char with CO_2 at elevated pressure. *Fuel,* 80 (11):1651-1658.

Aranda, G., Grootjes, A., Van der Meijden, C., Van der Drift, A., Gupta, D., Sonde, R. 2016. Conversion of high-ash coal under steam and CO_2 gasification conditions. *Fuel processing technology,* 141:16-30.

Aydar, E., Gul, S., Unlu, N., Akgun, F. & Livatyali, H. 2014. Effect of the type of gasifying agent on gas composition in a bubbling fluidized bed reactor. *Journal of the Energy Institute,* 87 (1):35-42.

Azimi, G., Keller, M., Mehdipoor, A. & Leion, H. 2012. Experimental evaluation and modeling of steam gasification and hydrogen inhibition in Chemical-Looping Combustion with solid fuel. *International Journal of Greenhouse Gas Control,* 11:1-10.

Bai, Y., Lv, P., Yang, X., Gao, M., Zhu, S., Yan, L. 2018. Gasification of coal char in H_2O/CO_2 atmospheres: Evolution of surface morphology and pore structure. *Fuel,* 218:236-246.

Bai, Y., Zhu, S., Luo, K., Gao, M., Yan, L. & Li, F. 2017. Coal char gasification in H_2O/CO_2: Release of alkali and alkaline earth metallic species and their effects on reactivity. *Applied Thermal Engineering,* 112:156-163.

Bell, D.A., Towler, B.F. & Fan, M. 2010. Coal gasification and its applications. William Andrew.

Bhatia, S.K. & Perlmutter, D. 1980. A random pore model for fluid-solid reactions: I. Isothermal, kinetic control. *AIChE Journal,* 26 (3):379-386.

Bhatia, S.K. & Vartak, B.J. 1996. Reaction of microporous solids: The discrete random pore model. *Carbon,* 34 (11):1383-1391.

Blackwood, J. & Ingeme, A. 1960. The reaction of carbon with carbon dioxide at high pressure. *Australian Journal of Chemistry,* 13 (2):194-209.

Blackwood, J. & McGrory, F. 1958. The carbon-steam reaction at high pressure. *Australian Journal of Chemistry,* 11 (1):16-33.

Botero, C., Field, R.P., Herzog, H.J. & Ghoniem, A.F. 2013. Impact of finite-rate kinetics on carbon conversion in a high-pressure, single-stage entrained flow gasifier with coal–CO_2 slurry feed. *Applied Energy,* 104:408-417.

Bunt, J.R. 2006. A new dissection methodology and investigation into coal property transformational behaviour impacting on a commercial-scale Sasol-Lurgi MK IV fixed-bed gasifier. Potchefstroom: NWU. (Thesis - PhD).

Burevski, D. 1982. The application of the Dubinin-Astakhov equation to the characterization of microporous carbons. *Colloid and Polymer Science,* 260 (6):623-627.

Chang, G., Xie, J., Huang, Y., Liu, H., Yin, X. & Wu, C. 2017. Gasification reactivity and pore structure development: Effect of intermittent addition of steam on Increasing reactivity of PKS Biochar with CO_2. *Energy & Fuels,* 31 (3):2887-2895.

Chen, C., Wang, J., Liu, W., Zhang, S., Yin, J., Luo, G. 2013. Effect of pyrolysis conditions on the char gasification with mixtures of CO_2 and H_2O. *Proceedings of the combustion institute,* 34 (2):2453-2460.

Chi, W.K. & Perlmutter, D.D. 1989. The effect of pore structure on the char-steam reaction. *AIChE Journal,* 35 (11):1791-1802.

Coetzee, G.H., Sakurovs, R., Neomagus, H.W.J.P., Everson, R.C., Mathews, J.P. & Bunt, J.R. 2017. Particle size influence on the pore development of nanopores in coal gasification chars: From micron to millimeter particles. *Carbon,* 112:37-46.

Coetzee, G.H., Sakurovs, R., Neomagus, H.W.J.P., Morpeth, L., Everson, R.C., Mathews, J.P. 2015. Pore development during gasification of South African inertinite-rich chars evaluated using small angle X-ray scattering. *Carbon,* 95:250-260.

Collot, A.-G. 2006. Matching gasification technologies to coal properties. *International Journal of Coal Geology,* 65 (3–4):191-212.

Devore, J.L. & Farnum, N.R. 2005. Applied Statistics for Engineers and Scientists. Thomson Brooks/Cole.

Di Blasi, C. 2009. Combustion and gasification rates of lignocellulosic chars. *Progress in energy and combustion science,* 35 (2):121-140.

DOE (Department of energy, South Africa). 2017. Coal resources. http://www.energy.gov.za/files/coal_frame.html Date of access: 24 March 2019.

Du toit, G. 2013. The influence of CO_2 on the steam gasification rate of a typical South African coal. Potchefstroom: NWU. (Dissertation - MEng).

Duman, G., Uddin, M.A. & Yanik, J. 2014. The effect of char properties on gasification reactivity. *Fuel processing technology,* 118:75-81.

Dupont, C., Jacob, S., Marrakchy, K.O., Hognon, C., Grateau, M., Labalette, F. 2016. How inorganic elements of biomass influence char steam gasification kinetics. *Energy,* 109:430-435.

Ergun, S. 1956. Kinetics of the reaction of carbon with carbon dioxide. *The Journal of Physical Chemistry,* 60 (4):480-485.

Everson, R.C., Neomagus, H.W., Kasaini, H. & Njapha, D. 2006. Reaction kinetics of pulverized coal-chars derived from inertinite-rich coal discards: gasification with carbon dioxide and steam. *Fuel,* 85 (7):1076-1082.

Everson, R.C., Neomagus, H.W.J.P., Kaitano, R., Falcon, R. & du Cann, V.M. 2008. Properties of high ash coal-char particles derived from inertinite-rich coal: II. Gasification kinetics with carbon dioxide. *Fuel,* 87 (15–16):3403-3408.

Farag, H.A.A., Ezzat, M.M., Amer, H. & Nashed, A.W. 2011. Natural gas dehydration by desiccant materials. *Alexandria Engineering Journal,* 50 (4):431-439.

Fatehi, H. & Bai, X.-S. 2017. Structural evolution of biomass char and its effect on the gasification rate. *Applied Energy,* 185:998-1006.

Feng, B. & Bhatia, S.K. 2003. Variation of the pore structure of coal chars during gasification. *Carbon,* 41 (3):507-523, 2003/01/01/.

Figueiredo, J.L. & Moulijn, J.A. 2012. Carbon and coal gasification: science and technology. Vol. 105: Springer Science & Business Media.

Fogler, H.S. 2013. Elements of Chemical Reaction Engineering. Pearson Education, Limited.

Fushimi, C., Wada, T. & Tsutsumi, A. 2011. Inhibition of steam gasification of biomass char by hydrogen and tar. *Biomass and bioenergy,* 35 (1):179-185.

Gadsby, J., Hinshelwood, C.N. & Sykes, K. 1946. The kinetics of the reactions of the steam-carbon system. *Proceedings of the Royal Society of London. Series A. Mathematical and Physical Sciences,* 187 (1009):129-151.

Gadsby, J., Long, F., Sleightholm, P. & Sykes, K. 1948. The mechanism of the carbon dioxide-carbon reaction. (*In* Proc. R. Soc. Lond. A organised by The Royal Society.

Gomez, A. & Mahinpey, N. 2015. Kinetic study of coal steam and CO_2 gasification: A new method to reduce interparticle diffusion. *Fuel,* 148:160-167.

Gomez, A., Silbermann, R. & Mahinpey, N. 2014. A comprehensive experimental procedure for CO_2 coal gasification: Is there really a maximum reaction rate?. *Applied Energy,* 124:73-81.

Gonzalez, V., Rußig, S., Schurz, M., Krzack, S., Kleeberg, J., Guhl, S. 2018. Experimental investigations on lignite char gasification kinetics using a pressurized drop tube reactor. *Fuel,* 224:348-356.

Gouws, S. 2017. The influence of carbon dioxide on the gasification rate of Highveld coal chars at elevated pressures. Potchefstroom: NWU. (Dissertation - MEng).

Gouws, S.M., Neomagus, H.W.J.P., Roberts, D.G., Bunt, J.R. & Everson, R.C. 2018. The effect of carbon dioxide partial pressure on the gasification rate and pore development of Highveld coal chars at elevated pressures. *Fuel processing technology,* 179:1-9.

Govind, R. & Shah, J. 1984. Modeling and simulation of an entrained flow coal gasifier. *AIChE Journal,* 30 (1):79-92.

Gräbner, M. 2014. Industrial coal gasification technologies covering baseline and high-ash coal. John Wiley & Sons.

Harris, D.J. & Smith, I.W. 1991. Intrinsic reactivity of petroleum coke and brown coal char to carbon dioxide, steam and oxygen. *In* Symposium (International) on Combustion organised by Elsevier.

Harvey, R. & Ruch, R. 1984. Overview of mineral matter in US coals. *Preprints of Papers-American Chemical Society, Division of Fuel Chemistry,* 29 (4):2-8.

Hattingh, B.B., Everson, R.C., Neomagus, H.W. & Bunt, J.R. 2011. Assessing the catalytic effect of coal ash constituents on the CO_2 gasification rate of high ash, South African coal. *Fuel processing technology,* 92 (10):2048-2054.

Hattingh, B.B., Everson, R.C., Neomagus, H.W., Bunt, J.R., Van Niekerk, D., Jordaan, J.H. 2013. Elucidation of the structural and molecular properties of typical South African coals. *Energy & Fuels,* 27 (6):3161-3172.

Henning, A. 2016. Evaluation of the gasification reactivity of Highveld coals for application in the coal to liquids process. Potchefstroom: NWU. (Dissertation - MEng).

Howaniec, N. 2019. Combined Effect of pressure and carbon dioxide activation on porous structure of lignite chars. *Materials,* 12 (8):1326.

Huan, W., Jiao, K., WANG, M.-j. & CHANG, L.-p. 2019. Structural evolution of a bituminous coal char related to its synchronized gasification behavior with H_2O and/or CO_2. *Journal of Fuel Chemistry and Technology,* 47 (4):393-401.

Huang, Z., Zhang, J., Zhao, Y., Zhang, H., Yue, G., Suda, T. 2010. Kinetic studies of char gasification by steam and CO_2 in the presence of H_2 and CO. *Fuel processing technology,* 91 (8):843-847.

Hurt, R., Sarofim, A. & Longwell, J. 1991. The role of microporous surface area in the gasification of chars from a sub-bituminous coal. *Fuel,* 70 (9):1079-1082.

Huttinger, K. 1989. Mechanisms of steam gasification and the role of hydrogen inhibition. *Prepr. Pap., Am. Chem. Soc., Div. Fuel Chem.;(United States),* 34 (CONF-8904169-).

Hüttinger, K.J. & Merdes, W.F. 1992. The carbon-steam reaction at elevated pressure: Formations of product gases and hydrogen inhibitions. *Carbon,* 30 (6):883-894.

IEO (International energy organisation, USA). 2016. World energy demand and economic outlook. https://www.eia.gov/outlooks/ieo/world.cfm Date of access: 24 March 2020.

Irfan, M.F., Usman, M.R. & Kusakabe, K. 2011. Coal gasification in CO_2 atmosphere and its kinetics since 1948: A brief review. *Energy,* 36 (1):12-40.

Jayaraman, K. & Gokalp, I. 2015. Effect of char generation method on steam, CO_2 and blended mixture gasification of high ash Turkish coals. *Fuel,* 153:320-327.

Jayaraman, K., Gokalp, I., Bonifaci, E. & Merlo, N. 2015. Kinetics of steam and CO_2 gasification of high ash coal–char produced under various heating rates. *Fuel,* 154:370-379.

Jayaraman, K., Gökalp, I. & Jeyakumar, S. 2017. Estimation of synergetic effects of CO_2 in high ash coal-char steam gasification. *Applied Thermal Engineering,* 110:991-998.

Jin, H., Fan, C., Wei, W., Zhang, D., Sun, J. & Cao, C. 2018a. Evolution of pore structure and produced gases of Zhundong coal particle during gasification in supercritical water. *The Journal of Supercritical Fluids,* 136:102-109.

Jin, H., Wang, C., Fan, C., Guo, L., Cao, C. & Cao, W. 2018b. Experimental investigation on the influence of the pyrolysis operating parameters upon the char reaction activity in supercritical water gasification. *International Journal of Hydrogen Energy*.

Kabe, T., Ishihara, A., Qian, E.W., Sutrisna, I.P. & Kabe, Y. 2004. Coal and coal-related compounds: structures, reactivity and catalytic reactions. Vol. 150: Elsevier.

Kabir, K.B., Tahmasebi, A., Bhattacharya, S. & Yu, J. 2016. Intrinsic kinetics of CO_2 gasification of a Victorian coal char. *Journal of Thermal Analysis and Calorimetry,* 123 (2):1685-1694.

Kajita, M., Kimura, T., Norinaga, K., Li, C.-Z. & Hayashi, J.-i. 2009. Catalytic and noncatalytic mechanisms in steam gasification of char from the pyrolysis of biomass. *Energy & Fuels,* 24 (1):108-116.

Kajitani, S., Hara, S. & Matsuda, H. 2002. Gasification rate analysis of coal char with a pressurized drop tube furnace. *Fuel,* 81 (5):539-546.

Kajitani, S., Suzuki, N., Ashizawa, M. & Hara, S. 2006. CO_2 gasification rate analysis of coal char in entrained flow coal gasifier. *Fuel,* 85 (2):163-169.

Kajitani, S., Tay, H.L., Zhang, S. & Li, C.Z. 2013. Mechanisms and kinetic modelling of steam gasification of brown coal in the presence of volatile-char interactions. *Fuel,* 103:7-13.

Katta, S. & Keairns, D.L. 1981. Study of kinetics of carbon gasification reactions. *Industrial & Engineering Chemistry Fundamentals,* 20 (1):6-13.

Keller, F., Küster, F. & Meyer, B. 2018. Determination of coal gasification kinetics from integral drop tube furnace experiments with steam and CO_2. *Fuel,* 218:425-438.

Kim, R.-G., Hwang, C.-W. & Jeon, C.-H. 2014. Kinetics of coal char gasification with CO_2: Impact of internal/external diffusion at high temperature and elevated pressure. *Applied Energy,* 129 (Supplement C):299-307.

Komarova, E., Guhl, S. & Meyer, B. 2015. Brown coal char CO_2-gasification kinetics with respect to the char structure. Part I: Char structure development. *Fuel,* 152:38-47.

Krishnamoorthy, V., Krishnamurthy, N. & Pisupati, S.V. 2019. Intrinsic Gasification Kinetics of Coal Chars Generated in a High-Pressure, High-Temperature Flow Reactor. *Chemical Engineering Journal*, 375:122028.

Kwon, T.-W., Kim, S.D. & Fung, D.P. 1988. Reaction kinetics of char—CO_2 gasification. *Fuel,* 67 (4):530-535.

La Villetta, M., Costa, M. & Massarotti, N. 2017. Modelling approaches to biomass gasification: A review with emphasis on the stoichiometric method. *Renewable and Sustainable Energy Reviews,* 74:71-88.

Lee, H.-H., Lee, J.-C., Joo, Y.-J., Oh, M. & Lee, C.-H. 2014a. Dynamic modeling of Shell entrained flow gasifier in an integrated gasification combined cycle process. *Applied Energy,* 131:425-440.

Lee, S., Speight, J.G. & Loyalka, S.K. 2014b. Handbook of alternative fuel technologies. CRC Press.

Li, J., Li, F., Liu, W., Liu, Z., Zhan, H., Zhang, Y. 2018. Influence of pressure on fluidized bed gasifier: Specific coal throughput and particle behavior. *Fuel,* 220:80-88.

Liu, G.-S., Rezaei, H., Lucas, J., Harris, D. & Wall, T. 2000a. Modelling of a pressurised entrained flow coal gasifier: the effect of reaction kinetics and char structure. *Fuel,* 79 (14):1767-1779.

Liu, G.-s., Tate, A., Bryant, G. & Wall, T. 2000b. Mathematical modeling of coal char reactivity with CO_2 at high pressures and temperatures. *Fuel,* 79 (10):1145-1154.

Liu, L., Cao, Y. & Liu, Q. 2015. Kinetics studies and structure characteristics of coal char under pressurized CO_2 gasification conditions. *Fuel,* 146:103-110.

Liu, L., Cao, Y., Liu, Q. & Yang, J. 2017. Experimental and kinetic studies of coal–CO_2 gasification in isothermal and pressurized conditions. *RSC Advances,* 7 (4):2193-2201.

Lowell, S., Shields, J.E., Thomas, M.A. & Thommes, M. 2012. Characterization of porous solids and powders: surface area, pore size and density. Vol. 16: Springer Science & Business Media.

Lussier, M., Zhang, Z. & Miller, D.J. 1998. Characterizing rate inhibition in steam/hydrogen gasification via analysis of adsorbed hydrogen. *Carbon,* 36 (9):1361-1369.

Ma, Z., Bai, J., Li, W., Bai, Z. & Kong, L. 2013. Mineral transformation in char and its effect on coal char gasification reactivity at high temperatures, Part 1: Mineral transformation in char. *Energy & Fuels,* 27 (8):4545-4554.

Malekshahian, M. & Hill, J.M. 2011. Kinetic analysis of CO_2 gasification of petroleum coke at high pressures. *Energy & Fuels,* 25 (9):4043-4048.

Marsh, H. 1987. Adsorption methods to study microporosity in coals and carbons—a critique. *Carbon,* 25 (1):49-58.

McKendry, P. 2002. Energy production from biomass (part 3): gasification technologies. *Bioresource technology,* 83 (1):55-63.

Megaritis, A., Zhuo, Y., Messenböck, R., Dugwell, D. & Kandiyoti, R. 1998. Pyrolysis and gasification in a bench-scale high-pressure fluidized-bed reactor. *Energy & Fuels,* 12 (1):144-151.

Meijer, R., Kapteijn, F. & Moulijn, J.A. 1994. Kinetics of the alkali-carbonate catalysed gasification of carbon: 3. H_2O gasification. *Fuel,* 73 (5):723-730.

Molina, A. & Mondragon, F. 1998. Reactivity of coal gasification with steam and CO_2. *Fuel,* 77 (15):1831-1839.

Morin, M., Pécate, S., Masi, E. & Hémati, M. 2017. Kinetic study and modelling of char combustion in TGA in isothermal conditions. *Fuel,* 203:522-536.

Moulijn, J.A. & Kapteijn, F. 1995. Towards a unified theory of reactions of carbon with oxygen-containing molecules. *Carbon,* 33 (8):1155-1165.

Mühlen, H.-J., van Heek, K.H. & Jüntgen, H. 1985. Kinetic studies of steam gasification of char in the presence of H_2, CO_2 and CO. *Fuel,* 64 (7):944-949.

Ng, S.H., Fung, D.P. & Kim, S.D. 1988. Study of the pore structure and reactivity of Canadian coal-derived chars. *Fuel,* 67 (5):700-706.

Nozaki, T., Adschiri, T. & Fujimoto, K. 1991. Comparison of steam gasification rate and carbon dioxide gasification rate through the surface oxide complexes. *Energy & Fuels,* 5 (4):610-611.

Nozaki, T., Adschiri, T. & Fujimoto, K. 1992. Coal char gasification under pressurized CO_2 atmosphere. *Fuel,* 71 (3):349-350.

Oakey, J. 2015. Fuel Flexible Energy Generation: Solid, Liquid and Gaseous Fuels. Woodhead Publishing.

Ochoa, J., Cassanello, M., Bonelli, P. & Cukierman, A. 2001. CO_2 gasification of Argentinean coal chars: a kinetic characterization. *Fuel processing technology,* 74 (3):161-176.

Okolo, G.N., Everson, R.C., Neomagus, H.W., Roberts, M.J. & Sakurovs, R. 2015a. Comparing the porosity and surface areas of coal as measured by gas adsorption, mercury intrusion and SAXS techniques. *Fuel,* 141:293-304.

Okolo, G.N., Neomagus, H.W.J.P., Everson, R.C., Roberts, M.J., Bunt, J.R., Sakurovs, R. 2015b. Chemical–structural properties of South African bituminous coals: Insights from wide angle XRD–carbon fraction analysis, ATR–FTIR, solid state 13C NMR, and HRTEM techniques. *Fuel,* 158:779-792.

Pan, J., Niu, Q., Wang, K., Shi, X. & Li, M. 2016. The closed pores of tectonically deformed coal studied by small-angle X-ray scattering and liquid nitrogen adsorption. *Microporous and Mesoporous Materials,* 224:245-252.

Park, H.Y. & Ahn, D.H. 2007. Gasification kinetics of five coal chars with CO_2 at elevated pressure. *Korean Journal of Chemical Engineering,* 24 (1):24-30.

Porada, S., Czerski, G., Grzywacz, P., Makowska, D. & Dziok, T. 2017. Comparison of the gasification of coals and their chars with CO_2 based on the formation kinetics of gaseous products. *Thermochimica Acta,* 653:97-105.

Rezaiyan, J. & Cheremisinoff, N.P. 2005. Gasification technologies: a primer for engineers and scientists. CRC press.

Roberts, D. & Harris, D. 2000. Char gasification with O_2, CO_2, and H_2O: Effects of pressure on intrinsic reaction kinetics. *Energy & Fuels,* 14 (2):483-489.

Roberts, D. & Harris, D. 2006. A kinetic analysis of coal char gasification reactions at high pressures. *Energy & Fuels,* 20 (6):2314-2320.

Roberts, D. & Harris, D. 2007. Char gasification in mixtures of CO_2 and H_2O: competition and inhibition. *Fuel,* 86 (17):2672-2678.

Roberts, D.G. & Harris, D.J. 2012. High-Pressure Char Gasification Kinetics: CO Inhibition of the C–CO_2 Reaction. *Energy & Fuels,* 26 (1):176-184.

Roberts, D.G., Hodge, E.M., Harris, D.J. & Stubington, J.F. 2010. Kinetics of char gasification with CO2 under regime II conditions: effects of temperature, reactant, and total pressure. *Energy & Fuels,* 24 (10):5300-5308.

Roberts, M.J., Everson, R.C., Neomagus, H.W., Van Niekerk, D., Mathews, J.P. & Branken, D.J. 2015. Influence of maceral composition on the structure, properties and behaviour of chars derived from South African coals. *Fuel,* 142:9-20.

Sahini, M. & Sahimi, M. 2003. Applications Of Percolation Theory. Taylor & Francis.

Saito, T., Nakayama, K., Lin, S. & Takarada, T. 2017. Kinetics of char and catalyzed char gasification at high steam partial pressures with or without H_2 for chemical looping coal combustion. *Journal of Chemical Engineering of Japan,* 50 (7):554-560.

Schmal, M., Monteiro, J.L.F. & Toscani, H. 1983. Gasification of high ash content coals with steam in a semibatch fluidized bed reactor. *Industrial & Engineering Chemistry Process Design and Development,* 22 (4):563-570.

Sha, X.-Z., Chen, Y.-G., Cao, J., Yang, Y.-M. & Ren, D.-Q. 1990. Effects of operating pressure on coal gasification. *Fuel,* 69 (5):656-659.

Shadle, L.J., Berry, D.A. & Syamlal, M. 2002. Coal conversion processes, gasification. *Kirk-Othmer Encyclopedia of Chemical Technology*.

Sing, K.S. 1985. Reporting physisorption data for gas/solid systems with special reference to the determination of surface area and porosity (Recommendations 1984). *Pure and applied chemistry,* 57 (4):603-619.

Smith, K.L., Smoot, L.D., Fletcher, T.H. & Pugmire, R.J. 2013. The structure and reaction processes of coal. Springer Science & Business Media.

Smoot, L.D. & Smith, P.J. 1985. Coal combustion and gasification. Springer Science & Business Media.

Speight, J.G. 2012. The Chemistry and Technology of Coal, Third Edition. Taylor & Francis.

Steibel, M., Halama, S., Geißler, A. & Spliethoff, H. 2017. Gasification kinetics of a bituminous coal at elevated pressures: Entrained flow experiments and numerical simulations. *Fuel,* 196:210-216.

Strange, J. & Walker Jr, P. 1976. Carbon-carbon dioxide reaction: Langmuir-Hinshelwood kinetics at intermediate pressures. *Carbon,* 14 (6):345-350.

Szekely, J. 2012. Gas-solid reactions. Elsevier.

Tanner, J. & Bhattacharya, S. 2016. Kinetics of CO_2 and steam gasification of Victorian brown coal chars. *Chemical Engineering Journal,* 285:331-340.

Tilghman, M.B. & Mitchell, R.E. 2015. Coal and biomass char reactivities in gasification and combustion environments. *Combustion and Flame,* 162 (9):3220-3235.

Tomaszewicz, M., Tomaszewicz, G. & Sciazko, M. 2017. Experimental study on kinetics of coal char–CO_2 reaction by means of pressurized thermogravimetric analysis. *Journal of Thermal Analysis and Calorimetry,* 130 (3):2315-2330.

Tremel, A., Haselsteiner, T., Kunze, C. & Spliethoff, H. 2012. Experimental investigation of high temperature and high pressure coal gasification. *Applied Energy,* 92:279-285.

Tremel, A. & Spliethoff, H. 2013. Gasification kinetics during entrained flow gasification–Part II: Intrinsic char reaction rate and surface area development. *Fuel,* 107:653-661.

van Dyk, J.C., Keyser, M.J. & Coertzen, M. 2006. Syngas production from South African coal sources using Sasol–Lurgi gasifiers. *International Journal of Coal Geology,* 65 (3–4):243-253.

Veca, E. & Adrover, A. 2014. Isothermal kinetics of char-coal gasification with pure CO_2. *Fuel,* 123:151-157.

Walker Jr, P., Rusinko Jr, F. & Austin, L.G. 1959. Gas reactions of carbon. *In* Advances in catalysis. Elsevier, 133-221.

Wall, T.F., Liu, G.-s., Wu, H.-w., Roberts, D.G., Benfell, K.E., Gupta, S. 2002. The effects of pressure on coal reactions during pulverised coal combustion and gasification. *Progress in energy and combustion science,* 28 (5):405-433.

Wang, F.Y. & Bhatia, S.K. 2001. A generalised dynamic model for char particle gasification with structure evolution and peripheral fragmentation. *Chemical Engineering Science,* 56 (12):3683-3697.

Wang, G., Zhang, J., Hou, X., Shao, J. & Geng, W. 2015. Study on CO_2 gasification properties and kinetics of biomass chars and anthracite char. *Bioresource technology,* 177:66-73.

Wang, M., Roberts, D.G., Kochanek, M.A., Harris, D.J., Chang, L. & Li, C.-Z. 2013. Raman spectroscopic investigations into links between intrinsic reactivity and char chemical structure. *Energy & Fuels,* 28 (1):285-290.

Wang, Y. & Bell, D.A. 2017. Competition between H_2O and CO_2 during the gasification of Powder River Basin coal. *Fuel,* 187:94-102.

Wang, Z.-H., Zhang, K., Li, Y., He, Y., Kuang, M., Li, Q., et al. 2016. Gasification characteristics of different rank coals at H_2O and CO_2 atmospheres. *Journal of Analytical and Applied Pyrolysis,* 122:76-83.

WEC (World energy council, USA). 2019. World energy resources. https://www.worldenergy.org/wp-content/uploads/2016/10/World-Energy-Resources-Full-report-2016.10.03.pdf Date of access: 29 March 2019.

Wills, B.A. & Finch, J. 2015. Wills' mineral processing technology: an introduction to the practical aspects of ore treatment and mineral recovery. Butterworth-Heinemann.

Ye, D., Agnew, J. & Zhang, D. 1998. Gasification of a South Australian low-rank coal with carbon dioxide and steam: kinetics and reactivity studies. *Fuel,* 77 (11):1209-1219.

Zhang, F., Xu, D., Wang, Y., Wang, Y., Gao, Y., Popa, T. 2015. Catalytic CO_2 gasification of a Powder River Basin coal. *Fuel processing technology,* 130:107-116.

Zhang, L., Huang, J., Fang, Y. & Wang, Y. 2006. Gasification reactivity and kinetics of typical Chinese anthracite chars with steam and CO_2. *Energy & Fuels,* 20 (3):1201-1210.

Zhang, R., Chen, Y., Lei, K. & Liu, D. 2017. The effects of specific surface area and ash on char gasification mechanisms in the mixture of H_2O, CO_2, H_2 and CO. *Fuel,* 209:109-116.

Zhang, Z., Lussier, M.G. & Miller, D.J. 2000. Stability of hydrogen adsorbed on Saran char. *Carbon,* 38 (9):1289-1296.

Zou, X., Ding, L., Liu, X., Guo, Q., Lu, H. & Gong, X. 2018. Study on effects of ash on the evolution of physical and chemical structures of char during CO_2 gasification. *Fuel,* 217:587-596.

APPENDIX A

(EXPERIMENTAL DESCRIPTION AND CONDITIONS)

A.1 Extended experimental description

The High-Pressure Fixed Bed Reactor (HPFBR) was built in-house to conduct high pressure gasification experiments. The rig is fabricated to withstand elevated pressures of up to 50 bar and temperatures of about 1000 °C. The gasification unit in which reactions take place consists of a vertical split furnace and reactor. The utilised reactor which is corrosion-resistant (93 cm C276 alloy) was supplied by Multi Alloys® and the furnace was supplied by Lenton® (Model: VST 12/100/200). The furnace provided with an overall heating length of 35 cm and was mounted on the vertical stand with a near hinge, allowing dislocation from the reactor vessel. It also consists of external insulation beyond the heated length. In order to control the heat provided by the furnace, an N-type thermocouple equipped with the furnace was used to measure the temperature and was further controlled by making use of a Eurotherm® PID temperature controller, model 201.

The reactor has an outside diameter of 2.7 cm and an inside diameter of 2.1 cm. The sample bed (quartz filter disc) is mounted and welded to a flange at the centre of the reactor and is capable of handling high temperatures. The quartz filter disc was supplied by Technical Glass Products® and consisted of a nominal pore size of -40+15 μm. At the top of the pipe, a T-type fitting provided by Swagelok® is equipped to facilitate a connection of a 650 x 3 mm K-type thermocouple (provided by WIKA®) and the reagent gas stream. The thermocouple is placed and positioned ~5 mm above the sample bed within the pipe. This thermocouple measures the reaction temperature and the readings are logged into a computer. The reaction or system pressure within the reactor vessel is also measured using a UniTrans pressure transmitter supplied by WIKA®. The pressure transmitter is capable of providing pressure readings from 0-40 bar(a) with pressure differences of 1.0 mbar. An EPC (Electronic Pressure Controller) supplied by Bronkhorst High-Tech® which is sealed with an EPDM material was used to electronically control the system pressure in the pipe from the computer using RS-232 standard communication. The EPC has an operating range of 0-80 bar(a) and the electronically controlled pressure is further logged on the computer.

The experimental rig is also equipped with a condenser unit, moisture trap, steam generator, controllers, flow meters, and gas analysers. The steam generation unit comprises a steam generator and an isocratic LS-Class® HPLC pump (Model: P-LS05S-8) capable of providing with

flow rate ranges of 0.01-4.0 ml/min and pressure ranges of 0-490 bar(a). The HPLC pump is used to pump de-ionised water from a 2.5 L water reservoir to the steam generator. The steam generator was manufactured in-house by making use of a (1) 5.5 m long stainless steel tube with an OD of 1/8", (2) two 9.52 x 177 mm cartridge heaters supplied by Thermon® SA, and (3) 20 cm long aluminium round bar with an OD of 60 mm supplied by Aluminium City®. The cartridge heaters are equipped with a J-type thermocouple and the temperature was monitored and controlled by making use of an auxiliary Shinko® temperature controller. Both the cartridge heaters with a power up to 490 W were mounted within the aluminium bar and the stainless steel tube was wrapped helically around with approximately 30 windings, 6 mm apart. The condenser unit consists of three high pressure stainless steel tubes contained in a 50L aluminium vessel (For ice-water bath) constructed in-house. The tubes are provided by swagelok® and can handle pressures of about 200 bar. These tubes (Two 1 L and 0.5 L) are equipped with a ¼" stainless steel piping providing an inlet and outlet path-way for the product gas and also a drainage system at the bottom. Each tube is equipped with a high pressure one valve that enables water to be removed connected to ¼" swagelok® pipe situated 10 cm from the bottom. To ensure efficient removal of moisture, the experimental rig is also equipped with two moisture traps constructed in-house which contains pellets of 3Å molecular sieves. These moisture traps are made from a 30 cm stainless steel pipe with a diameter of about 2 cm.

Three flow gas controllers supplied by supplied Bronkhorst High-Tech® were used to control and monitor the total flow rate of gas fed (N_2 and CO_2 gas) to the rig and product gas. These controllers were used to electronically control (via RS-232 communication) the concentration of each gas whereby the operating range was 0-5 NL/min and 0-0.75 NL/min for N_2 and CO_2 MFC, respectively. The total product gas rate was measured and logged on the computer using TMFM (Thermal Mass Flow Meter) of which has an operating range of 0-2.16 NL/min.

A.2 Evaluation of experimental conditions

A.2.1 Pyrolysis isothermal zone

To establish the position at which a sample holder must be located within the tube furnace, a temperature profile was examined at pyrolysis temperature and flow conditions. An external K-type thermocouple with a length of 100 cm was used to measure the heating zones temperatures throughout the length of the furnace with increments of 10 cm from both sides. The temperature distribution or profile that was obtained under these conditions is shown in Figure A-1.

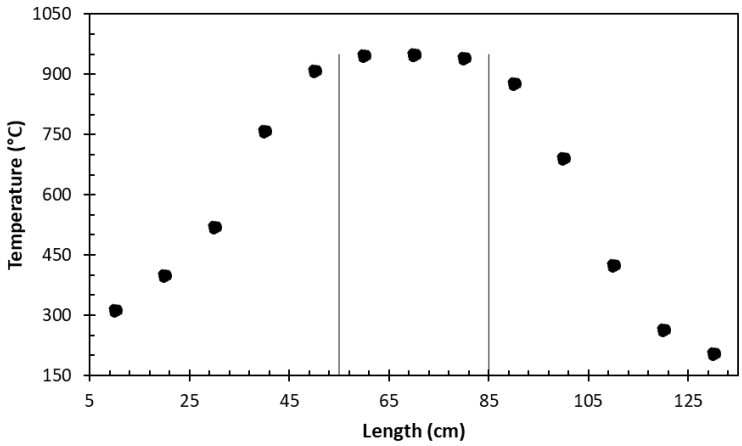

Figure A-1: Temperature profile of the tube furnace

The temperature was measured from both sides of the tube furnace over the tube length. As shown in Figure A-1 it was found that the sample holder must be located at a length of 55 cm from left-to-right and 45 cm from right-to-left, resulting in a heating zone of 300 mm within the centre of the furnace.

A.2.2 Gasification and steam generation temperature

The reaction and steam generation temperatures were monitored and logged into the computer. The temperature profiles of the selected temperatures are illustrated in Figure A-2.

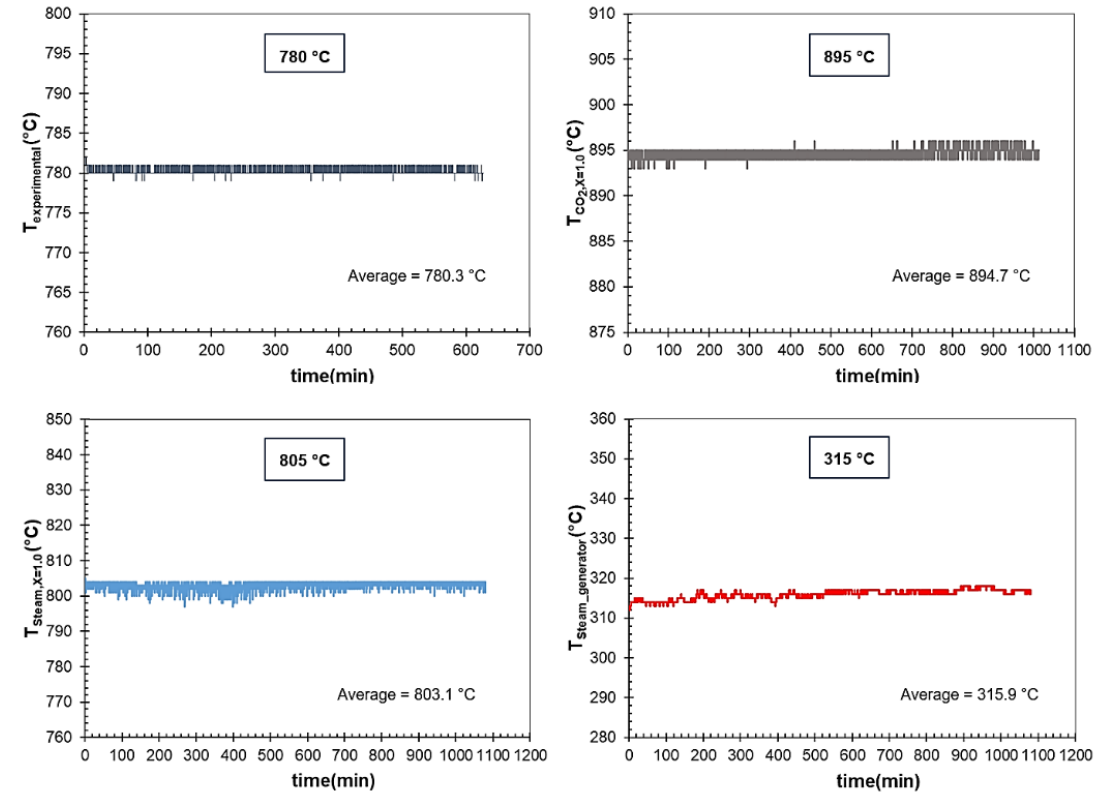

Figure A-2: Temperature profiles

For both the reaction and steam generation temperature, the deviations between the average and the desired temperature were found to less than 2%.

A.2.3 Total pressure

The total or system pressure was measured and logged through the entire gasification experiments and pressure profiles are presented in the following figure.

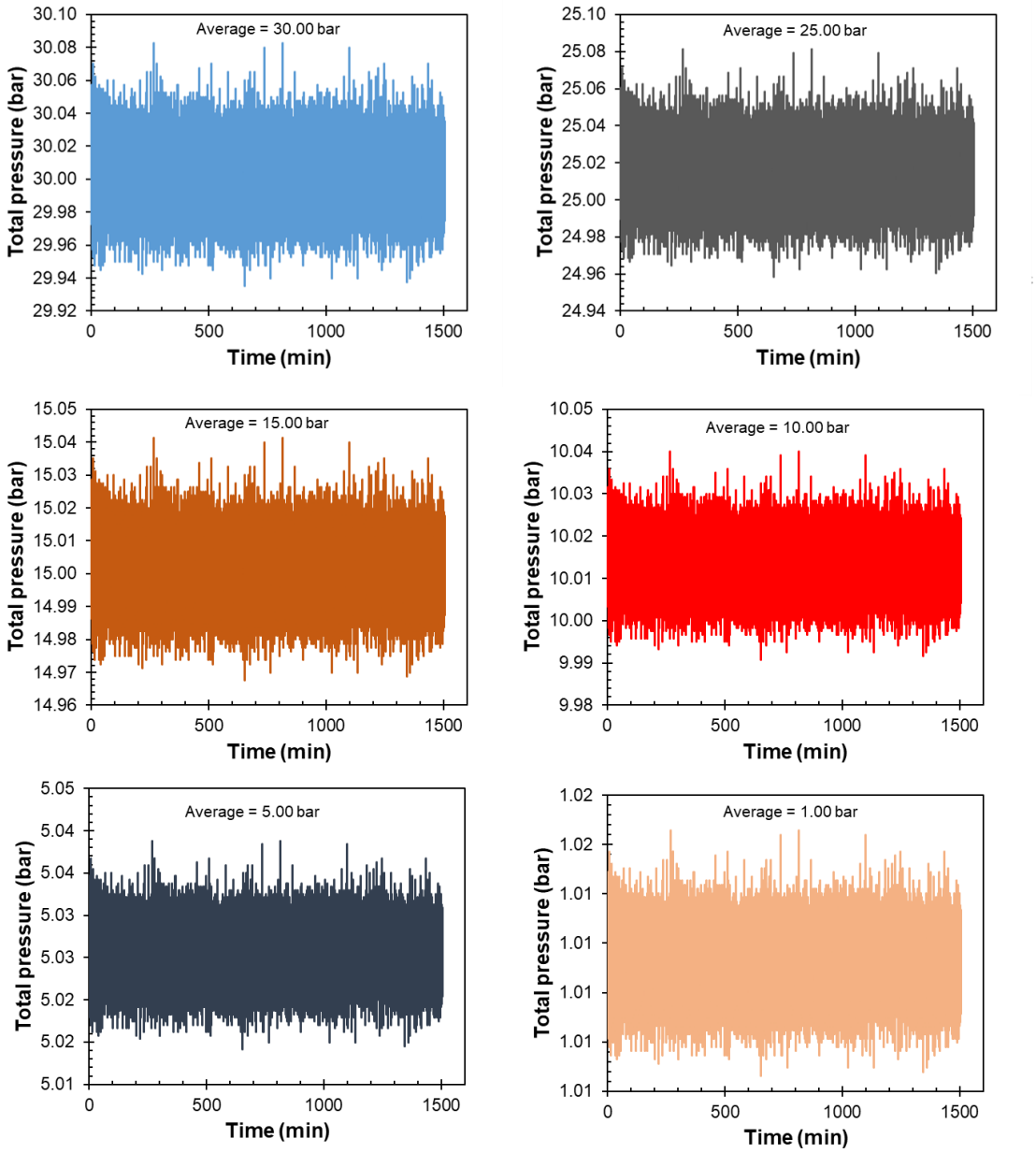

Figure A-3: Total or system pressure profiles

APPENDIX B

(EQUIPMENT CALIBRATION)

B.1 Mass flow controller

The mass flow controllers were utilised in the char gasification experiments to control the flow rates of N_2 and CO_2 gas fed to the reactor, which were re-calibrated prior to experimentation.

B.1.1 N_2 Mass flow controller

The N_2 Mass Flow Controller (MFC) supplied by Bronkhorst High-Tech® is capable of providing with the flow rate range of 0 to 5 NL/min. This MFC was re-calibrated to ensure that the specific amount of N_2 is present in the total gas stream. The bubble-flow meter with volume increments of 50 ml was used to monitor the actual N_2 flow rate at a certain MFC set-point under atmospheric conditions. In this case, MFC set-point ranging from 0.5-3.0 NL/min were selected and the actual flow rate was determined at each set-point. The measured actual flow rate was converted to standard flow using Equation (B.1) at standardised temperature and pressure of 0 °C and 1 atm, respectively.

$$\dot{V}_{STP} = \dot{V}_a \left(\frac{T_{STP}}{T_a}\right)\left(\frac{P_a}{P_{STP}}\right) \tag{B.1}$$

The calibration data was used to determine the N_2 flow rate required for conducting high N_2 concentrations experiments ranging from 60-100% (moles) of which resulted in a flow rate range of 1.2-2.0 NL/min with respect to the total gas flow rate used. The experiments required low concentrations ranging from 0-40% were conducted by using CO_2 MFC which was capable of providing with low flow rates (discussed in Appendix B.1.2). The results obtained for the actual flow rate and standard flow rate of the N_2 gas at each MFC set-point are summarised in Table B-1.

Table B-1: N_2 MFC calibration data

MFC set-point (NL/min)	N_2 flow rate (L/min)	N_2 flow rate (NL/min)
0.5	0.65	0.53
1.0	1.30	1.05
1.5	1.96	1.58
2.0	2.59	2.10
2.5	3.23	2.61
3.0	3.88	3.14

The results summarised in Table B-1 shown a form of linear behaviour and the linear regression model was used to determine the calibration curve that expresses the MFC set-point as a function of standard flow rate. In this case, the calibration curve was used as presented in Equation B.2 to determine a specific flow rate in conjunction with the MFC set point.

$$MFC_{set-point}(NL/min) = 0.959\dot{V}_{STP} - 0.010 \quad \text{(B.2)}$$

The model resulted in an R^2 value of 1 which implies that the model can sufficiently correlate the actual flow rate of N_2 gas in standardised conditions with the corresponding MFC set-point. Furthermore, the variance between the actual MFC set-point and the one determined from the calibration curve at a specific standard flow rate of nitrogen was found to be less than 1%.

The nitrogen MFC was utilised to conduct high concentrations of CO_2 experiments because of limitations on the CO_2 MFC set-point range especially for high partial pressures ranging from 20-30 bar. This was applied for the gasification experiments with pure CO_2 for the desired partial pressure. The nitrogen MFC was then re-calibrated at similar conditions and methods as discussed previously but in this case, CO_2 gas was used instead of N_2 gas. From the calibration data with CO_2, the calibration curve was derived and is given Equation B.3.

$$MFC_{set-point}(NL/min) = 1.195\dot{V}_{STP} - 0.119 \quad \text{(B.3)}$$

B.1.2 CO_2 Mass flow controller

The CO_2 MFC also supplied by Bronkhorst High-Tech® with a flow range of 0 to 0.75 NL/min was utilised to control the concentration of the CO_2 gas introduced in the reactor especially for low concentrations ranging from 10-40% (moles). The results of the actual flow rate and standard flow

rate obtained by making use of the bubble-flow meter and Equation B.1 respectively, are summarised in Table B-2.

Table B-2: CO_2 calibration data

MFC set-point (NL/min)	CO_2 flow rate (L/min)	CO_2 flow rate (NL/min)
0.2	0.28	0.23
0.3	0.41	0.33
0.4	0.55	0.45
0.5	0.67	0.55
0.6	0.83	0.67
0.7	0.98	0.80

As shown in Table B-2, the calibration data was obtained to relate the CO_2 MFC set-point with the actual flow rate at standard conditions. The correlation coefficient was also determined and was found to be 1 indicating a good correlation between the data points with a variance of less than 1%. From the calibration data, the calibration curve was determined for the CO_2 gas flow rate by making use of a linear regression method and is given in Equation B.4.

$$MFC_{set-point}(NL/min) = 0.879\dot{V}_{STP} + 0.008 \quad \text{(B.4)}$$

As for the low concentrations for N_2 gas, the CO_2 MFC was used since it is capable of providing with low flow rates less than 1 NL/min and this was done in accordance with the high partial pressures of CO_2 which required low flow rates of N_2 gas. In this case, the CO_2 MFC was re-calibrated using N_2 gas, and the calibration curve determined from the calibration data is given as follows:

$$MFC_{set-point}(NL/min) = 0.570\dot{V}_{STP} + 0.004 \quad \text{(B.5)}$$

B.2 Rotameter

The rotameter was used during the gasification experiments to illustrate and monitor the product gas flow rate admitted to the gas analysers. The rotameter was then calibrated by making use of the bubble-flow meter and the N_2 gas to determine the actual flow rate on the basis of standard conditions. The calibration data results obtained are presented in the following table.

Table B-3: Rotameter calibration data

N_2 actual flow (NL/min)	Rotameter flow (L/min)
0.5	1.50
1.0	2.50
2.0	4.75
3.0	6.75
4.0	8.75
5.0	10.75

In this case, the nitrogen flow rate was controlled by using the MFC and based on the knowledge of the actual flow rate at standard conditions provided from the calibration data, the N_2 gas flow rate was varied from 0.5-5.0 NL/min while monitoring the reading on the rotameter. Based on the results obtained, the reading on the rotameter was kept at 2.5 L/min by purging the total gas (2 NL/min) which is equivalent to 1 NL/min of the product gas for safety and accuracy of the measuring equipment.

B.3 HPLC pump

The HPLC pump was used for char-steam gasification experiments to pump the de-ionised water from the water reservoir to the steam generator and also provide the desired pressure of the steam. This pump is capable of providing with the liquid flow rate range of 0-4 ml/min (0.001 accuracy) and pressure ranges of 1-490 bar.

The water flow rate was calibrated by means of changing the pump set-point and monitoring the actual flow rate at atmospheric pressure. This was conducted by pumping the de-ionised water (0.1-3 ml/min set points) from the water reservoir into a 50 ml graduated cylinder to measure the actual volume of the water at a specific time. The procedure was repeated five times to evaluate the precision and accuracy of the pump. The average actual flow rate was then obtained from the time and volume data at each set-point and the results are summarised in Table B-4.

Table B-4: Pump flow rate calibration data

Set-point flow rate (ml/min)	Average actual flow rate (ml/min)
0.100	0.090
0.500	0.477
1.000	0.950
1.500	1.470
2.000	1.960
2.500	2.450
3.000	2.940

The calibration curve was then derived from the obtained data in order to provide an equation that relates the pump set-point flow rate and the actual flow rate of the de-ionised water. The linear regression method was used to derive the equation and is given as follows with a correlation coefficient (R^2) of 0.9992:

$$Pump\ flow\ rate_{set-point}(L/min) = 1.0142\dot{V}_{\ actual} + 0.0167 \qquad \text{(B.6)}$$

From the derived equation, the pump flow rate set-point can be obtained for a specific water flow rate desired for a specific gasification experiment. The desired actual flow rate will depend on the concentration of the steam required for conducting the gasification experiments at certain steam partial pressure and the discussions are covered in Appendix B.4.

B.4 Steam flow rate

The steam flow rate was correlated to the water flow rate fed to the steam generator based on the water balance. ASPEN simulation (at atmospheric pressure) and water balance experiments (at high pressures) were performed to evaluate the correlation efficiency between the water flow rate and the actual steam flow rate.

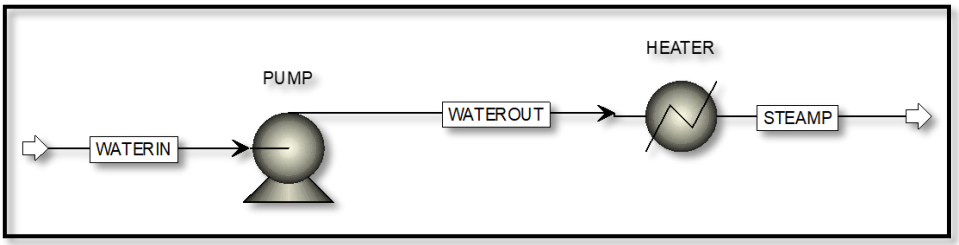

Figure B-1: Water balance and evaluation of steam flow rates using ASPEN simulation

Based on the total flow rate of 2 NL/min used in this study, the steam flow rate at standard conditions was determined and therefore correlated to the subsequent water flow rate. The results of the steam flow rate correlated to the water flow rate using mass balance and ASPEN simulation are summarised in Table B-5.

Table B-5: Results of correlating steam flow rate and water flow rate using mass balance and ASPEN simulation

y_{steam} (mol%)	V_{steam} (NL/min)	V_{water} (ml/min)	ASPEN-water flow rate (ml/min)
5	0.1	0.080	0.082
10	0.2	0.161	0.164
15	0.3	0.241	0.245
20	0.4	0.322	0.327
25	0.5	0.402	0.409
30	0.6	0.482	0.491
35	0.7	0.563	0.572
40	0.8	0.643	0.654
50	1.0	0.804	0.818
60	1.2	0.965	0.981
70	1.4	1.126	1.144
80	1.6	1.286	1.308
90	1.8	1.447	1.471
100	2	1.608	1.635

From Table B-5, it was observed that the correlation of steam flow rate and water flow rate can be described using the ASPEN results and mass balance calculations. Using the linear regression method the steam flow rate can be related to water flow rate using Equation B.7.

$$\dot{V}_{water}(ml/min) = 0.804\dot{V}_{steam}(nL/min) \quad \text{(B.7)}$$

To evaluate the applicability of Equation B.7 for high pressures, water balance on the steam fed to the reactor and collected in the condenser was done on the selected high pressure steam gasification experiments. The results and conditions are summarised in Table B-6.

Table B-6: Results of water balance at high pressures

y_{steam} (mol%)	P_{total} (bar)	V_{water} (ml/min)	t_{run} (min)	$V_{in,t}$ (ml)	$V_{out,f}$ (ml)	%Difference
50	5	0.804	238	192	196	2
50	10	0.804	298	240	244	2
66.7	15	1.073	285	306	315	3
50	15	0.804	302	243	257	6
75	20	1.206	223	269	277	3
66.7	30	1.073	259	278	289	4

As shown in Table B-6, the total water fed to the reactor and collected at the end of the experiment is almost in the same order with a %difference of less than 6. Therefore, Equation B.7 is suitable in describing the relationship between the inlet water and steam flow rate.

B.5 NDIR gas analyser

The CO and CO_2 gas analyser (NDIR) were used to measure the carbon reacted during gasification experiments. To accurately measure the CO and CO_2 concentrations, the analysers were calibrated to correct for span-drift using known standard gas concentrations. The known CO (2800 and 1450 ppm) and CO_2 (1900 and 1050 ppm) were used to provide the calibration curve. For the evaluation of cross-reference between the analysis of CO and CO_2, CO calibration was fed to the CO_2 analyser and vice-verse for CO analyser. The cross-reference was seen to be less than 50 ppm and 10 ppm for CO_2 and CO analyser, respectively.

The calibration curves developed were aimed to determine the “true” concentrations of CO and CO_2 measured from the product gas. The standard calibration gases were fed to the analysers and the readings were recorded. The results of the detected concentrations using the calibration gases are summarised in Table B-7.

Table B-7: Calibration results for the CO and CO_2 analyser

CO analyser		**CO_2 analyser**	
CO,detected (ppm)	CO,actual (ppm)	CO_2,detected (ppm)	CO_2,actual (ppm)
1175	0	0	0
1185	0	100	0
1450	2600	1050	1200
2800	4845	1900	1900
2800	4900	1900	2100

A linear regression method was used to relate the detected concentration and the "true" concentration resulting in the following equations:

$$[CO]_{true} = 2.7374[CO]_{detected} - 2682.8 \quad \text{(B.8)}$$

$$[CO_2]_{true} = 1.0816[CO_2]_{detected} - 30.679 \quad \text{(B.9)}$$

Due to trivial span-drift, the gas analysers were calibrated regularly and the calibration curves were re-calculated.

APPENDIX C

(MEASUREMENTS AND CALCULATIONS)

C.1 Determination of char gasification rates

C.1.1 Specific reaction rate (Char-CO_2 experiments)

The coal char gasification with CO_2 results in the formation of carbon monoxide as a product. Based on the experimental methodology described in detail in Chapter 4, the concentration of CO that is formed is monitored and logged, from which the true CO concentration is determined using the calibration curve described in Appendix B.5. From the CO concentration, the rate of carbon consumed during gasification, carbon conversion, and the specific reaction rate was determined.

Rate of converted carbon (r_c)

To determine the specific reaction rate for the consumption or conversion of the carbon within the char that is reacting with CO_2, the stoichiometry of the overall reaction is used. In this case, the rate of carbon converted is directly determined from the measured rate of CO produced. The rate of carbon converted at a specific instant is then calculated with the following equation;

$$r_c = \frac{1}{2}\left(\frac{\dot{V}_T}{\hat{V}_{STP}}\right)[CO]MW_c \qquad \text{(C.1)}$$

Where r_c is the rate of carbon converted at an instant, [CO] is the true CO concentration produced, MW_c is the molecular weight of carbon, $\dot{V}_T$ is the total standard volume flow rate of product gas, $\hat{V}_{STP}$ is the standard molar volume at standard temperature and pressure.

Since the true CO concentration is in terms of parts per million (ppm), then the rate at which carbon is converted is expressed in terms of 10^5 (g/s). From Equation C.1, the total standard volume flow rate of the product gas is converted to a total molar flow rate, from which the molar flow rate of CO produced is obtained based on the measured CO concentration. Thereafter, the stoichiometry of the overall CO_2 gasification is used to convert the determined molar flow rate of CO produced to carbon converted or consumed. In most applications and literature, the specific reaction rate is expressed in terms of the mass of carbon converted at certain time interval per mass of carbon fed, as a result, the determined molar flow rate of carbon converted is further transformed to rate of carbon converted at any instant, by utilising the molecular weight of carbon.

Carbon conversion (*X*)

At this stage, it evident that during char-CO_2 gasification, the carbon within the char matrix is converted to CO and the rate at which carbon is converted can be determined by making use of Equation B.1. To determine the specific reaction rate, the carbon conversion is determined from the rate of carbon converted to measure the reaction's progress. The carbon conversion is expressed as the mass of carbon converted at a certain interval (cumulative) per mass of carbon fed to the reactor. This expression is illustrated in Equation C.2 as follows;

$$X = \frac{\Delta m_{C,t}}{m_{C,0}} = \frac{\Delta m_{C,t}}{m_{Char}\left(1 - x_{ash,d.b}\right)x_{C,daf}} \cong \frac{m_{C,0} - m_{C,t}}{m_{C,0}} \qquad \text{(C.2)}$$

Where X is carbon conversion, $m_{C,0}$ is mass of carbon fed (initial), m_{Char} is mass of char sample, $x_{ash,d.b}$ is the weight percentage of ash on a dry basis or moisture-free basis, $x_{C,daf}$ is the weight percentage of carbon within the char at dry-ash free, Δm_c is the carbon cumulative mass from the initial time to s certain time (t). The carbon cumulative mass is determined by taking an integral on the rate of carbon converted and further approximated by numerical integral based on the trapezoidal rule, as expressed and simplified in Equation C.3.

The mass of carbon fed which is given in the denominator of Equation C.2 is attributed to the amount of carbon present in the char sample. In detail, the char fed into the reactor has a certain amount of volatile matter, ash, and fixed carbon, as a result, the amount of carbon fed into the reactor is mainly the amount of carbon present in the char sample on a dry-ash free basis.

$$\Delta m_{C,t} = \int_{t_0}^{t_i} \dot{r}_c dt \approx \frac{\Delta t}{2}\left[\sum_{i=1}^{n}\left(r_C(t_{i-1}) + r_C(t_i)\right)\right] \qquad \text{(C.3)}$$

From Equation C.3, t is time, and Δt is a time interval which is 2 seconds in this case, since the concentration of CO is logged every 2 seconds interval.

Moreover, the specific reaction rate for the converted carbon is determined from the knowledge of the carbon conversion as expressed in Equation C.4.

$$r_s = \frac{1}{1 - X}\frac{dX}{dt} = \frac{1}{m_{C,0} - \Delta m_{C,t}}\frac{d\Delta m_C}{dt} = \frac{1}{m_{C,t}}\frac{dm_{C,t}}{dt} \qquad \text{(C.4)}$$

Where r_s (g/g/s) is specific reaction rate.

The specific reaction rate or specific reactivity represented by Equation C.4 is the rate of change of carbon converted normalised with the unreacted carbon mass present the char sample. Consequently, the derivative term ($\frac{dX}{dt}$) in Equation C.4 can be further simplified to;

$$\frac{dX}{dt} = \frac{\Delta X}{\Delta t} = \frac{X_i - X_{i-1}}{t_i - t_{i-1}} \tag{C.5}$$

Equation C.4 and C.5 are used to determine the specific reaction rates for the char-CO_2 gasification experiments.

C.1.2 Specific reaction rate (Char-steam experiments)

The specific reaction rate for steam gasification experiments depends on the quantity of the CO and also CO_2 produced during the reaction of which is attributed to the overall carbon converted. Based on the stoichiometry of the carbon-steam and water-shift reaction, one mole of carbon is converted to form one mole of hydrogen and carbon monoxide of which can further react with one mole of water to form one mole of carbon dioxide.

$$C + H_2O \rightarrow CO + H_2 \tag{R2.4}$$

$$CO + H_2O \rightarrow CO_2 + H_2 \tag{R2.6}$$

The known concentration of CO and CO_2 the specific reaction rate for steam gasification can be obtained. In this case, the rate of carbon converted is equivalent to the sum rate of CO and CO_2 produced. That is;

$$r_c = r_{CO} + r_{CO_2} \tag{C.6}$$

Using the stoichiometry, the above equation can be further simplified and described as follows;

$$r_c = 1.\left(\frac{\dot{V}_T}{\hat{V}_{STP}}\right)[CO]MW_c + 1.\left(\frac{\dot{V}_T}{\hat{V}_{STP}}\right)[CO_2]MW_c \tag{C.7}$$

Which then result in the following equation;

$$r_c = \left(\frac{\dot{V}_T}{\hat{V}_{STP}}\right)([CO] + [CO_2])MW_c \tag{C.8}$$

From the rate of carbon converted, the char-carbon conversion during steam gasification can then be determined by making use of Equation C.3 from which the specific reaction rate can be obtained using Equation C.2 and C.4.

C.2 Determination of model parameters

The well-established kinetic and structural models were utilised to provide the kinetic data and also fit the experimental data. These models were used for various gasification data obtained at fixed conditions.

C.2.1 nth-order rate law

The nth-order model also known as the Power-law model was used to fit the experimental data based on the determination of the fitting parameters such as the reaction order and the rate constant. The model is based on representing the reaction rate as a function of reactant partial pressure and is given as follows;

$$r_s = k_s {p_i}^n \tag{C.9}$$

Where

$$k_s = k_0 \exp\left(\frac{-E_a}{RT}\right) \tag{C.10}$$

The kinetic parameters were determined based on the measured reaction rate from the char-gas gasification reactions by means of varying the reactant partial pressure. In this case, the kinetic parameters such as the pre-exponential factor and the activation energy of the reactions were not evaluated since the previous consistent studies on the Highveld coals have shown conclusive results.

In order to obtain the reaction order and the rate constant, the Power-law model was linearised by using linearisation method of which resulted in the following equation;

$$ln(r_s) = ln(k_s) + n.ln(p_i) \tag{C.11}$$

From the plot of $ln(r_s)$ against $ln(p_i)$ which is generally a straight line, the reaction order was determined from the slope of the equation and the rate constant was determined by taking the natural logarithm of the intercept.

C.2.2 LH reaction rate model

The Langmuir-Hinshelwood (LH) rate model which is derived from the char-gas reaction mechanism was used to also fit the experimental data due to its applicability to represent the experimental data at high reactant partial pressures.

$$r_{s,4\%} = \frac{[C_t]k_1 p_i}{1 + {k_1}/{k_3}\, p_i + {k_2}/{k_3}\, p_j} \tag{C.12}$$

And for the intrinsic reaction rate;

$$r_i^{"} = \frac{c\, p_i}{1 + {k_1}/{k_3}\, p_i + {k_2}/{k_3}\, p_j} \tag{C.13}$$

where p_i is the partial pressure of steam or CO_2 and p_j is the partial pressure of CO for CO_2 gasification and H_2 for steam gasification. These equations have been previously used at low pressures and also high pressures from which the reactant partial pressures of the product gas (CO and H_2) were low resulting to insignificant effect on the rate model and therefore the P_{CO} and $P_{H2} \approx 0$ (Chen *et al.*, 2013; Hüttinger & Merdes, 1992; Kwon *et al.*, 1988; Liu *et al.*, 2017; Roberts & Harris, 2006; Tomaszewicz *et al.*, 2017; Wang & Bell, 2017). These results were also in accordance with the observed experimental results whereby the CO partial pressure was low in such a way that the rate expression reduced to the following equation.

$$r_{s,4\%}(g/g_c/s) = \frac{[C_t]k_1 p_i}{1 + {k_1}/{k_3}\, p_i} \tag{C.14}$$

And for the intrinsic reaction rate;

$$r_i^{"}(g/m^2/s) = \frac{c\, p_i}{1 + {k_1}/{k_3}\, p_i} \tag{C.15}$$

To fit the experimental data using the above-mentioned rate models, the kinetic parameters were firstly determined. These parameters can be obtained from the measured experimental data by expressing the reaction rate as a function of reactant partial pressure (linearisation method) or by making use of the least-square method. In this case, the least-square method was used since it was observed to be the most suitable method because the linearisation method showed uncertainties above reactant partial pressure of 5 bar as also observed by Tomaszewicz *et al.* (2017).

$$Minimisation = \left[\sum_{i=1}^{N}\left(r_{exp,i} - r_{cal,i}\right)^2\right] \quad \text{(C.16)}$$

To execute this method, the reaction rate was firstly calculated from the estimated kinetic constant the squared deviations between the experimental and calculated data were determined. The sum of the squared deviations was minimised by making use of SOLVER add-in in Microsoft Excel® with regards to the approximation of the kinetic constants represented by the $[Ct]k_1$ and k_1/k_3 terms.

C.2.3 RPM model

The Random-Pore Model (RPM) which incorporates the structural changes during the char conversion was also used for fitting the experimental data.

$$\frac{dX}{dt} = k_p(1-X)\sqrt{1-\psi ln(1-X)} \quad \text{(C.17)}$$

This equation represented the overall reaction as a function of structural parameters and conversion of which was further simplified to describe the specific or apparent reaction rate and the equation results as follows;

$$r_s = \frac{dX}{dt}\frac{1}{(1-X)} = r_{s,0}\sqrt{1-\psi ln(1-X)} \quad \text{(C.18)}$$

where the initial rate is given by the following equation:

$$r_{s,0} = \frac{k_s S_0}{(1-\varepsilon_0)} \quad \text{(C.19)}$$

The RPM for the description of the specific reaction rate is mostly used in terms of data fitting where the initial reaction rate ($r_{s,0}$) and the structural parameters (ψ) are estimated. The leas-squares method was also used to determine the fitting parameters and this method has been widely used for the determination of RPM parameters (Duman *et al.*, 2014; Kajitani *et al.*, 2002; Tremel & Spliethoff, 2013; Wang *et al.*, 2015).

C.3 Uncertainties and precision determination

C.3.1 Repeatability and reproducibility

The repeatability and reproducibility of the experimental data play a major role in the accuracy of the reported data. The uncertainties with regards to the specific reaction rate data measured through the experimental method were determined by making use of the t-methods as described further by Devore and Farnum (2005). The confidence interval can, therefore, be determined with the knowledge of the t-distribution by making use of the following equation:

$$CI = \bar{x} \pm t_{critical\_value} \frac{s}{\sqrt{n}} \tag{C.20}$$

Where s is the standard deviation of the repeated runs, n is the number of experimental runs on the same conditions, and t is the critical value obtained from a specific confidence level and degrees of freedom (n-1). In this case, the experimental uncertainties which might result from the data handling, measuring equipment, etc. was determined based on the 95% confidence level with three repeated runs of which resulted in two degrees of freedom and t critical value of 4.303.

The experimental error for this uncertainties can, therefore, be calculated from the standard error (SE) and the mean as follows;

$$error(\%) = \left(t_{critical_{value}} \frac{s}{\sqrt{n}} \Big/ \bar{x} \right) \times 100 \tag{C.21}$$

C.3.2 Experimental data and models

The experimental data was used to determine the parameters of the kinetic models and the results were further evaluated in terms of deviations between the experimental data and the kinetic models. The relative/deviation error was calculated using the following equation:

$$error\ (\%) = \left[\frac{\sqrt{\left(\sum_{i=1}^{N} \left(r_{exp,i} - r_{cal,i} \right)^2 \right) / N}}{r_{exp}(max)} \right] \times 100 \tag{C.22}$$

This method provides the quantified deviations between the experimental data and kinetic models which can be ascribed to the experimental errors in association with the limited range of the equipment.

C.3.3 Quality of fit (QOF)

The quality of fit (QOF) was used to calculate the accuracy of the model in predicting the experimental results and it is expressed in Equation C.23.

$$QOF\ (\%) = \left[1 - \frac{\sum_{i=1}^{N} \frac{\left|r_{exp,i} - r_{cal,i}\right|}{r_{exp,i}}}{N}\right] \times 100 \qquad \text{(C.23)}$$

Where N is the number of data points, $r_{exp,i}$ is the experimental value at a specific point, and $r_{cal,i}$ is the calculated value using the model.

APPENDIX D

(EXTENDED EXPERIMENTAL RESULTS)

D.1 Coal pyrolysis

Coal pyrolysis was done on 12 batches of representative coal and the results of the char and gas yield are summarised in Table D-1.

Table D-1: Summary of pyrolysis char and gas yield results

Sample no.	Initial mass (g)	Final mass (g)	Char yield (wt%)	Gas yield (wt%)
1	146.2	112.3	76.8	23.2
2	150.0	114.1	76.1	23.9
3	152.2	115.7	76.0	24.0
4	150.7	114.9	76.2	23.8
5	148.9	113.9	76.5	23.5
6	153.9	117.4	76.3	23.7
7	157.4	120.13	76.3	23.7
8	152.1	116.8	76.8	23.2
9	153.8	117.7	76.5	23.5
10	151.6	115.9	76.4	23.6
11	150.3	114.9	76.4	23.6
12	152.3	116.15	76.3	23.7
Total	1819.4	1389.7	76.4	23.6

The gas yield was found to be relatively 23.6 wt% which is based on total volatiles (inherent moisture and volatile matter) driven-off during coal devolatilisation.

D.2 Gasification experiments

D.2.1 CO ad CO_2 concentration profiles

Using the NDIR gas analysers, raw data was obtained and true concentrations were measured by making use of the calibration curves (Appendix B.5). The results of the determined CO concentration profiles for both steam and CO_2 gasification experiments are shown in Figure D-1.

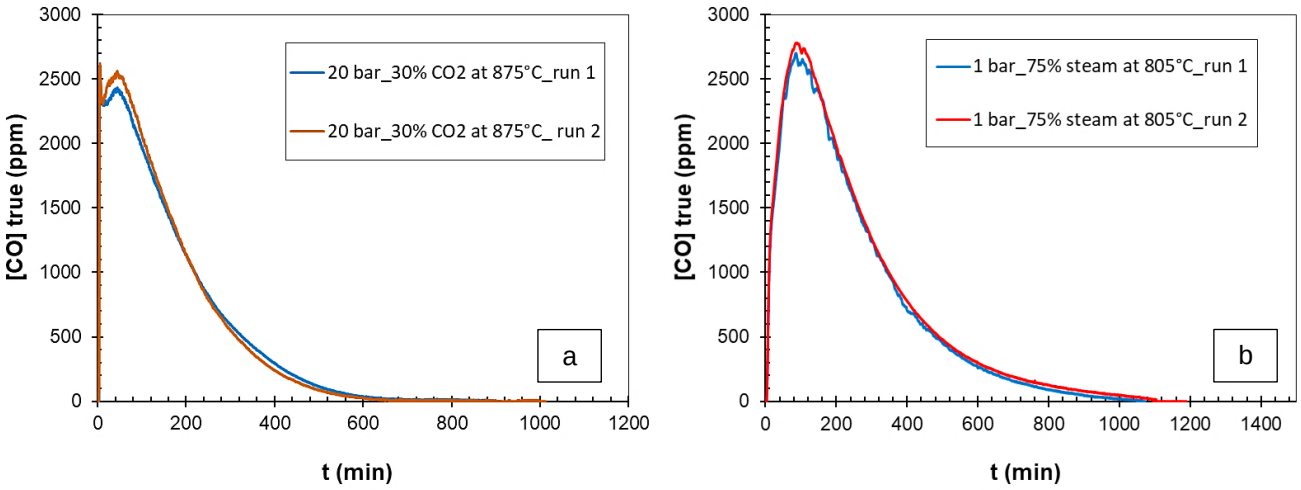

Figure D-1: CO concentration profiles for (a) CO_2 and (b) steam gasification experiments

As shown in Figure D-1, the CO concentration measured in the product gas, increased rapidly in the early stage of gasification reactions and then decreased as the reactions proceeded to an extent where CO concentration was significantly low and levelled off.

The CO_2 concentration was also measured (Due to water-shift reaction) in conjunction with the CO concentration in the product gas for the char-steam gasification experiments. The measured CO_2 concentration profile was further converted to true CO_2 concentration using the calibration data provided in Appendix B.5. The results of the measured CO_2 concentration and CO/CO_2 ratio are illustrated in Figure D-2.

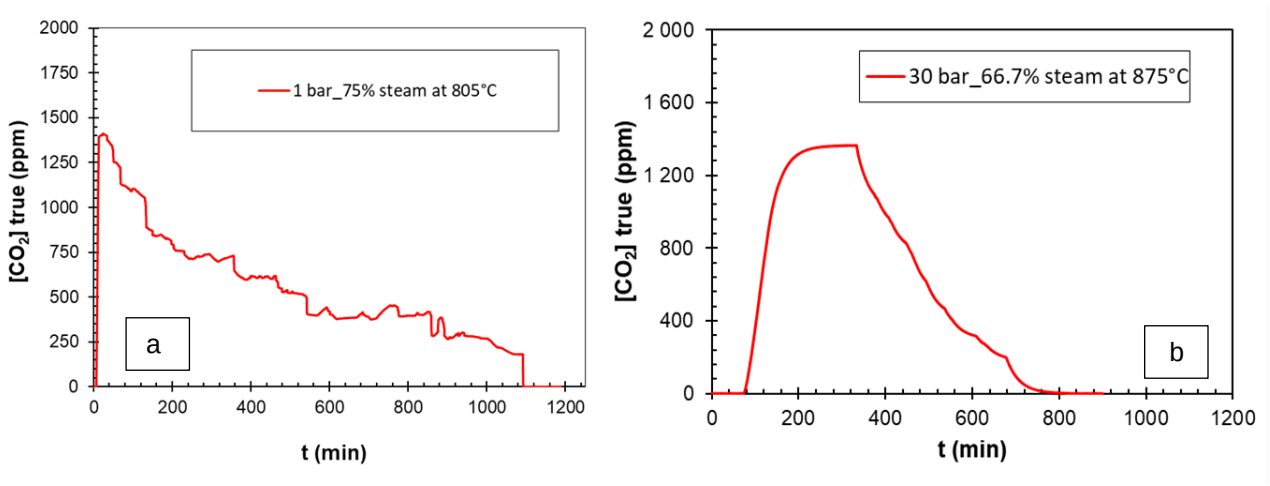

Figure D-2: CO_2 concentration profiles (a) 0.75 bar steam at 805 °C, (2) 20 bar steam at 875 °C and (c) CO/CO_2 ratio at 0.75 bar steam at 805 °C

D.2.2 Carbon mass balance

From the measurements of the gasification product concentrations (Appendix D.2.1), the carbon conversion was determined using the methods described in C.1.1 and C.1.2 for CO_2 and steam gasification, respectively. The carbon conversions were found to be 97.2 and 95.2% with an ash yield of 98.5 and 98.9% from the proximate analysis of the remaining residue for steam and CO_2, respectively. From these results, the mass of carbon converted was determined and compared with the converted mass of carbon from the experimental. Equation D.1 shows the expression used to calculate the mass of carbon converted.

$$m_c(cal) = m_{c,0} - m_{c,t} \tag{D.1}$$

where $m_{c,0}$ is the initial mass of carbon and $m_{c,t}$ is the mass of carbon at time t, which is the final time in this case.

$$m_{c,0} = m_{char}\left(1 - x_{ash,0}\right)x_{c,daf} \tag{D.2}$$

and

$$m_{c,t} = m_{char}\left(1 - x_{ash,t}\right)x_{c,daf} \tag{D.3}$$

From the proximate analysis results of the remaining residue, the mass of carbon after gasification was calculated and found to be 0.2884 g and 2903 g for steam and CO_2, respectively. Table D-2 shows a comparison of the calculated and experimental results of the converted mass of carbon.

Table D-2: Carbon balance results

Steam gasification			CO_2 gasification		
$m_{c,cal}$ (g)	$m_{c,exp}$ (g)	abs. error	$m_{c,cal}$ (g)	$m_{c,exp}$ (g)	abs. error
0.2884	0.2907	**1%**	0.2934	0.2845	**3%**

As shown in Table D-2, the maximum absolute error between the calculated and experimental converted carbon balance is 3%. These results indicate that the measurements of carbon conversion from the experimental data correlate well with the calculated values.

D.2.3 Carbon conversion profiles

- ***Char-CO_2 experiments***

Char-CO_2 experiments were conducted at a temperature of 780 °C and CO_2 partial pressure range of 1-30 bar and the carbon conversion profiles (10, 20, and 30%) as a function of time are shown in Figure D-3.

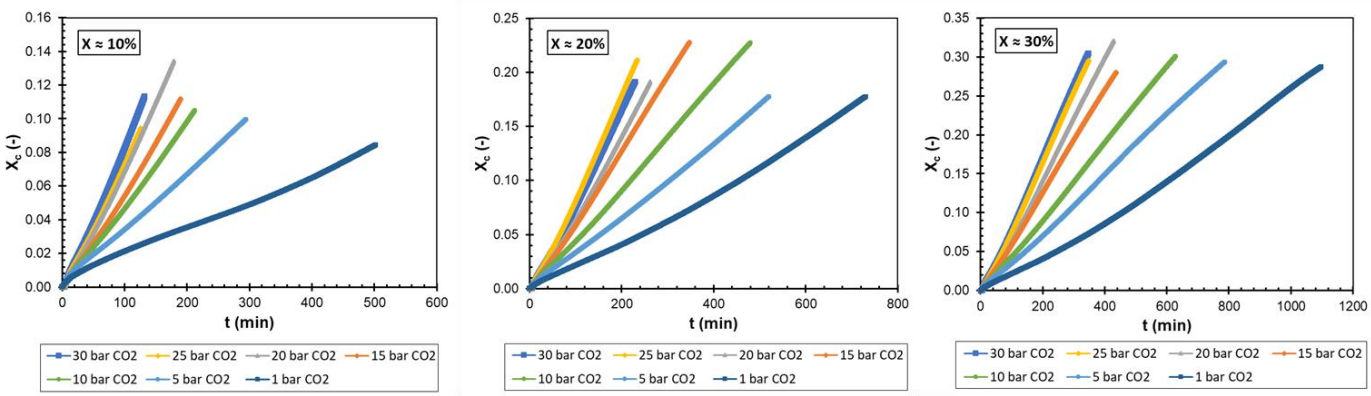

Figure D-3: Carbon conversion profiles against time for CO_2 gasification experiments

- ***Char-steam experiments***

Char-steam gasification experiments were conducted at a temperature of 740 °C and steam partial pressure of 2.5 up to 20 bar. The measured carbon conversion profiles as a function of time are shown in Figure D-4.

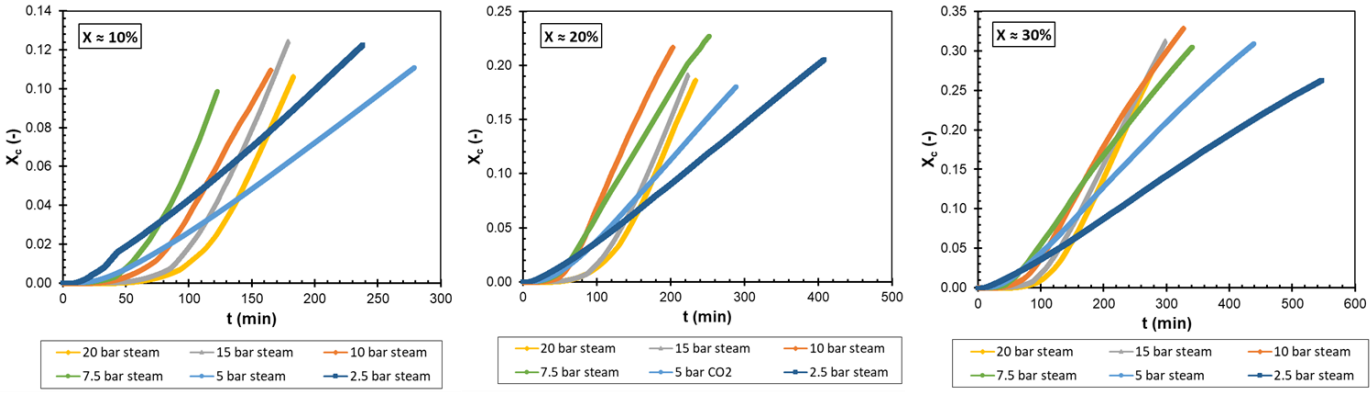

Figure D-4: Carbon conversion profiles against time for steam gasification experiments

Unlike with CO_2 experiments, the carbon conversion measured from char-steam reactions increases slowly with time in the early stage and these effects are the result of pressure. As the steam partial pressure increases, this effect also increases whereby at 20 bar steam the conversion starts to increase significantly after 100 minutes for the evaluated conversion range.

D.3 Kinetic modelling

D.3.1 Power law (n^{th}-order) model

The PL model was used to determine the kinetic parameters which include reaction order from the specific reaction rate data at 4% conversion and intrinsic reaction rate data at 10, 20, and 30% conversion for steam and CO_2. Figure D-5 shows the specific rate data fitted to the PL model.

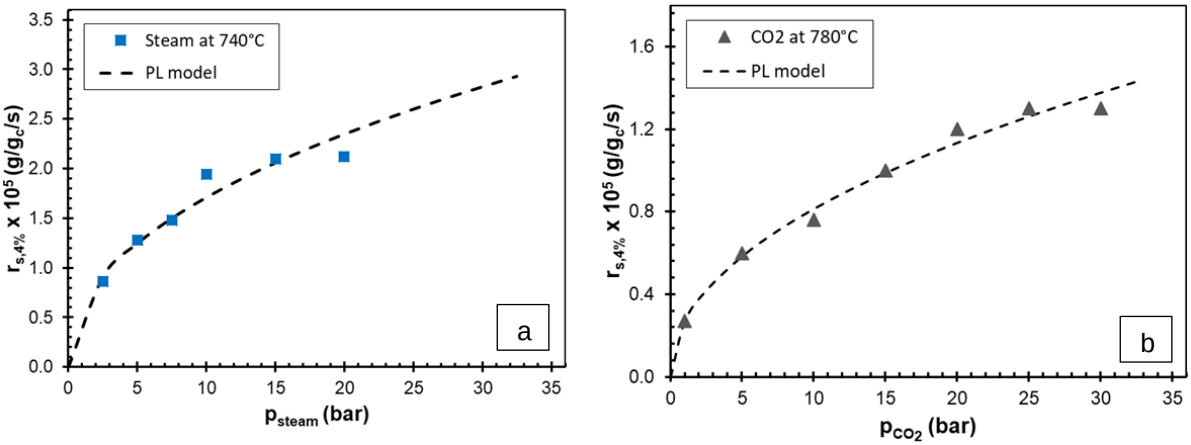

Figure D-5: Specific reaction rate and PL model results for (a) steam and (b) CO_2 measured at 4% conversion

The kinetic parameters and the relative error between the specific rate determined from PL and the experimental data are summarised in Table D-3.

Table D-3: PL model parameters and deviation error results obtained from specific rate data at 4% conversion

	Steam results	CO_2 results
n (-)	0.46	0.48
k_s (1/s)	$6.0x10^{-6}$	$2.7x10^{-6}$
Relative error (%)	6.4	3.6

For the intrinsic reaction which is simply the specific reaction rate normalised to the subsequent micropore surface area at carbon conversions of 10, 20, and 30%, the correlation of the Power-law model and the experimental data is illustrated in Figure D-6.

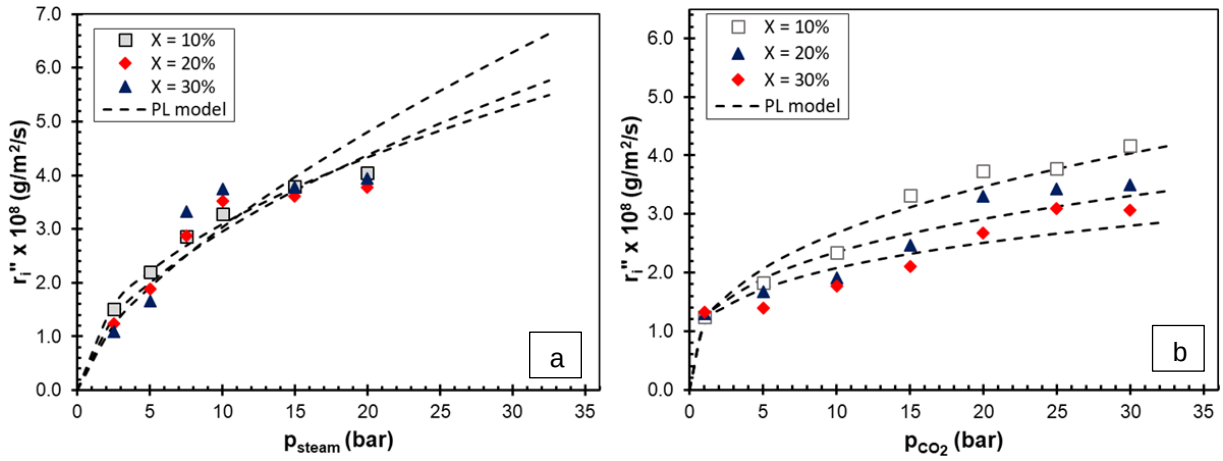

Figure D-6: Intrinsic reaction rate and PL model at 10, 20 and 30% for (a) steam and (b) CO_2

The determined kinetic parameters at conversions of 10, 20, and 30% from the intrinsic rate data are summarised in Table D-4.

Table D-4: PL model parameters and deviation error results obtained from intrinsic rate data

X	CO_2 results		Steam results	
	n $(-)$	k_s $(g/m^2.s.bar)$	n $(-)$	k_s $(g/m^2.s.bar)$
10%	0.37	$1.1x10^{-8}$	0.49	$1.0x10^{-8}$
20%	0.31	$1.2x10^{-8}$	0.57	$8.0x10^{-9}$
30%	0.27	$1.1x10^{-8}$	0.66	$6.6x10^{-9}$

The relative error was found to be 4.0, 9.9, and 14.9% for steam and 5.0, 8.3, and 9.3% for CO_2 at conversions of 10, 20, and 30%, respectively.

D.3.2 Langmuir-Hinshelwood model

LH model was used together with the specific rate data measured at 4% conversion to compare and evaluate the measured kinetic parameters from the reported results. Figure D-7 shows the LH model results fitted to the experimental data.

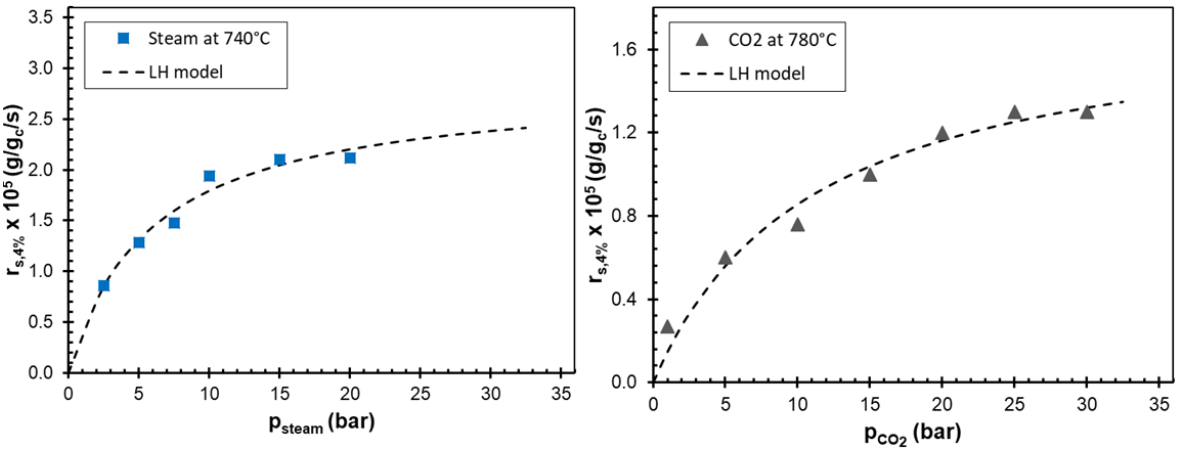

Figure D-7: LH model results fitted to specific rate obtained at 4% conversion

The LH kinetic parameters are summarised in Table D-5.

Table D-5: LH model parameters obtained from specific rate data at 4% conversion

	CO_2 results		Steam results	
	$[C_t]k_1$ $(1/bar.s)$	k_1/k_3 $(1/bar)$	$[C_t]k_1$ $(1/bar.s)$	k_1/k_3 $(1/bar)$
X = 4%	1.6x10^{-6}	0.09	4.8x10^{-6}	0.17
Relative error (%)	**5.1**		**4.1**	

The obtained kinetic parameters compare well with the results reported by Roberts and Harris (2006) who found the $[C_t]k_1$ value of 3.3-8.7x10^{-6} (1/bar.s) and a k_1/k_3 value of 0.07-0.47 (1/bar) for both steam and CO_2 gasification.

D.4 Random-Pore Model (RPM)

D.4.1 Specific reaction rate

The Random-Pore Model (RPM) described by Bhatia and Perlmutter (1980) (for isothermal and chemical controlled conditions) was used (Equation C.18) to model the specific reaction rate measured at a conversion range of 4-30% at different steam and CO_2 partial pressures. The structural parameter (ψ) and initial rate were obtained from the measured specific rate data and

the method is described in Appendix C.2.3. A comparison of the specific rate measured from the experimental data and determined from the RPM rate equation is illustrated in Figure D-8.

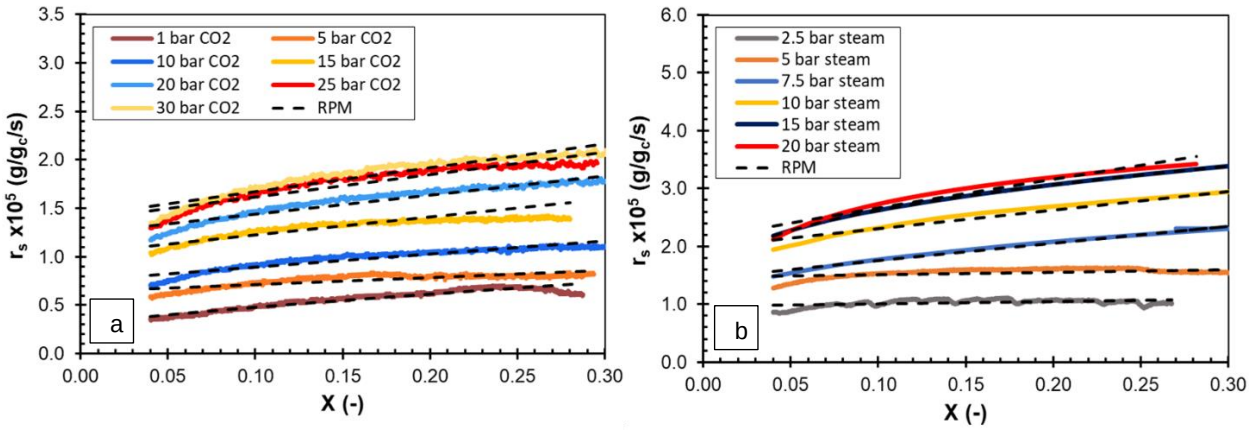

Figure D-8: Comparison of specific reaction rate of (a) CO_2 and (b) steam against conversion using RPM

It can be seen that the RPM can describe well the specific reaction rate for the evaluated steam and CO_2 partial pressure range over the conversion of 4-30%. The deviations between the RPM and experimental data results were found to be lower than 0.5% indicating a good fit. Several authors have also found the RPM to be able to predict well the experimental data measured at both high and low partial pressures for steam and CO_2 (Gouws, 2017; Jayaraman *et al.*, 2015; Kajitani *et al.*, 2002; Tomaszewicz *et al.*, 2017; Wang *et al.*, 2015). The fitted values of the structural parameter and initial rate are summarised in Table D-6.

Table D-6: Summary of the fitted RPM parameters for CO_2 and steam

CO_2 results (780 °C)			**Steam results (740 °C)**		
CO_2 pressure *(bar)*	ψ $(-)$	$r_{s,0}$ $(g/g_c/s)$	***Steam pressure*** *(bar)*	ψ $(-)$	$r_{s,0}$ $(g/g_c/s)$
1	13.3	0.3	2.5	0.8	1.0
5	2.2	0.6	5	0.5	1.5
10	3.9	0.8	7.5	4.7	1.4
15	3.9	1.0	10	3.4	2.0
20	3.3	1.2	15	4.5	2.1
25	3.6	1.4	20	5.4	2.1
30	3.7	1.4	-	-	-

The determined structural parameter results for steam and CO_2 are in agreement with the reported results in the literature (Gouws, 2017; Jayaraman *et al.*, 2015; Kajitani *et al.*, 2002; Tomaszewicz *et al.*, 2017; Wang *et al.*, 2015). The structural parameter measured from the reactivity data is not a good indicator of pore development during gasification because it provides values that are not suitable to predict the surface area (Kajitani *et al.*, 2002). However, the ψ

values suggests that the structural parameter has some dependency on reactant partial pressure as shown in Table D-6. These results corresponds well with the observed pore development occurring from the onset of gasification at a constant conversion. The initial reactivity is found to be similarly affected by the reactant partial pressure as observed from the reactivity results and similar results have been obtained (Gouws, 2017; Kajitani *et al.*, 2002).

D.4.2 Pore development: Structural parameter

The structural parameter measured from the micropore surface area development was found to be constant for steam gasification. As for CO_2 gasification, it was observed that this parameter is dependent on CO_2 partial pressure and can be described by the n^{th}-order type equation as shown in Figure D-9. The correlation coefficient (R^2) of 0.938 was found which indicates a strong relationship between the structural parameter and CO_2 partial pressure.

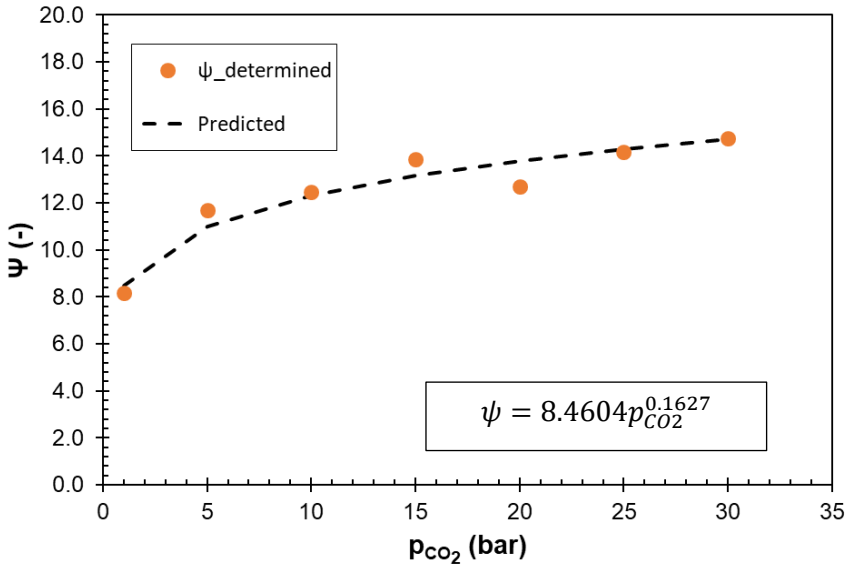

Figure D-9: Prediction of the structural parameter as a function of CO_2 partial pressure

The deviations between the determined and predicted ψ value was found to be less than 10% indicating that the n^{th}-order type equation can be used to predict the changes in the structural parameter with CO_2 partial pressure.

D.5 Combined models

The combined models were used to predict the specific reaction rate based on the determined kinetic and structural parameters from the measured intrinsic kinetic data. The model is based on the existing proposed models that describe the effects of reactant partial pressure on reaction rate (LH type model) and pore development (RPM) during gasification as shown in Equation D.4

$$r_s = \frac{cp_i}{1 + {k_1}/{k_3}\, p_i} S_{m,0}\sqrt{1 - \psi \ln(1 - X)} \qquad \text{(D.4)}$$

The quality of fit (QOF) was measured for the evaluated reactant partial pressure range and the results are summarised in Table D-7.

Table D-7: QOF results of the modelled specific reaction rate for steam and CO_2 gasification

Quality of fit (QOF)							
$\boldsymbol{P_{CO2}}$	1 bar	5 bar	10 bar	15 bar	20 bar	25 bar	30 bar
QOF	94%	72%	69%	87%	87%	88%	90%
$\boldsymbol{P_{Steam}}$	2.5 bar	5 bar	7.5 bar	10 bar	15 bar	20 bar	-
QOF	83%	82%	90%	85%	87%	89%	-